Yuwei Hu
Fenghua Li
Dongxue Han
Li Niu

Biocompatible Graphene for Bioanalytical Applications

SpringerBriefs in Molecular Science

Yuwei Hu · Fenghua Li
Dongxue Han · Li Niu

Biocompatible Graphene for Bioanalytical Applications

Yuwei Hu
Engineering Laboratory for Modern
    Analytical Techniques c/o, State Key
    Laboratory of Electroanalytical
    Chemistry
Changchun Institute
    of Applied Chemistry
Chinese Academy of Sciences
Changchun
China

Fenghua Li
Engineering Laboratory for Modern
    Analytical Techniques c/o, State Key
    Laboratory of Electroanalytical
    Chemistry
Changchun Institute
    of Applied Chemistry
Chinese Academy of Sciences
Changchun
China

Dongxue Han
Engineering Laboratory for Modern
    Analytical Techniques c/o, State Key
    Laboratory of Electroanalytical
    Chemistry
Changchun Institute
    of Applied Chemistry
Chinese Academy of Sciences
Changchun
China

Li Niu
Engineering Laboratory for Modern
    Analytical Techniques c/o, State Key
    Laboratory of Electroanalytical
    Chemistry
Changchun Institute
    of Applied Chemistry
Chinese Academy of Sciences
Changchun
China

Preface

Over the past few decades, various nanomaterials, such as gold nanoparticles, carbon nanotubes, quantum dots, magnetic beads, polymers, carbon dots, etc., have received intense scientific attention and offered promising applications in biosensing, energy, medicine, imaging, electronics, as well as the interdisciplinary fields, attributing to their unique optical, electrical, chemical, and mechanical properties. However, interests and efforts are always devoted to finding new materials and exploring their new properties to fulfill the ever-increasing needs, and great progress has been achieved in these aspects. As the newly found material, graphene, a single layer of sp^2-bonded carbon atoms arranged in a two-dimensional honeycomb lattice, has gained scientific attention from all over the world since its first total discovery in 2004 by K.S. Novoselov and A.K. Geim. The unique structure and atom configuration of graphene endows it with outstanding properties, such as large theoretical surface area up to 2,630 m^2/g, high charge carrier mobility at room temperature ($\sim 2.5 \times 10^5$ cm^2/V s), good optical transparency (~ 97.7 %), excellent thermal conductivity (~ 5000 W/m K), high Young's modulus (~ 1.1 TPa), and quantum hall effect, etc., which are much more beneficial for its applications in sensing, energy storage, flexible electronic devices, etc. In the area of sensing, graphene has achieved a great success, but there are hurdles that must be overcome. The main challenges include the exfoliation of high quality single-layer graphene sheets, the prevention of self-aggregation of graphene sheets into a graphite-like structure, the biocompatibility and maximized performance under physiological conditions, which are the main focuses of the current volume.

We present the biocompatible graphene in bioanalytical applications, including the use of simulations and bioinformatics-driven approaches for predictive modeling of the interaction between graphene and biomolecules, various biomaterials decorated graphene based on covalent or non-covalent modes, the enhancement of analytical performances, the effective transduction of recognition event to the detectable signals through optical, electrochemical, mechanical, electronic, and other methods, the effective versatile/multiplexed targets recognition, the cytotoxicity and sophisticated in-vivo imaging, etc. We highlight the recent progress in bioassays toward various targets, for example, DNA, amino acid, peptide, protein,

enzyme, antigen, glucose, DA, AA, UA, ATP, NADH, cell imaging and drug delivery, gas, other molecules and ions, etc. Along this line, particular emphasis is placed on the well-designed strategies for graphene platform construction and target determination. Also, future challenges and prospects of graphene in bioanalytical applications are discussed.

We believe those who wish to have a complete overview of biocompatible graphene in the bioassay fields, wise strategies to decorate graphene, and signal transduction ways to maximize analytical performances, would benefit from this book. Great appreciation is given to all authors, who made great contributions to the book. And, of course, the organizational support from Springer in the production of this book is gratefully acknowledged.

<div align="right">

Yuwei Hu
Fenghua Li
Dongxue Han
Li Niu

</div>

Contents

Chapter 1
Introduction

Abstract IUPAC defines graphene as a single carbon layer of the graphite structure, describing its nature by analogy to a polycyclic aromatic hydrocarbon of quasi infinite size. This unique intrinsic structure endows graphene with remarkable properties, which actually are largely determined by the methods used to fabricate and exfoliate graphene sheets. Besides using the appropriate synthesis methods, one commonly adopted strategy to improve and expand the performance of graphene is to incorporate functional materials into graphene basal plane or edges based on covalent or noncovalent interactions. Among these materials, biological materials, such as DNA, peptide, protein, etc., behave as good candidates due to their unique structure, biocompatibility, and renewability. Exfoliation and functionalization of graphene using these materials are highlighted.

Keywords Graphene · Functional materials · Exfoliation · DNA · Peptide · Protein

Back to 1840s, German scientist Schafhaeutl reported the intercalation (insertion of a small-molecule species, such as an acid or alkali metal, in between carbon lamellae) and exfoliation of graphite (held by van der Waals forces among individual layers) with sulfuric and nitric acids, which was the earliest report of graphite oxide and graphite intercalation compounds. As early as the 1940s, a series of theoretical analyses suggested that these layers—if isolated—might exhibit extraordinary electronic characteristics. As time goes on, chemical and thermal exfoliation, growth on transition-metal substrate, epitaxial sublimation of silicon from silicon carbide, and micromechanically exfoliating graphite have been adopted to exfoliate graphite. Interesting and important results were obtained, which acted as prelude and paved the way for the finally successful exfoliation of graphite. A specific illustration of the historical account of graphene would be found at Ref. [1]. Till 2004 [2], Novoselov and Geim obtained single graphene layer with a scotch tape and proved the thermodynamically stable existence of the two-dimensional material at finite temperatures, leading the world into a 'graphene age'. Since then, tremendous amount of efforts has been devoted to investigating the properties, fabrication, and applications of the thinnest material. Now the

exciting show of graphene is still ongoing and great advancements have been achieved in the fields of physics, chemistry, materials, biology, and medicine, as well as other interdisciplinary fields.

IUPAC defines graphene as 'a single carbon layer of the graphite structure, describing its nature by analogy to a polycyclic aromatic hydrocarbon (PAH) of quasi infinite size' [3]. PAH is a common name given to aromatic hydrocarbons, which contain more than two unsubstituted fused benzene rings. Graphene molecule is defined as large PAHs having sizes of 1–5 nm, while nanographene can be a graphene fragment ranging from 1 to 100 nm in size. Once the size of the hexagonal sp^2 carbon network exceeds 100 nm, they can be directly regarded as graphene, as recently presented in an excellent review [4]. There are also graphene nanoribbons (GNPs) [5–7], which are graphene strips with a width of less than 10 nm and length/width ratio higher than 10, and graphene quantum dots (GQDs) [8], which are relatively regular-shaped graphene units with sizes ranging from several to 100 nm. Despite the size and shape differences, the structure and composition of these graphenes are basically the same, in which sp^2-bonded carbon atoms arrange in a two-dimensional honeycomb lattice. The graphene honeycomb lattice is composed of two equivalent sublattices of carbon atoms bonded together with σ bonds. Each carbon atom in the lattice has a π orbital that contributes to a delocalized network of electrons. The unique intrinsic structure endows graphene with remarkable properties, such as large theoretical surface area (2,630 m^2/g) [9], high charge carrier mobility at room temperature ($\sim 2.5 \times 10^5$ cm^2/V s) [10], good optical transparency (~ 97.7 %) [11], excellent thermal conductivity ($\sim 5,000$ W/m K) [12], high Young's modulus (~ 1.1 TPa) [13], and quantum hall effect [14]. These electronic, optical, thermal, and mechanical properties make graphene far superior to its counterparts [15]. In reality, these superior properties are largely determined by the methods which graphene is synthesized. In general, the most often adopted methods for graphene preparation include mechanical exfoliation [2, 16], epitaxial growth [17, 18], chemical vapor deposition (CVD) [19–23], reduction of graphene derivatives (viz. graphene oxide) [24–27], longitudinal 'unzipping' of CNTs [28, 29], etc. Besides the above mentioned properties, large difference in graphene size, defect, edge, chemical composition, number of layers, reactivity, and dispersibility, etc. would also be observed with different synthesis strategies. To best facilitate the application of graphene, one should particularly pay attention to the preparation method and the properties. Detailed discussion of the properties and synthesis of graphene is out of the scope of this book, which might be found in some excellent reviews [4, 30–38].

One common strategy to improve and expand the performance of graphene is to incorporate functional materials, such as inorganic nanoparticles [39–42], organic structures [43–50], polymers [51–55], biomaterials [56–61], into graphene basal plane or edges based on covalent or non-covalent interactions. The incorporation of these functional materials into graphene sheets has two main merits: (a) efficiently exfoliating graphene sheets. The high cohesive van der Waals energy (5.9 kJ/mol) tends to adhere graphitic sheets to one another [62]. While the outstanding physical and chemical properties of graphene are largely associated with its single-layer

sheets. (b) Tailored-modification and synergic-effect resulting in the graphene-based composites with superior properties, which are beneficial for practical performances. Researches into graphene-based applications, such as biosensing, electronics, energy, photovoltaics, catalysis, and so on, have been flourishing and great progress has been made in the past few years, and many review papers have been dedicated to these topics [15, 63–77]. In this book, we will present recent advances on graphene and biocompatible materials decorated graphene in bioanalytical applications toward detection of DNA, RNA, amino acid, peptide, protein, enzyme, antigen, glucose, DA, AA, UA, ATP, NADH, gas, other molecules and ions, etc. as well as cell imaging and drug delivery via various well-designed strategies. First, exfoliation and functionalization of graphene by biomaterials, such as DNA, peptides, and protein, are highlighted. Comparing with organic polymers, surfactants, or nanoparticles, biological molecules emerge as appealing as functional materials due to their unique structure, biocompatibility, and renewability, which guarantee properties that are different from other substances. Then, significant developments in the exploration of graphene and its hybrids for bioanalytical applications employing various techniques are presented. The interaction mechanisms of graphene with these targets and the signal-transduction manners are also revealed.

Being first isolated by mechanical exfoliation using the 'scotch tape' method, graphene can be prepared via 'top-down' strategies, as well as 'bottom-up' synthesis approaches [75]. Despite these advances in the isolation of graphene, the ability to generically tailor its physical and chemical properties has been limited by its delicate structure. Different fabrication methods result in graphenes that differ in size, defect, edge, chemical composition, number of layers, reactivity, and dispersibility, etc. and hence the properties, performances. Besides, the aggregation, poor dispersity, or solubility in most common solvents of graphene sheets represents one of the main obstacles encountering researchers. To date, the most often adopted strategy to solve this problem is incorporating functional materials into graphene sheets. The unique π-conjugated structure, oxygenic groups, and large surface area of graphene enable it to be a good platform for functional materials anchoring based on covalent or non-covalent binding. Covalent functionalization can trigger symmetry breakage of the graphene lattice, thereby altering its properties. Non-covalent modification strategies may be limited in the scope of applicability. A general method for chemical and biological modification of graphene with specific binding motifs—while retaining the excellent properties of graphene—is thus highly desired [60]. Among these functional materials, biological molecules, such as DNA, peptides, proteins, serve as good candidates due to their unique structure, properties, and biocompatibility. The combination of graphene and biomolecules demonstrates a new type of nano-biomaterials, leading to a successful incorporation of the properties of two different components that represent important features for potential applications ranging from advanced biomedical systems by means of very sensitive sensors and biosensors to highly efficient electronics- and optics-based biotechnology.

Previous studies have illustrated that hydrophobic carbon nanotubes (CNTs) could be functionalized with single-stranded DNA (ssDNA) through non-covalent π–π stacking interactions involving both purine and pyrimidine bases of DNA molecules [78]. The negatively charged phosphate backbones are oriented away from the surface of the nanotube to produce a hydrophilic outer layer that facilitates dispersal of the wrapped CNTs in aqueous medium. Inspired by this approach, for the first time, the use of ssDNA in the preparation of stable aqueous suspensions of graphene single sheets with concentrations as high as 2.5 mg/mL was demonstrated by Mann and coworkers [79]. The spontaneous assembly of novel graphene-based bio-nanocomposites had ordered lamellar nanostructures in which the entrapped biomolecules were located specifically within the gallery regions of graphene sheets. DNA molecules were adsorbed principally through hydrophobic as well as weak electrostatic/hydrogen bonding interactions between primary amines of the nitrogen bases, and the carboxylic and phenolic groups of the graphene sheets. As a consequence, the biopolymer was oriented such that the charged and polar moieties of the sugar-phosphate backbone were exposed to the solvent. The co-assembly of a wide range of functional molecules such as dyes, electron transfer agents, protein, and enzymes, or different types of metallic, semiconducting, or catalytic nanoparticles with ssDNA-stabilized graphene sheets represented a new general route to graphene-based lamellar materials. In a similar manner, thiol and pyrene-labeled ssDNA were used to exfoliate graphene sheets, and the resulting bioconjugates were then employed to scaffold the self-assembly of gold nanoparticles [80, 81]. The particular advantages of employing DNA are its unique molecular structure, conformation, and the ability to hybridize with the complementary sequences and the unwinding of duplex under certain conditions, which results in DNA conformational transition. Based on these, DNA-directed reversible assemblies of graphene sheets under pH-responsive [82] and heat-controlled [56] conditions were successfully achieved. These studies provide a new insight for the assembly of functionalized graphene with other building blocks, especially biomolecules, which will help the rational design and preparation of hierarchical graphene-based materials. A more specific illustration of the interaction mechanisms of DNA assembly on graphene sheets would be revealed in the following DNA detection part.

Peptides are molecules containing a broad chemical diversity (acidity, hydrophobicity, etc.) that can be achieved within a relatively compact size. A powerful yet benign approach for chemical functionalization of graphene via comprehensively screened phage displayed peptides was demonstrated by Cui et al. [60]. Results showed that graphene could be selectively recognized even in nanometer-defined strips. Further, modification of graphene with bifunctional peptides revealed both the ability to impart selective recognition of gold nanoparticles and the development of an ultrasensitive graphene-based TNT sensor. Despite the extensive investigation into the integration of graphene and NPs, the control of the size, array density, and position of various NPs on isolated graphene is still a big challenge. Recently, in a controllable manner, spontaneous organization of various nanoparticles (i.e., Pt, Au, Pd, and Ru) was achieved by employing programmed-peptides

as directing agents and graphene as preformed 2D templates [83]. The resultant hybrid materials showed high electrocatalytic activity in the electrooxidation of methanol. Different from the usually adopted methods employing graphene as the template, a straightforward peptide-graphene hybrid assembly into core-shell nanowires was demonstrated by single-step solution processing based on electrostatic attraction [57]. The resultant core-shell nanowires exhibited electroconductivity through their continuous graphene shell. Further processing via thermal calcinations of peptide cores led to highly entangled networks of the hollow graphene shell, whose remarkable performance as a supercapacitor electrode was demonstrated.

Proteins are complex amphiphilic biopolymers, featuring hydrophobic and hydrophilic patches on their surfaces, which make them well-known for the adhesiveness to solid surfaces. Based on the unique structures and properties, proteins, such as bovine serum albumin (BSA) [59], β-lactoglobulin [84], and hydrophobins [58, 85], are adopted for the efficient exfoliation and functionalization of graphene sheets. In the first example, Liu et al. [59] reported a BSA-based, environmentally friendly one-step reduction/decoration strategy to produce protein-conjugated GO and reduced GO (rGO) nanosheets. BSA acted as both a reducing and a decorating agent at a suitable pH value and reaction temperature. They further demonstrated that the incorporation of protein as a 'universal glue' molecule successfully turned GO and rGO into general platforms toward the efficient assembly of nanoparticles with varying sizes, shapes, compositions, and surface properties.

In the exfoliation of graphene, lowering of the high surface tension between water and the surface of graphite seems to be an effective strategy. Since amphiphilic hydrophobin forms a monolayer whose sides have significantly different surface energies, the mixing enthalpy of graphene flakes coated with hydrophobin can be expressed in terms of the surface-energy differences between graphene and the hydrophobic side of the protein, and the solvent and hydrophilic side of the protein. As these energy differences are smaller than those of a non-coated system, the adsorption of hydrophobin on the surface of graphene is expected to lead to a stable graphene dispersion [58]. According to this, graphene exfoliation was carried out by exposing mixtures of HFBI protein and graphite to ultrasonic waves (Fig. 1.1a). Through opening of the basal planes and stabilization of the individual sheets, this process resulted in mixtures of graphite and graphene flakes with a variety of thicknesses. Some examples of bright-field TEM images of exfoliated graphite/graphene sheets were shown in Fig. 1.1b. Exfoliation can also be carried out by using variants of these proteins that contain not only the surface-active hydrophobin part, which attaches to the graphite surface, but also a second part with a specified functionality. In a followed study, the protein was genetically engineered to connect graphene and native nanofibrillated cellulose, so that it self-assembled at the interfaces, leading to cohesion and alignment [85]. Binding to graphene was achieved by the hydrophobin HFBI, and binding to cellulose was achieved by using a protein denoted as a cellulose-binding domain, which was tethered to HFBI by amino acid linkers, eventually forming a complex called
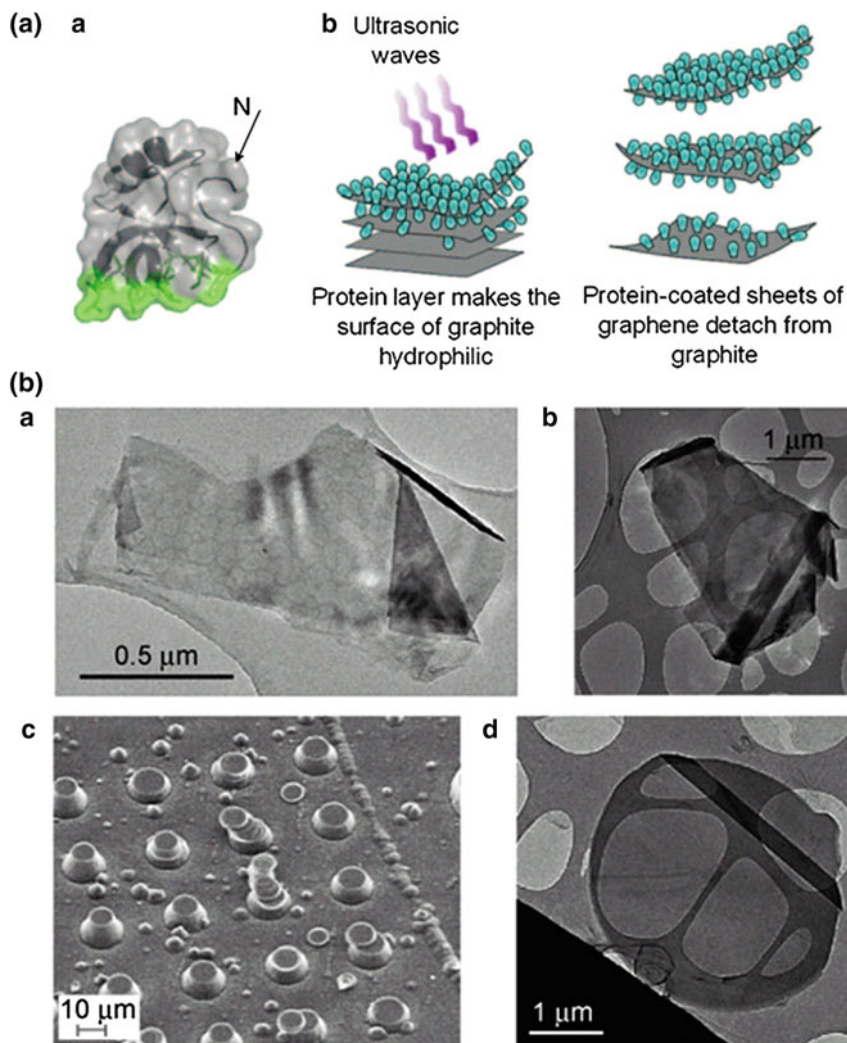
Fig. 1.1 a Schematic illustration of exfoliation and functionalization of graphene by hydropho-bins. (*a*) Structure of the HFBI protein. (*b*) HFBI-facilitated exfoliation of graphene. **b** TEM micrographs of exfoliated thin graphene/graphite flakes. (*a*) TEM image of a flake exfoliated from Kish graphite with HFBI by sonication for 2 min with an ultrasonic probe. (*b*) TEM image of a flake exfoliated from Kish graphite with HFBI by sonication for 40 min in an ultrasonic bath. (*c*) SEM image of lithographically formed HOPG micropillars. (*d*) TEM image of a thin sheet exfoliated from the HOPG micropillars. Reprinted from Ref. [58] by permission of John Wiley & Sons Ltd

'diblock proteins'. As revealed by the authors, the precise engineering of the molecular structures opens endless opportunities to design and fine-tune materials properties.

References

1. Dreyer, D.R., Ruoff, R.S., Bielawski, C.W.: From conception to realization: an historical account of graphene and some perspectives for its future. Angew. Chem. Int. Ed. **49**, 9336–9344 (2010)
2. Novoselov, K.S., Geim, A.K., Morozov, S.V., Jiang, D., Zhang, Y., Dubonos, S.V., Grigorieva, I.V., Firsov, A.A.: Electric field effect in atomically thin carbon films. Science **306**, 666–669 (2004)
3. Fitzer, E., Kochling, K.H., Boehm, H.P., Marsh, H.: Recommended terminology for the description of carbon as a solid (IUPAC recommendations 1995). Pure Appl. Chem. **67**, 473–506 (1995)
4. Chen, L., Hernandez, Y., Feng, X., Mullen, K.: From nanographene and graphene nanoribbons to graphene sheets: chemical synthesis. Angew. Chem. Int. Ed. **51**, 7640–7654 (2012)
5. Cai, J., Ruffieux, P., Jaafar, R., Bieri, M., Braun, T., Blankenburg, S., Muoth, M., Seitsonen, A.P., Saleh, M., Feng, X., Mullen, K., Fasel, R.: Atomically precise bottom-up fabrication of graphene nanoribbons. Nature **466**, 470–473 (2010)
6. Jia, X., Hofmann, M., Meunier, V., Sumpter, B.G., Campos-Delgado, J., Romo-Herrera, J.M., Son, H., Hsieh, Y.P., Reina, A., Kong, J., Terrones, M., Dresselhaus, M.S.: Controlled formation of sharp zigzag and armchair edges in graphitic nanoribbons. Science **323**, 1701–1705 (2009)
7. Li, X., Wang, X., Zhang, L., Lee, S., Dai, H.: Chemically derived, ultrasmooth graphene nanoribbon semiconductors. Science **319**, 1229–1232 (2008)
8. Lu, J., Yeo, P.S.E., Gan, C.K., Wu, P., Loh, K.P.: Transforming C60 molecules into graphene quantum dots. Nat. Nanotechnol. **6**, 247–252 (2011)
9. Stoller, M.D., Park, S., Zhu, Y., An, J., Ruoff, R.S.: Graphene-based ultracapacitors. Nano Lett. **8**, 3498–3502 (2008)
10. Orlita, M., Faugeras, C., Plochocka, P., Neugebauer, P., Martinez, G., Maude, D.K., Barra, A. L., Sprinkle, M., Berger, C., de Heer, W.A., Potemski, M.: Approaching the Dirac point in high-mobility multilayer epitaxial graphene. Phys. Rev. Lett. **101**, 267601–267604 (2008)
11. Nair, R.R., Blake, P., Grigorenko, A.N., Novoselov, K.S., Booth, T.J., Stauber, T., Peres, N. M., Geim, A.K.: Fine structure constant defines visual transparency of graphene. Science **320**, 1308 (2008)
12. Balandin, A.A., Ghosh, S., Bao, W., Calizo, I., Teweldebrhan, D., Miao, F., Lau, C.N.: Superior thermal conductivity of single-layer graphene. Nano Lett. **8**, 902–907 (2008)
13. Lee, C., Wei, X., Kysar, J.W., Hone, J.: Measurement of the elastic properties and intrinsic strength of monolayer graphene. Science **321**, 385–388 (2008)
14. Novoselov, K.S., Jiang, Z., Zhang, Y., Morozov, S.V., Stormer, H.L., Zeitler, U., Maan, J.C., Boebinger, G.S., Kim, P., Geim, A.K.: Room-temperature quantum Hall effect in graphene. Science **315**, 1379 (2007)
15. Pumera, M.: Electrochemistry of graphene: new horizons for sensing and energy storage. Chem. Rec. **9**, 211–223 (2009)
16. Novoselov, K.S., Jiang, D., Schedin, F., Booth, T.J., Khotkevich, V.V., Morozov, S.V., Geim, A.K.: Two-dimensional atomic crystals. Proc. Natl. Acad. Sci. U.S.A. **102**, 10451–10453 (2005)
17. Hertel, S., Waldmann, D., Jobst, J., Albert, A., Albrecht, M., Reshanov, S., Schoner, A., Krieger, M., Weber, H.B.: Tailoring the graphene/silicon carbide interface for monolithic wafer-scale electronics. Nat. Commun. **3**, 957 (2012)
18. Berger, C., Song, Z., Li, X., Wu, X., Brown, N., Naud, C., Mayou, D., Li, T., Hass, J., Marchenkov, A.N., Conrad, E.H., First, P.N., de Heer, W.A.: Electronic confinement and coherence in patterned epitaxial graphene. Science **312**, 1191–1196 (2006)
19. Gomez De Arco, L., Zhang, Y., Schlenker, C.W., Ryu, K., Thompson, M.E., Zhou, C.: Continuous, highly flexible, and transparent graphene films by chemical vapor deposition for organic photovoltaics. ACS Nano **4**, 2865–2873 (2010)

20. Wang, Y., Zheng, Y., Xu, X.F., Dubuisson, E., Bao, Q.L., Lu, J., Loh, K.P.: Electrochemical delamination of CVD-grown graphene film: toward the recyclable use of copper catalyst. ACS Nano **5**, 9927–9933 (2011)
21. Ismach, A., Druzgalski, C., Penwell, S., Schwartzberg, A., Zheng, M., Javey, A., Bokor, J., Zhang, Y.: Direct chemical vapor deposition of graphene on dielectric surfaces. Nano Lett. **10**, 1542–1548 (2010)
22. Sun, Z., Yan, Z., Yao, J., Beitler, E., Zhu, Y., Tour, J.M.: Growth of graphene from solid carbon sources. Nature **468**, 549–552 (2010)
23. Li, X., Cai, W., An, J., Kim, S., Nah, J., Yang, D., Piner, R., Velamakanni, A., Jung, I., Tutuc, E., Banerjee, S.K., Colombo, L., Ruoff, R.S.: Large-area synthesis of high-quality and uniform graphene films on copper foils. Science **324**, 1312–1314 (2009)
24. Hummers, W.S., Offeman, R.E.: Preparation of graphitic oxide. J. Am. Chem. Soc. **80**, 1339 (1958)
25. Stankovich, S., Dikin, D.A., Piner, R.D., Kohlhaas, K.A., Kleinhammes, A., Jia, Y., Wu, Y., Nguyen, S.T., Ruoff, R.S.: Synthesis of graphene-based nanosheets via chemical reduction of exfoliated graphite oxide. Carbon **45**, 1558–1565 (2007)
26. Gan, S., Zhong, L., Wu, T., Han, D., Zhang, J., Ulstrup, J., Chi, Q., Niu, L.: Spontaneous and fast growth of large-area graphene nanofilms facilitated by oil/water interfaces. Adv. Mater. **24**, 3958–3964 (2012)
27. Li, D., Muller, M.B., Gilje, S., Kaner, R.B., Wallace, G.G.: Processable aqueous dispersions of graphene nanosheets. Nat. Nanotechnol. **3**, 101–105 (2008)
28. Jiao, L., Zhang, L., Wang, X., Diankov, G., Dai, H.: Narrow graphene nanoribbons from carbon nanotubes. Nature **458**, 877–880 (2009)
29. Kosynkin, D.V., Higginbotham, A.L., Sinitskii, A., Lomeda, J.R., Dimiev, A., Price, B.K., Tour, J.M.: Longitudinal unzipping of carbon nanotubes to form graphene nanoribbons. Nature **458**, 872–876 (2009)
30. Dreyer, D.R., Park, S., Bielawski, C.W., Ruoff, R.S.: The chemistry of graphene oxide. Chem. Soc. Rev. **39**, 228–240 (2010)
31. Zhu, Y., Murali, S., Cai, W., Li, X., Suk, J.W., Potts, J.R., Ruoff, R.S.: Graphene and graphene oxide: synthesis, properties, and applications. Adv. Mater. **22**, 3906–3924 (2010)
32. Wei, W., Qu, X.: Extraordinary physical properties of functionalized graphene. Small **8**, 2138–2151 (2012)
33. Rao, C.N.R., Biswas, K., Subrahmanyam, K.S., Govindaraj, A.: Graphene, the new nanocarbon. J. Mater. Chem. **19**, 2457–2469 (2009)
34. Castro Neto, A.H., Peres, N.M.R., Novoselov, K.S., Geim, A.K.: The electronic properties of graphene. Rev. Mod. Phys. **81**, 109–162 (2009)
35. Allen, M.J., Tung, V.C., Kaner, R.B.: Honeycomb carbon: a review of graphene. Chem. Rev. **110**, 132–145 (2010)
36. Rao, C.N., Sood, A.K., Subrahmanyam, K.S., Govindaraj, A.: Graphene: the new two-dimensional nanomaterial. Angew. Chem. Int. Ed. **48**, 7752–7777 (2009)
37. Huang, X., Qi, X., Boey, F., Zhang, H.: Graphene-based composites. Chem. Soc. Rev. **41**, 666–686 (2012)
38. Compton, O.C., Nguyen, S.T.: Graphene oxide, highly reduced graphene oxide, and graphene: versatile building blocks for carbon-based materials. Small **6**, 711–723 (2010)
39. Williams, G., Seger, B., Kamat, P.V.: TiO_2-graphene nanocomposites. UV-assisted photocatalytic reduction of graphene oxide. ACS Nano **2**, 1487–1491 (2008)
40. Muszynski, R., Seger, B., Kamat, P.V.: Decorating graphene sheets with gold nanoparticles. J. Phys. Chem. C **112**, 5263–5266 (2008)
41. Carara, S., Batista, R., Chacham, H.: Modifications in graphene electron states due to a deposited lattice of Au nanoparticles: Density functional calculations. Phys. Rev. B **80**, 115435–115437 (2009)
42. Huang, X., Zhou, X., Wu, S., Wei, Y., Qi, X., Zhang, J., Boey, F., Zhang, H.: Reduced graphene oxide-templated photochemical synthesis and in situ assembly of Au nanodots to orderly patterned Au nanodot chains. Small **6**, 513–516 (2010)

43. Wang, S., Goh, B.M., Manga, K.K., Bao, Q.L., Yang, P., Loh, K.P.: Graphene as atomic template and structural scaffold in the synthesis of graphene-organic hybrid wire with photovoltaic properties. ACS Nano **4**, 6180–6186 (2010)

44. Backes, C., Hauke, F., Hirsch, A.: The potential of perylene bisimide derivatives for the solubilization of carbon nanotubes and graphene. Adv. Mater. **23**, 2588–2601 (2011)

45. Kozhemyakina, N.V., Englert, J.M., Yang, G., Spiecker, E., Schmidt, C.D., Hauke, F., Hirsch, A.: Non-covalent chemistry of graphene: electronic communication with dendronized perylene bisimides. Adv. Mater. **22**, 5483–5487 (2010)

46. Englert, J.M., Röhrl, J., Schmidt, C.D., Graupner, R., Hundhausen, M., Hauke, F., Hirsch, A.: Soluble graphene: generation of aqueous graphene solutions aided by a perylenebisimide-based bolaamphiphile. Adv. Mater. **21**, 4265–4269 (2009)

47. Su, Q., Pang, S., Alijani, V., Li, C., Feng, X., Müllen, K.: Composites of graphene with large aromatic molecules. Adv. Mater. **21**, 3191–3195 (2009)

48. Xu, Y., Liu, Z., Zhang, X., Wang, Y., Tian, J., Huang, Y., Ma, Y., Zhang, X., Chen, Y.: A graphene hybrid material covalently functionalized with porphyrin: synthesis and optical limiting property. Adv. Mater. **21**, 1275–1279 (2009)

49. Englert, J.M., Dotzer, C., Yang, G., Schmid, M., Papp, C., Gottfried, J.M., Steinruck, H.P., Spiecker, E., Hauke, F., Hirsch, A.: Covalent bulk functionalization of graphene. Nat. Chem. **3**, 279–286 (2011)

50. Englert, J.M., Rohrl, J., Schmidt, C.D., Graupner, R., Hundhausen, M., Hauke, F., Hirsch, A.: Soluble graphene: generation of aqueous graphene solutions aided by a perylenebisimide-based bolaamphiphile. Adv. Mater. **21**, 4265–4269 (2009)

51. Kovtyukhova, N.I., Ollivier, P.J., Martin, B.R., Mallouk, T.E., Chizhik, S.A., Buzaneva, E.V., Gorchinskiy, A.D.: Layer-by-layer assembly of ultrathin composite films from micron-sized graphite oxide sheets and polycations. Chem. Mater. **11**, 771–778 (1999)

52. Kulkarni, D.D., Choi, I., Singamaneni, S.S., Tsukruk, V.V.: Graphene oxide–polyelectrolyte nanomembranes. ACS Nano **4**, 4667–4676 (2010)

53. Park, S., Dikin, D.A., Nguyen, S.T., Ruoff, R.S.: Graphene oxide sheets chemically cross-linked by polyallylamine. J. Phys. Chem. C **113**, 15801–15804 (2009)

54. Yang, H., Zhang, Q., Shan, C., Li, F., Han, D., Niu, L.: Stable, conductive supramolecular composite of graphene sheets with conjugated polyelectrolyte. Langmuir **26**, 6708–6712 (2010)

55. Zhuang, X.D., Chen, Y., Liu, G., Li, P.P., Zhu, C.X., Kang, E.T., Noeh, K.G., Zhang, B., Zhu, J.H., Li, Y.X.: Conjugated-polymer-functionalized graphene oxide: synthesis and nonvolatile rewritable memory effect. Adv. Mater. **22**, 1731–1735 (2010)

56. Xu, Y.X., Wu, Q.O., Sun, Y.Q., Bai, H., Shi, G.Q.: Three-dimensional self-assembly of graphene oxide and DNA into multifunctional hydrogels. ACS Nano **4**, 7358–7362 (2010)

57. Han, T.H., Lee, W.J., Lee, D.H., Kim, J.E., Choi, E.Y., Kim, S.O.: Peptide/graphene hybrid assembly into core/shell nanowires. Adv. Mater. **22**, 2060–2064 (2010)

58. Laaksonen, P., Kainlauri, M., Laaksonen, T., Shchepetov, A., Jiang, H., Ahopelto, J., Linder, M.B.: Interfacial engineering by proteins: exfoliation and functionalization of graphene by hydrophobins. Angew. Chem. Int. Ed. **49**, 4946–4949 (2010)

59. Liu, J., Fu, S., Yuan, B., Li, Y., Deng, Z.: Toward a universal "adhesive nanosheet" for the assembly of multiple nanoparticles based on a protein-induced reduction decoration of graphene oxide. J. Am. Chem. Soc. **132**, 7279–7281 (2010)

60. Cui, Y., Kim, S.N., Jones, S.E., Wissler, L.L., Naik, R.R., McAlpine, M.C.: Chemical functionalization of graphene enabled by phage displayed peptides. Nano Lett. **10**, 4559–4565 (2010)

61. Yun, J.M., Kim, K.N., Kim, J.Y., Shin, D.O., Lee, W.J., Lee, S.H., Lieberman, M., Kim, S.O.: DNA origami nanopatterning on chemically modified graphene. Angew. Chem. Int. Ed. **51**, 912–915 (2012)

62. Zacharia, R., Ulbricht, H., Hertel, T.: Interlayer cohesive energy of graphite from thermal desorption of polyaromatic hydrocarbons. Phys. Rev. B **69**, 155406 (2004)

63. Wan, X.J., Huang, Y., Chen, Y.S.: Focusing on energy and optoelectronic applications: a journey for graphene and graphene oxide at large scale. Acc. Chem. Res. **45**, 598–607 (2012)

64. Artiles, M.S., Rout, C.S., Fisher, T.S.: Graphene-based hybrid materials and devices for biosensing. Adv. Drug Deliv. Rev. **63**, 1352–1360 (2011)
65. Yang, W., Ratinac, K.R., Ringer, S.P., Thordarson, P., Gooding, J.J., Braet, F.: Carbon nanomaterials in biosensors: should you use nanotubes or graphene? Angew. Chem. Int. Ed. **49**, 2114–2138 (2010)
66. Kuila, T., Bose, S., Khanra, P., Mishra, A.K., Kim, N.H., Lee, J.H.: Recent advances in graphene-based biosensors. Biosens. Bioelectron. **26**, 4637–4648 (2011)
67. Chen, D., Feng, H., Li, J.: Graphene oxide: preparation, functionalization, and electrochemical applications. Chem. Rev. **112**, 6027–6053 (2012)
68. Chen, Y., Zhang, B., Liu, G., Zhuang, X., Kang, E.T.: Graphene and its derivatives: switching ON and OFF. Chem. Soc. Rev. **41**, 4688–4707 (2012)
69. Wu, J.S., Pisula, W., Mullen, K.: Graphenes as potential material for electronics. Chem. Rev. **107**, 718–747 (2007)
70. Shao, Y., Wang, J., Wu, H., Liu, J., Aksay, I.A., Lin, Y.: Graphene based electrochemical sensors and biosensors: a review. Electroanalysis **22**, 1027–1036 (2010)
71. Pumera, M.: Graphene-based nanomaterials for energy storage. Energy Environ. Sci. **4**, 668–674 (2011)
72. Guo, S., Dong, S.: Graphene and its derivative-based sensing materials for analytical devices. J. Mater. Chem. **21**, 18503–18516 (2011)
73. Yao, J., Sun, Y., Yang, M., Duan, Y.: Chemistry, physics and biology of graphene-based nanomaterials: new horizons for sensing, imaging and medicine. J. Mater. Chem. **22**, 14313–14329 (2012)
74. Pumera, M.: Graphene in biosensing. Mater. Today **14**, 308–315 (2011)
75. Kochmann, S., Hirsch, T., Wolfbeis, O.S.: Graphenes in chemical sensors and biosensors. TrAC Trends Anal. Chem. **39**, 87–113 (2012)
76. Pumera, M., Ambrosi, A., Bonanni, A., Chng, E.L.K., Poh, H.L.: Graphene for electrochemical sensing and biosensing. TrAC Trends Anal. Chem. **29**, 954–965 (2010)
77. Pumera, M.: Graphene-based nanomaterials for energy storage. Energy Environ. Sci. **4**, 668–674 (2011)
78. Zheng, M., Jagota, A., Strano, M.S., Santos, A.P., Barone, P., Chou, S.G., Diner, B.A., Dresselhaus, M.S., McLean, R.S., Onoa, G.B., Samsonidze, G.G., Semke, E.D., Usrey, M., Walls, D.J.: Structure-based carbon nanotube sorting by sequence-dependent DNA assembly. Science **302**, 1545–1548 (2003)
79. Patil, A.J., Vickery, J.L., Scott, T.B., Mann, S.: Aqueous stabilization and self-assembly of graphene sheets into layered bio-nanocomposites using DNA. Adv. Mater. **21**, 3159–3164 (2009)
80. Liu, J., Li, Y., Li, Y., Li, J., Deng, Z.: Noncovalent DNA decorations of graphene oxide and reduced graphene oxide toward water-soluble metal–carbon hybrid nanostructures via self-assembly. J. Mater. Chem. **20**, 900–906 (2010)
81. Liu, F., Choi, J.Y., Seo, T.S.: DNA mediated water-dispersible graphene fabrication and gold nanoparticle-graphene hybrid. Chem. Commun. **46**, 2844–2846 (2010)
82. Qu, K., Ren, J., Qu, X.: pH-responsive, DNA-directed reversible assembly of graphene oxide. Mol. BioSyst. **7**, 2681–2687 (2011)
83. Choi, B.G., Yang, M.H., Park, T.J., Huh, Y.S., Lee, S.Y., Hong, W.H., Park, H.: Programmable peptide-directed two dimensional arrays of various nanoparticles on graphene sheets. Nanoscale **3**, 3208–3213 (2011)
84. Lu, F., Zhang, S., Gao, H., Jia, H., Zheng, L.: Protein-decorated reduced oxide graphene composite and its application to SERS. ACS Appl. Mater. Interfaces **4**, 3278–3284 (2012)
85. Laaksonen, P., Walther, A., Malho, J.M., Kainlauri, M., Ikkala, O., Linder, M.B.: Genetic engineering of biomimetic nanocomposites: diblock proteins, graphene, and nanofibrillated cellulose. Angew. Chem. Int. Ed. **50**, 8688–8691 (2011)

Chapter 2
Graphene for DNA Biosensing

Abstract Graphene (or GO) is an excellent candidate for biomolecules anchoring and detection due to its large surface area (up to 2,630 m^2/g) and unique sp^2 (sp^2/sp^3)-bonded network. According to the binding affinity difference between single-stranded DNA (ssDNA) and double-stranded DNA (dsDNA) to graphene sheet, GO has been successfully adopted as a platform to discriminate DNA sequences. Fluorescent, electrochemical, electrical, surface-enhanced Raman scattering (SERS) and other methods have been utilized to achieve the sensitive, selective, and accurate DNA recognition. Both theoretical and experimental results illustrate that ssDNA sequences are adsorbed on the surface of graphene sheet with all nucleobases lying nearly flat. DNA or RNA sequencing through graphene nanopore, nanogap, and nanoribbon has also attracted much interest because it is a label-free, amplification-free, and single-molecule approach that can be scaled up for high-throughput DNA or RNA analysis. Meanwhile, miRNA detection is achieved by forming DNA–miRNA duplex helixes, and strong emission is observed due to the poor interaction between the helix and GO.

Keywords DNA sequencing · miRNA detection · Fluorescent spectroscopy · Electrochemical method · Electrical method · Graphene nanopore · Graphene nanogap · Graphene nanoribbon

2.1 Investigation of DNA and Graphene Binding Interaction

The large surface area (up to 2,630 m^2/g) and unique sp^2 (sp^2/sp^3)-bonded network make graphene (GO) an excellent candidate for biomolecules anchoring and detection. Taking DNA for the first example, various strategies have been adopted to nucleic acid sequence recognition [1–10]. To better illustrate the interaction, how nucleobases interact with graphene should be addressed, which may be inspired by the interaction of nucleobases with CNTs [11–13] and highly oriented pyrolytic graphite (HOPG) [14].

Single-stranded DNA (ssDNA) strand is unwound double-stranded helix (dsDNA), which is held together by hydrogen bonds between the bases linked to two ssDNA strands. It consists of one long polymer of simple units called nucleotides, with backbones made of alternating sugars (deoxyribose) and phosphate groups, with the nucleobases (G, T, A, C abbreviated for guanine, adenine, thymine, cytosine, respectively) attached to the sugars. Employing various strategies and techniques, researchers tried to illustrate the interactions between DNA and graphene. Molecular dynamics (MD) simulations of ssDNA and dsDNA anchored via an aliphatic linker to a graphene surface were performed in order to investigate the role of the surface charge density in the structure and orientation of attached DNA [15]. A considerable difference in the behavior of the ssDNA and dsDNA anchored to graphene layer was observed. The rigid dsDNA kept its geometry close to the canonical B-DNA form and interacted with graphene surface by the nearest base pairs. The flexible ssDNA intended to maximize the attraction to graphene surface by exploiting more bases for the interaction, namely 'lying' on the surface with bases as the anchor. This interaction was also investigated by isothermal titration calorimetry (ITC) [16]. ITC is an ultrasensitive tool to study binding interactions in aqueous solutions. Experimental results showed the relative interaction energies of nucleobases decreasing in the order of G > A > T > C, with the position of T and C interchangeable. Theoretical calculations including van der Waals interaction and solvation energies gave the similar trend G > A $\sim$ T > C. Using first-principles investigation, the calculated binding energy was found to be G > A $\sim$ T $\sim$ C > U, where U represents uracil in RNA [17]. And the stabilizing factor in the interaction between the base molecules and graphene sheet is dominated by the molecular polarizability that allows a weakly attractive dispersion force to be induced between them. These interaction magnitudes are similar to those found between bases with SWCNTs [18].

Based on the binding energy difference, the anchoring of DNA sequences on graphene may present as different morphologies. Recently, Postma and coworker demonstrated that DNA assembled into two distinct patterns, small spherical particles and elongated networks, on graphene surface [19]. According to the AFM results of poly-A, C, T, G assembling on graphene (Fig. 2.1a), they found that these common mechanisms, e.g., hydrogen bonding, base stacking, electrostatic, van der Waals, and hydrophobic interactions, could not explain these observations. Alternatively, they concluded a different mechanism (Fig. 2.1b), where E_b and E_g represented the interbase binding energy and base–graphene binding energy, respectively. Hence, they argued that the root cause of DNA assembling in distinct patterns is a crossover in the balance between the two energies, i.e., $E_b > E_g$ or $E_b < E_g$. When $E_b > E_g$, meaning that the interbase coupling is more energetically favorable than binding to graphene, the DNA (A, C) assembled into spheres to maximize E_b (Fig. 2.1b A). When $E_b < E_g$, meaning that the base–graphene interaction is more energetically favorable than interbase, the DNA (G, T) stretched out across graphene surface to maximize the energy and resulted in network formation (Fig. 2.1b B). This hypothesis was supported by the fact that $E_g(G) > E_g(A) \sim E_g(T) \sim E_g(C)$ and $E_b(G) \sim E_b(T) > E_b(A) \sim E_b(C)$. They also
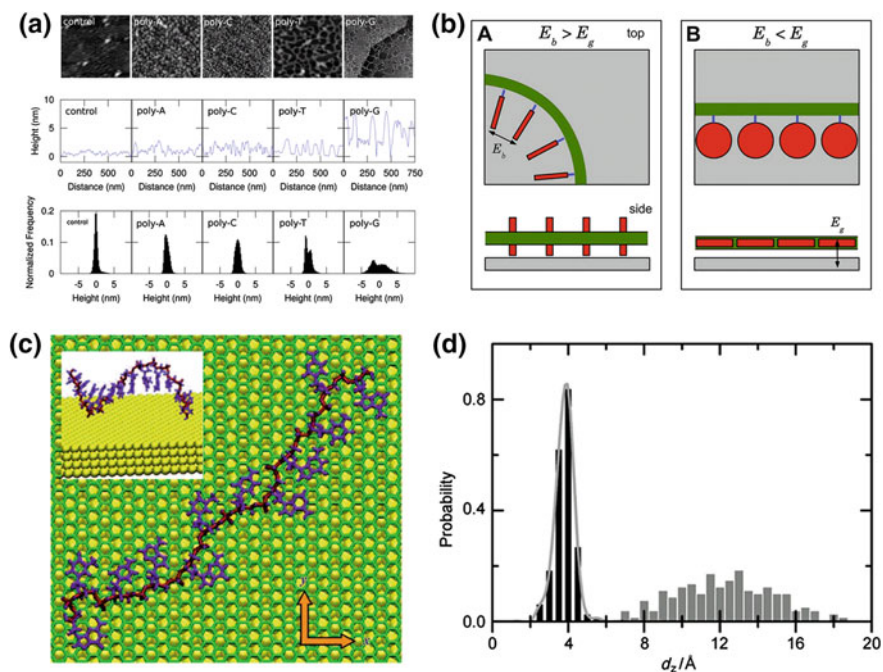
Fig. 2.1 a Atomic force micrographs of graphene with and without ssDNA, line scans, and histograms. **b** DNA assembles onto graphene (*gray*) into spheres (*A*) or networks (*B*). The nucleotides (*red*) can rotate around the link (*blue*) to the sugar phosphate backbone (*green*) to either maximize the interbase binding energy E_b (*A*) or the base–graphene binding energy E_g (*B*). Reprinted from Ref. [19]. **c** Schematic representation of an ssDNA nucleobase on the surface of the graphene-on-Au(111) material. The nucleobases and the backbone of the ssDNA are shown in *violet* and *dark red*, respectively. The graphene sheet is shown in *green*. The Au(111) surface is indicated by *yellow* spheres and sticks. The *inset* is a typical conformation of ssDNA on Au(111). **d** Probability of finding the atoms in the nucleobases of ssDNA at a distance d_z from the graphene-on-Au(111) surface (*black columns*) and the Au(111) surface (*gray columns*), respectively. Reprinted from Ref. [20] by permission of John Wiley & Sons Ltd.

estimated that the critical interbase interaction strength that separated network formation from sphere assembly was ∼0.3–0.5 eV.

Both above-mentioned theoretical and experimental results illustrate that ssDNA sequences are adsorbed on graphene sheet surface with all nucleobases lying nearly flat (Fig. 2.1c). To more specifically and directly elucidate the interaction, MD simulations were carried out [20]. A clear distance of ∼4.0 Å was observed in Fig. 2.1d (black). This distance was quite close to the van der Waals distance between a carbon atom in graphene and carbon/oxygen/nitrogen atoms, which are the main elements in nucleobases. This showed that most of the atoms in the nucleobases were directly adsorbed by graphene, which was strong enough to destroy the helical structure of ssDNA. A comparison was also carried out, in which the same ssDNA was adsorbed on Au(111) surface (Fig. 2.1d [gray]). The distance

had a wide distribution from 7.0 to ∼18.5 Å. Hence, ssDNA still retained its helical structure on the Au(111) surface (Fig. 2.1c inset) as the segment with six nucleobases in bulk water. Besides, the developed graphene-on-Au(111) composite was very stable, and the conductivity of this material was excellent, which resulted in a very high signal-to-noise ratio of the resonant currents through different nucleobases. Then, this hybrid held the potential for single-molecule DNA sequencing via AFM or STM.

Using scanning tunneling spectroscopy, Ahmed et al. [21] calculated the tunneling conductance and electronic local density of states (LDOS) for DNA nucleobases at various orientations on graphene surface and showed that the different nucleobases had significantly different LDOS peaks (fingerprints), allowing differentiation via local tunneling conductance. Besides, a plane orientation of DNA nucleobases with respect to graphene surface was the most stable state, which favored π–π stacking between the bases and aromatic carbons in graphene. This conclusion is in consistent with above-mentioned research results.

2.2 DNA Biosensing Employing Graphene Platform

Although the nucleobases–graphene binding energy is slightly different via various strategies and equipments, one might be certain that ssDNA could be adsorbed on graphene sheet surface coupling crossover of several interaction forces and employing nucleobases as the anchors. This is also the root cause that ssDNA binds more strongly to graphene than dsDNA does [19], in which nucleobases are entrapped and shielded by the phosphate–deoxyribose backbones. According to the binding affinity difference between ssDNA and dsDNA to graphene sheet, graphene (GO) has been successfully adopted as a platform to discriminate DNA sequences. Several methods, such as fluorescent, electrochemical, electrical, and SERS, have been utilized to achieve the sensitive, selective, and accurate DNA recognition.

2.2.1 Fluorescent Assay

In a typical fluorescent manner (Fig. 2.2a) [4], fluorescent dye-labeled ssDNA was adsorbed on graphene surface. Then, the fluorescence of dye-labeled ssDNA was completely quenched due to the fluorescent resonance energy transfer (FRET). In the presence of a target, the hybridization between dye-labeled ssDNA and target sequence altered the conformation of ssDNA and disturbed the binding between the dye-labeled ssDNA and graphene. This behavior might originate from the fact that DNA nucleobases matching is more energetically favorable than binding with graphene. The formed dye-labeled dsDNA left from graphene surface, resulting in the restoration of dye fluorescence. Based on the mechanism, both hairpin DNA and molecular beacon (MB) were designed for homogeneous DNA detection [5, 6].
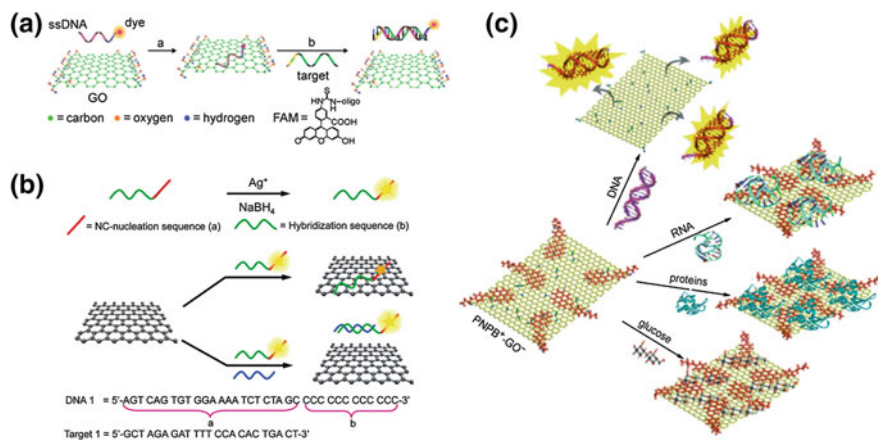
Fig. 2.2 a Schematic representation of the target-induced fluorescence change of the ssDNA–FAM–GO complex. FAM is the fluorescein-based fluorescent dye. Reprinted from Ref. [4] by permission of John Wiley & Sons Ltd. **b** Schematic representation of the preparation of silver nanoclusters on DNA scaffolds in aqueous solution and the assay for DNA detection using AgNCs-GO nanohybrid materials. Reprinted from Ref. [31] by permission of The Royal Society of Chemistry. **c** Sensing by PNP^+GO^-. DNA can complex efficiently with PNP^+ to form ionic complex PNP^+DNA^- and thus switches on the fluorescence. Other biomolecules undergo π–π stacking on GO but do not remove PNP^+ from GO, and thus, fluorescence remains quenched. Reprinted from Ref. [33] by permission from John Wiley & Sons Ltd.

dsDNA was also detected by the formation of triplex DNA with dye-labeled ssDNA [22]. As a nanoquencher, graphene shows super-quenching capacity with a wide energy transfer range, which may quench the fluorescence of different dyes simultaneously. Fan and coworkers devised a multicolor fluorescent DNA analysis manner [1], in which multiple ssDNA sequences labeled with different dyes were anchored on graphene. Hybridization to multiple DNA targets in the same solution led to fluorescence recovery of different dyes. The multicolor biosensor might also be suitable for the detection of a range of analytes.

Due to the different graphene fabrication methods, the carbon-to-oxygen (C/O) ratios in GO might differ at a large level, also the sp^3/sp^2 bonded network structure. This may have a great impact on GO's ability for fluorescence quenching of adsorbed dyes and the binding interactions to ssDNA, resulting in a broad range of DNA detection sensitivity. In fact, rGO, in which the oxygenic groups are partially or totally reduced, might not be directly used in the detection due to the strong tendency to aggregate [23]. To get a deeper insight into this, properties of GO samples with tuned C/O ratios (1.1, 1.3, 1.6, and 1.9) were fairly investigated [24]. Results showed that GO with high C/O ratio bound more strongly to ssDNA and quenched the fluorescence of organic chromophores more effectively than that with low C/O ratio. The loading amount of fluorophore-labeled ssDNA at least oxidized GO (C/O ratio = 1.9) was four times than that at GO with C/O ratio of 1.1. With the tunable chemical compositions, GO nanosheets offer a broad range of materials with

different fluorescence quenching efficiencies and binding affinity with ssDNAs, which exhibit the great potential in biological applications.

Importantly, the binding of ssDNA to graphene in solution may be influenced by other elements, such as ssDNA length, ions, pH, organic solvent, and temperature, which then contribute to the hybridization accuracy and efficiency. Experiments were carried out by Liu and coworkers to study these impacts on DNA adsorption and desorption [25]. By using dye-labeled ssDNA, they found that shorter ssDNA bound to graphene with higher kinetics and higher adsorption efficiency. Adsorption was also favored by low pH value and high ionic strength. Desorption could occur by adding the complementary DNA to form dsDNA, adding the same ssDNA to exchange, and increasing temperature. These findings are important for further understanding the interactions between DNA and graphene and optimizing DNA and graphene-based devices and sensors. On the other hand, the self-assembly of graphene in aqueous solution can be tuned with ions to form colloidal stacked graphene, which may be powerful platforms for capturing dsDNA [26, 27].

Besides taking fluorescent dye as label, FRET could also happen between quantum dots (QDs) and GO. Dong et al. [28] designed MB-modified QDs to recognize target. The strong interaction between MB and GO resulted in the fluorescence quenching of QDs. After hybridization with target, the interaction between target-bound MB and GO was weakened, leading to the restoration of QD fluorescence. Due to the ultrasmall size (composed of a few to hundred atoms), good biocompatibility, and excellent photostability, fluorescent metal nanoclusters, e.g., Au and Ag, have attracted much attention and been widely used in biological applications [29, 30]. By taking advantage of Ag nanoclusters' optical features and GO's super-quenching capacity, a kind of sensitive fluorescent DNA detection manner was proposed [31]. ssDNA consisted of hybridization sequence, which was for target detection, and nucleation sequence, which was for Ag nanocluster formation (Fig. 2.2b). The fluorescence of ssDNA–Ag nanoclusters was quenched by GO and recovered after hybridization with target sequence, which was similar to the above fluorophore-labeled detection manner. This strategy avoided the direct labeling process of probe DNA or target DNA; however, the nucleation process needs to be precisely controlled. Moreover, due to the tunable fluorescence of Ag nanoclusters, multiple and simultaneous DNA detection was achieved, which was an obvious improvement in the present study.

These labeling manners possess high sensitivity, good selectivity, etc., while at the mean time, they need DNA sequences to be previously fluorophore-labeled. Labeling step incorporated into nucleic acid assay has shortcomings of limited labeling efficiency, complex multistep analysis, and contamination to samples [32]. Eliminating the tedious labeling process, a GO–organic dye charge transfer complex was fabricated by Loh and coworkers [33]. The positively charged and fluorescent pyrene derivative, namely 4-(1-pyrenylvinyl)-N-butylpyridinium bromide (PNPB), could interact with negatively charged GO to form PNP^+GO^- complex. The fluorescence of PNP^+ was quenched due to the charge–transfer interactions between PNP^+ and GO. Negatively charged dsDNA bound to PNP^+ through ion-exchange process, resulting in the release of PNP^+-dsDNA from GO and a

fluorescence 'turn-on' manner (Fig. 2.2c). This simple, efficient ion-exchange strategy could distinguish dsDNA from other biomolecules, such as protein, RNA, glucose, and surfactants, while one issue concerning it might be the selectivity toward ssDNA, or the capability to target DNA sequence hybridization detection. Because of the different binding ability of graphene (GO) to ssDNA and dsDNA, the current concept might be extended to label-free fluorescent DNA detection.

With the aid of DNA ligase, fluorescent DNA single-nucleotide polymorphism (SNP) detection was achieved based on the quenching capacity of graphene [34]. By using in situ-generated hydroxyl radical ($^\cdot$OH), which caused DNA damage by abstracting an H atom from phosphate backbone, the interaction between ssDNA and graphene was regulated. It also probed the $^\cdot$OH-induced ssDNA damage and exhibited the potential in screening antioxidants in DNA repair and anticancer therapy [35].

2.2.2 Electrochemical Assay

Recently, there has been an increasing interest in electrochemical devices for DNA biosensing since they allow a simple, fast, and sensitive analysis without usage of expensive equipment. Among these, electrochemical impedance spectroscopy (EIS) is often used due to its truly label-free manner and high sensitivity. EIS is a powerful method to analyze the complex electrical resistance of a system and is also sensitive to surface phenomena and changes of bulk properties. Thus, in the field of biosensing, it is particularly suited to the detection of binding events and sensitive to changes in interfacial impedance upon biorecognition events occurring at the surface/electrolyte interface. In addition, it is also a valuable tool in characterizing surface modifications, e.g., on transducer devices during the immobilization procedure of recognition elements. A thorough introduction to EIS theory, experiment, and applications could be found in a book [36] and reviews concerning EIS biosensing [37–40].

Graphene's unique 2D structure and properties, such as rapid heterogeneous electron transfer, make it an excellent candidate in EIS DNA biosensing. It provides the essential elements that an electrochemical substrate needs, e.g., large surface area, various functional groups (–OH, –COOH, –C=O, epoxide, etc.), good conductivity, and high affinity for molecule binding. A review on graphene for impedimetric biosensing has been published recently [41], while at this part, we mainly focus on the comparative studies of these strategies.

Based on the unique structure of ssDNA and graphene, physical adsorption, especially π–π stacking, dominates their direct interactions between the aromatic rings of nucleobases and the hexagonal cells of graphene sheets. Both linear and hairpin DNA probes had been adsorbed on graphene. After hybridization with cDNA, an impedance 'signal-off' assay was observed due to the detachment of dsDNA from graphene surface (employing $[Fe(CN)_6]^{3-/4-}$ as the redox indicator) [3, 42]. To keep dsDNA on graphene surface and gain 'signal-on' process, covalent

immobilization of ssDNA was often adopted using graphene's own oxygenic groups, such as –COOH [43]. There are extensive nuclear magnetic resonance, infrared spectroscopic, and electron diffraction evidences for the presence of –COOH, –OH, and –C=O groups at the edge of the GO sheet, while the basal plane is covered with mostly epoxide and –OH groups [44]. Hence, it would be necessary to decorate the basal plane with –COOH for covalent binding reactions. Recently, Loh and coworkers fabricated anodized epitaxial graphene (EG) platform, which contained large amount of –COOH groups [8]. After activation by EDC and NHS, NH$_2$–ssDNA could be covalently immobilized on graphene and hybridization detection was carried out in phosphate buffer solution. Wide dynamic range and more sensitive response than π–π stacking immobilization manner were observed. However, one main obstacle for applying this strategy might be the preparation of anodized EG, which depends highly on the equipment. Our group proposed a very easy way to introduce –COOH on graphene for DNA biosensing [7]. 3,4,9,10-Perylene tetracarboxylic acid (PTCA), bearing π-conjugated perylene ring and carboxylic acid groups, was used to decorate graphene. Based on the π–π stacking and hydrophobic interactions between the perylene ring and the basal plane of graphene, PTCA molecules separated graphene sheets efficiently and decorated them with plenty of –COOH. This method resolved the graphene aggregation problem, and the resulting hybrids dispersed well in aqueous solution. After activation, NH$_2$–ssDNA was covalently immobilized on the hybrid, which presented as 'lying' structure (Fig. 2.3a). Hybridization to cDNA induced the 'lying' ssDNA to 'standing' dsDNA, which caused the graphene interfacial property changes, e.g., negative charge and conformation. Employing [Fe(CN)$_6$]$^{3-/4-}$, a 'turn-on' impedance signal was observed with the increment of cDNA concentration (Fig. 2.3b). In a recent research, we optimized the experimental procedure [9]. ssDNA was designed to consist of two parts, the immobilization sequence and the probe sequence. The immobilization part was for anchoring ssDNA and dsDNA on graphene, which eliminated the previous graphene decoration steps and simplified the procedure efficiently. The hybridization between probe and target induced the formation of dsDNA, which stood on graphene surface due to the anchoring by the immobilization sequence.

Instead of occupying the π–π stacking between DNA nucleobases and graphene, an optional way might be through the negatively charged phosphate backbones of DNA. In this manner, the nucleobases are free for efficient hybridization. Onto the PTCA-modified graphene surface, Au NPs were deposited using amine-terminated ionic liquid (NH$_2$-IL) as the reductant and capping agent [45]. Au NPs with mean diameter of 3 nm dispersed uniformly on graphene, and their outer layer was positively charged imidazole termini, which increased the surface area of graphene and provided large amount of attachment points for ssDNA immobilization. Based on the electrostatic interaction and adsorption effect, ssDNA was conveniently immobilized and its nucleobases were free to hybridize with cDNA. The HIV-1 pol gene sequences were satisfactorily detected with low detection limit of 3.4×10^{-14} M. In a similar manner, we designed a positively charged perylene derivative PDI, *N,N*-bis-(1-aminopropyl-3-propylimidazol salt)-3,4,9,10-perylene
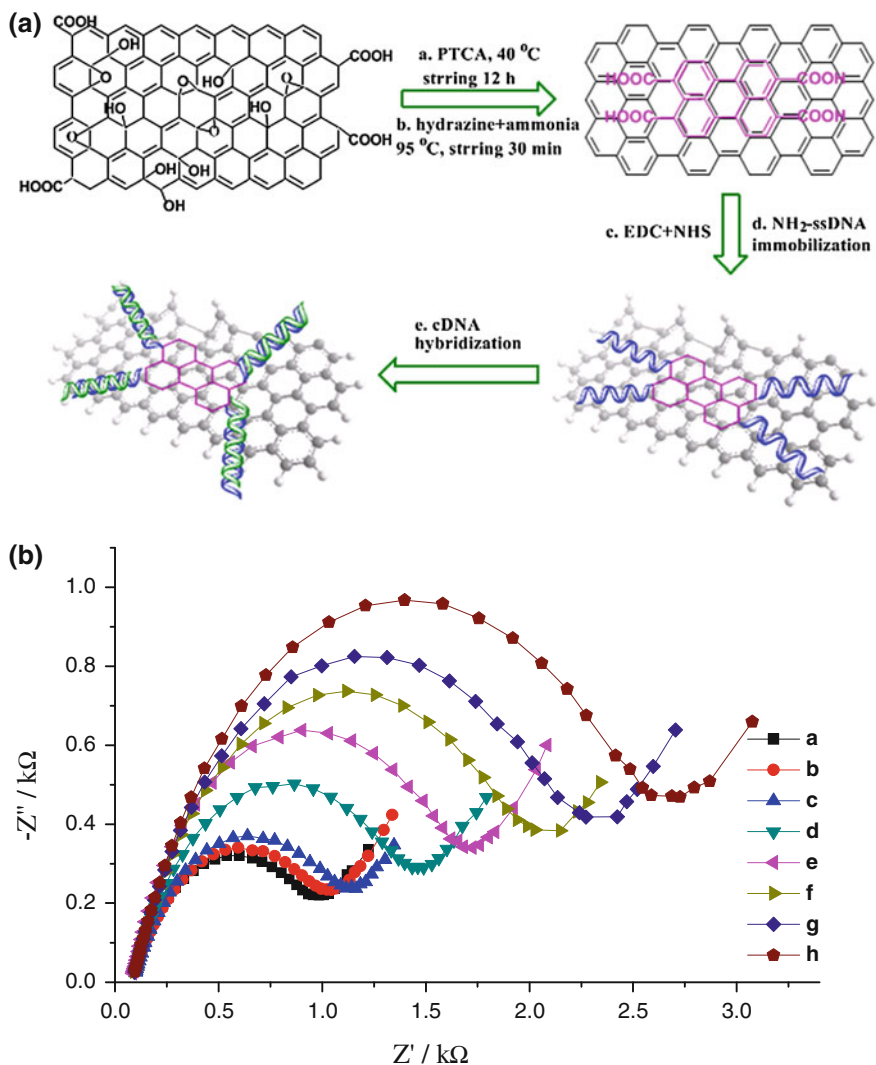
Fig. 2.3 a Schematic representation of graphene functionalization with PTCA, ssDNA immobilization, and hybridization. **b** Nyquist diagrams recorded at ssDNA immobilized PTCA/graphene/GCE (*a*) and after hybridization with its complementary human immunodeficiency virus 1 (HIV-1) pol gene sequences of different concentrations from 1.0×10^{-12} to 1.0×10^{-6} M (b–h). Reprinted from Ref. [7] by permission form The Royal Society of Chemistry

tetracarboxylic acid diimide, to decorate graphene [46]. UV–vis and TEM characterizations illustrated that PDIs self-assembled into pentamer or hexamer, which were uniformly scattered on graphene sheets and beneficial for electrostatic ssDNA immobilization. After hybridization, the formed dsDNA stayed on PDI/graphene, causing an increase of R_{et} value. The 'signal-on' process exhibited high sensitivity

and reproducibility. More importantly, the rational design, tailoring, and decoration of graphene endow it with desired properties (dispersive, structural, photoelectrical, and conductive, etc.), which may hold great potential applications in electronics, photovoltaics, and nanodevices. Another impedimetric DNA detection based on reduced GO-modified electrode could be found in Ref. [47].

Another electrochemical label-free DNA detection method is through the direct oxidation of the four nucleobases, without the need of hybridization or labeling molecules. At some point, this strategy is the simplest, while most electrode materials' narrow potential window, high background or slow electron transfer rate restrict their applications [48, 49]. A comparative study of different carbon electrodes for DNA oxidation is illustrated in Ref. [50]. Recently, a nanocarbon film electrode with wide potential window and high activity was successfully used for DNA SNP detection [51]. As an alternative, graphene also fits the requirements well. For instance, Zhou et al. [52] used chemically reduced graphene oxide (CR-GO)-modified GCE for direct nucleobase detection. Comparing with GCE or graphite-modified GCE, negatively moved oxidation potentials and enhanced peak currents were obtained at graphene/GCE. Besides, the quantitative SNP detection at physiological pH was well accomplished. Meanwhile, Pumera and coworkers showed that the oxidation signals of four nucleobases at stacked graphene nanofibers were two to four times higher than those on CNT-based electrode, also higher than edge-plane pyrolytic graphite, glassy carbon, or graphite microparticle-based electrodes [53]. Also, anodized epitaxial graphene was found to exhibit superior electroanalytical performances for nucleobase oxidation compared to carbon electrodes, such as boron-doped diamond, carbon nanotubes, and glassy carbon [54]. Much progress was achieved by Akhavan et al. [55] by using reduced graphene nanowalls (RGNWs), which had a very large surface area and edge-plane defects. To the electrochemical detection of DNA bases (as the free form or in ssDNA and dsDNA), the RGNW electrode exhibited higher current and lower anodic potential as compared to other electrodes (Fig. 2.4a). The high electrochemical activity of the RGNWs could be assigned to better electron exchange between the four bases and the edge-plane-like defective sites of the sheets as active sites for oxidation of DNA bases. The linear dynamic detection range for dsDNA at RGNWs was from 0.1 fM to 10 mM (detection limit to be 9.4 zM, $\sim$5 dsDNA/mL), while it was from 2.0 pM to <10 mM (detection limit to be 5.4 fM) at reduced graphene nanosheets (RGNSs). The RGNWs was also efficient in label-free detection of SNPs of 20 zM oligonucleotides ($\sim$10 DNA/mL) with a specific sequence (Fig. 2.4b). This is the first report on electrochemical sensing of nucleic acids at single-DNA levels.

Based on the direct oxidation of guanines, another aspect would be the detection of DNA damage. A graphene-ionic liquid-Nafion/(horseradish peroxidase (HRP)/dsDNA)$_n$ film was firstly constructed on pyrolytic graphite electrode. DNA damage was induced by incubating the modified electrode in acrylamide (AA) or AA + H_2O_2 solution at 37 °C. AA or its epoxide, glycidamide, could form adduct with dsDNA, which disrupted the double helix structure and made guanines exposed. The DPV signals of guanines represented the degree of dsDNA damage [56].
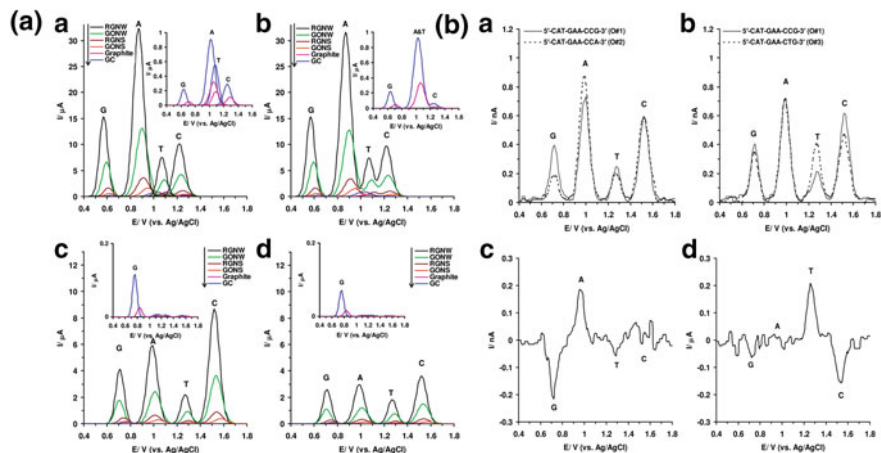
Fig. 2.4 **a** Differential pulse voltammetry (*DPV*) profiles of the RGNW, GONW, RGNS, and GONS electrodes as compared to the graphite and GC electrodes for the detection of (*a*) the four free bases of DNA (*G*, *A*, *T*, and *C*) separately, (*b*) an equimolar mixture of *G*, *A*, *T*, and *C*, (*c*) ssDNA, and (*d*) dsDNA, with a concentration of 0.1 μM for all of the species applied in (*a*)–(*d*) in 0.1 M PBS as supporting electrolyte at pH 7.0. **b** Detection of SNPs of oligonucleotides by using DPVs of the single-base mismatched oligonucleotides obtained through (*a*) G → A mutation (O#2) and (*b*) C → T mutation (O#3), as compared to the base oligonucleotide (O#1) at the surface of the RGNW electrode. (*c*), (*d*) present subtraction of the DPVs shown in (*a*) and (*b*), respectively. Concentration of the different oligonucleotides was 20 zM in 0.1 mM PBS at pH 7.0. Reprinted with permission from Ref. [55] Copyright 2012 American Chemical Society

As mentioned above, plenty of oxygenic groups, e.g., hydroxyl, carboxy, epoxide, carbonyl, aldehyde, peroxide, ether, and ester, present at the basal planes or edges of GO sheets. Using electrochemical methods, GO can be reduced with an irreversibly cathodic peak at negative potentials [57, 58]. According to the researches [59, 60], the hydroxy is not able to be further electrochemically reduced. The reduction of epoxide, aldehyde, and peroxide takes place at potentials around −0.9 to −1.5 V (vs. Ag/AgCl) in neutral buffers. And the reduction of carbonyl, carboxy, and ester groups takes place at potentials around −2.1 V in strongly acidic media. Hence, based on the electrochemical reduction signal, it is feasible to selectively reduce oxygenic groups and subsequently quantify the amount, which makes the composition and property of GO tunable. More importantly, the inherent redox activity can be utilized in electrochemical investigation. Recently, GO nanoplatelets (size value ∼37 nm) were employed as the electrochemical label for DNA analysis [61]. According to the different binding ability of GO nanoplatelets to fully matched dsDNA, one-base-mismatched dsDNA, and unhybridized sequences, GO reduction signals with varying intensities were observed. This allowed the discrimination of SNPs related to Alzheimer's disease. Though the electrochemical reduction mechanism of GO is not yet thoroughly investigated, one might be certain that hydrogen ions participate in the reduction process. It may get a hint from the thermal reduction of GO in deionized water [62].

Differential pulse voltammetry (DPV) also represents a sensitive method for DNA detection based on the electrochemical signals of intercalators or tags, such as adriamycin [63], daunomycin [64, 65], methylene blue [66], and Au [67]. Without these intercalators or tags, an ultrasensitive and selective DNA detection by using stand-displacement DNA polymerization and parallel-motif DNA triplex system as dual amplifications was realized on ferrocene-appended poly(ethyleneimine)/graphene–mesoporous silica–gold nanoparticle hybrids (Fc-PEI/GSGHs)$_n$ [68]. The detection limit reached as low as 10 fM, and it discriminated the SNP.

2.2.3 Electrical Assay

Above, we mentioned the optical and electrochemical DNA detection employing graphene. As an attractive alternative, electrical detection also possesses real-time, label-free, sensitive, and rapid measurement qualities [69–71]. Graphene's large surface area, biocompatibility, and exceptional and unique electronic properties, such as ultrahigh mobility, low charge scattering, and ambipolar field effect, might make it superior than CNTs for field-effect transistors (FETs) [69]. In FETs, ssDNA fragments acted as negative potential gating agents, resulting in an increase of the hole density in graphene layers, to be 1.8×10^{12} cm^{-2} [71]. This increased density was consistent with the Raman frequency shifts in the G peak and 2D band positions and the corresponding changes in the G peak full width at half maximum. Ab initio calculations using density functional theory rule out significant charge transfer or modification of the graphene band structure in the presence of ssDNA fragments. The sensitivity of electrical DNA detection strongly depends on the size and shape of graphene, wrinkles on graphene surface, and the oxidation degree of graphene. Using CVD-grown, large-sized graphene films, Dong et al. [69] constructed FETs for DNA hybridization with single-base specificity. The $V_{g,min}$ was significantly left-shifted with the addition of probe DNA sequences, suggesting that DNA molecules *n*-doped the graphene film. The left shift in $V_{g,min}$ increased with the increasing concentration of the complementary DNA, especially in the 0.01–10 nM range. As for the one-base mismatched DNA detection, left shift in $V_{g,min}$ was less noticeable. Results illustrated that $V_{g,min}$ shift appeared to be a good indicator for DNA detection with a concentration as low as 0.01 nM and for detection of single-base mutation, which is thought as the key to the diagnosis of genetic diseases and realization of personalized medicine. Furthermore, adding nanoparticles, such as Au and Pt, could increase the loading amount of ssDNA and extend dynamic detection range [69, 72].

Usually, the CVD-grown graphene is compromised by high cost and suffers from alignment and reproducibility issues when integrated into prefabricated circuitry. Chemically modified graphenes with adjustable surface chemistry have offered competitive results in biological FETs [72–74]. In the label-free detection, one of the pressing problems was the response to non-specific binding. To mitigate the non-specific effect, Stine and coworkers designed rGO-based bioFET devices,
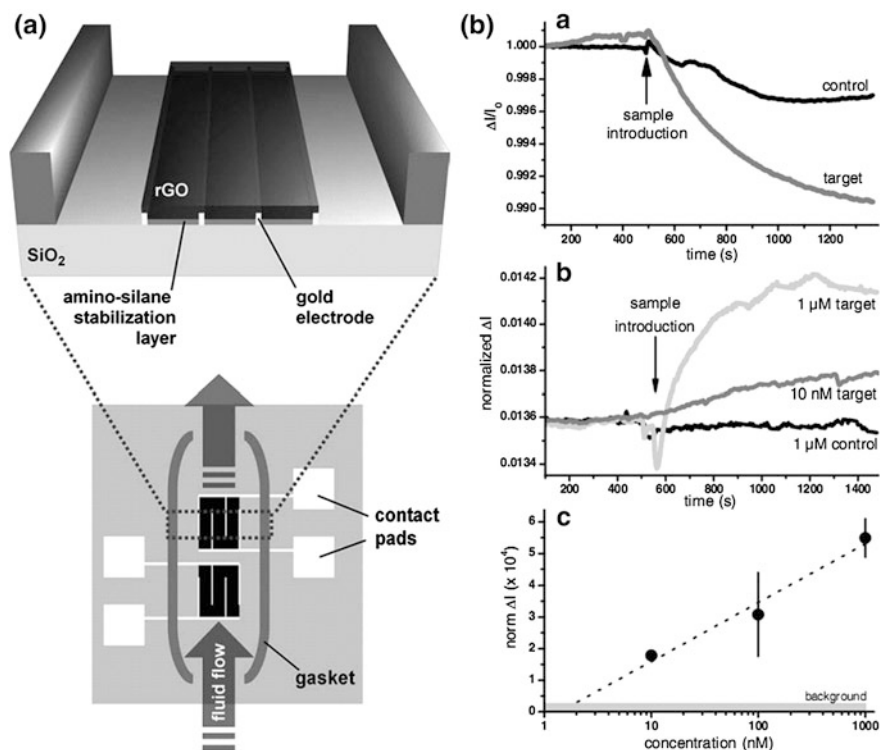
Fig. 2.5 **a** rGO-based FET sensor schematic. The two devices are isolated inside the gasket of the flow cell, with one acting as a reference device to eliminate interference from non-specific biological adhesion (*bottom*). The enlarged area (not to scale) shows the GO deposited on top of the prefabricated electrodes. **b** Functionalized rGO FET devices for DNA detection. (*a*) Response of single FET devices after exposure to both target and non-complementary control DNA solutions. (*b*) Response of differential measurements using one of the FET devices as an internal reference. (*c*) Signal versus target concentration. Reprinted from Ref. [73] by permission from John Wiley & Sons Ltd.

in which the side-by-side devices were exposed to the same sample solution with one device acting as an internal reference for subtracting common sources of interferences, such as pH changes and non-specific biological adhesion (Fig. 2.5a) [73]. The performance of a single isolated FET device (without a reference FET) was shown in Fig. 2.5b *a*. Though a larger change in current was seen for the target solution due to preferential binding of the complementary strand, the sensor clearly responded to both complementary and non-complementary DNA exposure. In the usage of a second FET as a reference, the limitation was overcome (Fig. 2.5b *b*). The electrical signal was a differential change between this reference device and the device functionalized with the probe DNA. Clear responses were seen when switching from pure buffer to the two solutions containing the complementary target, but introduction of the non-complementary strand showed no significant

response, with the signal returning to the baseline after the noise caused by switching the feed line. Limit of detection fell near 2 nM (Fig. 2.5b *c*), placing it in the upper range of the results seen for nanowire/nanotube sensors in similar salt solutions. Moreover, the ability to incorporate a reference sensor by spin coating identical side-by-side devices offers a distinct advantage over similar CNT FETs, as the variability between nanotubes and the bottom-up construction of such devices makes this difficult.

In graphene-based biological FETs, several factors could be optimized, including (a) tailoring the device geometry to maximize the effect of bound targets on conduction pathways, (b) manipulating graphene conductivity, surface groups, and morphology to control the device selectivity and sensitivity, (c) optimizing the density of biological probes to obtain the maximum number of bound targets, and (d) switching the binding affinity or polarity specificity for versatile probe immobilization and target detection.

2.2.4 Other Detection Manners

Based on the unique structure of graphene and its π–π interaction with DNA, other methods, such as colorimetry [75–77], SERS [78], chemiluminescence [79], and mass spectrometry (MS) [80], have been applied to sensitive and multiplex DNA detection. Taking SERS for instance, researches have been carried out to study the Raman spectrum of graphene [81, 82] and its role in Raman enhancement [83]. It is found that the Raman signals of molecules on monolayer graphene are stronger than those on the SiO_2/Si substrate, and the intensity decreases roughly with the increase of the number of graphene layers. Based on the charge transfer of graphene and chemical enhancement mechanism, graphene leads to an enhancement factor of 2–17 [83]. Though it is not clear for the precise origin and further investigation is still needed, one might expand these properties for practical application. Fabricating high-quality graphene with CVD and combining the electromagnetic enhancement of Au nanoparticles, He and coworkers developed the gold-decorated graphene, serving as a highly efficient SERS-active substrate, to facilitate the immobilization of dye-labeled DNAs [78]. A low detection limit of 10 pM was obtained. Also, it realized the simultaneously detection of more types of target DNAs on the same substrate with single-laser excitation.

Due to its double helix structure and the base pairing, DNA-mediated assembled structures can be designed and controlled as a desirable and reversible route. For the first time, DNA hybridization-induced controllable assembly of GO nanosheets was illustrated by Tang et al. [84]. Two single-stranded sequences, DNA_1 and DNA_2, were separately added to GO solutions to form DNA_1–GO and DNA_2–GO complexes, respectively. DNA_1 had a target-specific sequence complementary to target DNA (T-DNA) and a $d(GT)_{15}$ tail at the 5′ terminus to facilitate the assembly of DNA_1 on GO nanosheets. DNA_2 also had a complementary sequence to T-DNA with a $d(GT)_{15}$ tail at the 3′ terminus. In the mixture of the two DNA_1–GO and

DNA$_2$–GO complexes, T-DNA hybridized with both DNA$_1$ and DNA$_2$, which resulted in an assembly of GO nanosheets. Such assembly process was expected to produce the layered structure with tunable interlayer spacing. In particular, it was observed that the size of the GO assembly was concentration dependent and base mismatch sensitive to target DNA, as revealed by dynamic light scattering (DLS) technique. A readily achieved detection limit of 1 pM was observed, and single-base-mismatched DNA was directly discriminated from the perfectly complementary ones.

2.2.5 DNA Sequencing Through Graphene Nanopore, Nanogap, and Nanoribbon

DNA or RNA sequencing through nanopores has attracted much interest because it is a label-free, amplification-free, and single-molecule approach that can be scaled for high-throughput DNA or RNA analysis [85–95]. The concept is simple, which is based on the resistive pulse technique, or Coulter Counter method. A single nanopore is placed in an electrochemical system with electrolytes. Ions are driven through the pore by an applied voltage, resulting in an ionic current. DNA could also be driven through the pore, influencing the flow of ions. As the pore diameter is sufficiently small, DNA is forced to pass through as a linear stand (opposite to the randomly coiled configuration in free solution), then its properties, length, and, ultimately, nucleobase sequence could be determined based on the duration of current blockage and variations in its magnitude [86, 89]. To make this approach practical and reliable, some issues should be resolved, for example, suppressing stochastic nucleobase motions, controlling DNA translocation rate, and resolving the signal overlap between different nucleobases [91]. Among these nanopore materials (e.g., α-hemolysin, SiN, Al$_2$O$_3$), graphene is particularly suitable for electronic DNA sequencing because the thickness of a single layer is comparable to the spacing between nucleotides in ssDNA (0.32–0.52 nm) [85]. For instance, Garaj et al. [90], Schneider et al. [92], and Merchant et al. [94] all succeeded in detecting individual dsDNA using graphene nanopores (Fig. 2.6a). A multilayered graphene–Al$_2$O$_3$ nanopore was also fabricated, which exhibited low electrical noise (lower than pure graphene nanopore), and was sensitive to electrolyte pH at low KCl concentration [96]. The folded and unfolded transport of single-DNA molecules and RecA-coated DNA complexes could be discerned with high temporal resolution, while a question still remains: Is single-base resolution with a graphene nanopore feasible? To achieve this, one might need to slow down the translocation rate of DNA through nanopores. Also, the nucleotides' geometric fluctuation-induced conductance fluctuations should be reduced. Theoretical investigation suggests that using transverse-conductance-based sequencing in the proper geometry could realize DNA sequencing with an error rate of 0 % [93]. Recently, MD simulations in conjunction with electronic transport calculations revealed that edge-
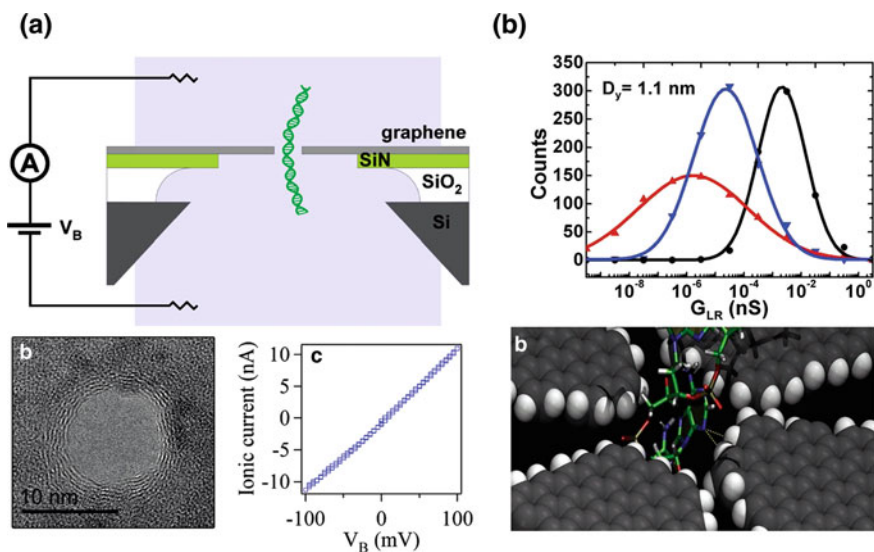
Fig. 2.6 a Graphene nanopore devices. (*a*) Device schematic. Few-layer graphene (1–5 nm thick) is suspended over a 1-µm-diameter hole in a 40-nm-thick SiN membrane. The SiN membrane is suspended over an approximately 50×50 µm^2 aperture in a silicon chip coated with a 5-µm SiO$_2$ layer. The device is inserted into a PDMS measurement cell with microfluidic channels that form reservoirs in contact with either side of the chip. A bias voltage, V_B, is applied between the reservoirs to drive DNA through the nanopore. (*b*) TEM image of a nanopore in a graphene membrane. Scale bar is 10 nm. The rings surrounding the pore are indicative of the number of graphene layers that form the membrane. (*c*) Ionic current–voltage measurement for this 10-nm graphene nanopore device in 1 M KCl, pH 9. Reprinted with permission from Ref. [94] Copyright 2010 American Chemical Society. **b** Edge-hydrogenated graphene nanopore. (*a*) Transverse differential conductance (G_d) distribution curves of poly(dA)$_{30}$ translocating through a nanopore using edge-hydrogenated graphene electrodes (*black line*), unhydrogenated electrodes (*red line*), and pseudo-hydrogenated electrodes (*blue line*). The nanopore inner diameter (D_y) amounts to 1.1 nm, the longitudinal driving field has a strength of $E_x = 5$ kcal mol^{-1} Å^{-1}, and the transverse bias voltage V_0 is set at 3.2 V, which is near the position of a characteristic eigen level of adenine. (*b*) A snapshot extracted from the molecular dynamics simulation of the DNA translocation through the nanopore, showing a moment when two H bonds (*dotted yellow lines*) are formed simultaneously between the nitrogen atom of a DNA nucleobase and two H atoms attached to the graphene edge. For the sake of clarity, only relevant atoms from the edge-hydrogenated graphene electrodes and the DNA molecule have been visualized, omitting water molecules, counter ions, and the SiN membrane. Reprinted from Ref. [97] by permission from John Wiley & Sons Ltd.

hydrogenated graphene nanopore could facilitate the temporary formation of H bonds with suitable atomic sites in the translocating DNA molecule (Fig. 2.6b) [97]. As a consequence, it reduced the translocation speed of DNA and the average conductivity was drastically raised by about 3 orders of magnitude while exhibiting significantly reduced statistical variance. At the same time, the variation in the conductance was significantly reduced, leading to a faster and more reliable identification of the four nucleotide types. The picosiemens tunneling conductance

facilitated reading the nucleotide sequence at a much greater speed than what was possible with only femtoampere tunneling currents. This strategy makes an improvement to the fast and reliable nucleotide identification.

Besides the nanopores, graphene nanogaps and nanoribbons are theoretically investigated in DNA sequencing [93, 98, 99]. In the graphene nanoribbons manner, nucleobases interacted with graphene nanoribbons through π–π stacking. As a DNA strand passed through the nanochannel, the distinct conductance characteristics of the graphene nanoribbons (calculated using a method based on density functional theory coupled to non-equilibrium green function theory) allowed the different nucleotides to be distinguished using a data mining technique and a two-dimensional transient autocorrelation analysis [99]. It is believed that further effort and development would be needed to realize the direct label-free DNA sequencing in real time and high resolution.

2.2.6 DNA Cleavage

The performances of above-mentioned graphene are greatly dependent on its large surface area and the few layers' presence, especially the monodispersed single layers. The unique properties of graphene are highly associated with the single-layer existence. When the lateral size of graphene becomes relatively small, e.g., graphene quantum dots (GQDs), the interaction with DNA might change as well. Different from the poor interaction affinity between dsDNA and large graphene sheets, nanosized graphene sheets intercalate and stack into the planes between the base pairs of dsDNA, which induces dsDNA cleavage. Combining with Cu^{2+} ions, which showed high affinity to DNA, GO/Cu^{2+} system exhibited improved cleavage of dsDNA. The specific interaction mechanism could be found in Ref. [100]. As it is illustrated, the cleavage efficiency was still low and the concentration of Cu^{2+} was high because the size of GO sheets was not well tailored. In a followed study, GQDs were largely produced with photo-Fenton reaction (Fe^{2+}/Fe^{3+}/H_2O_2 reagent under UV irradiation) [101]. Comparing with the micrometer-sized GO sheets, the GQDs with smaller lateral size performed as a better intercalator to DNA. This exhibits the potential applications of GQDs in biological and medical research.

2.3 RNA Detection

Like DNA, RNA is assembled as a chain of nucleotides (G, A, U, C), but is usually single stranded. MicroRNAs (miRNAs) are small, endogenous, non-coding RNAs (approximately 18–25 nucleotides), which play crucial roles in cell proliferation, differentiation, and apoptosis. The sensitive, rapid, and multiple miRNA detection is of great importance. Similar to the above-mentioned fluorescent DNA detection strategies, firstly, ssDNAs labeled with different dyes are adsorbed on GO, where

minimal fluorescence is observed. Upon the recognition of specific target miRNA, DNA–miRNA duplex helixes form and strong emission is observed due to the poor interaction between the helix and GO [102]. Employing isothermal strand-dis-placement polymerase reaction (ISDPR) to amplify the detection signal, a low detection limit of 2.1 fM with a linear range of four orders of magnitude was realized. In a similar manner, DNase I was used to cleave DNA and release miRNA. It acted on ssDNA and dsDNA, chromatin, and DNA in DNA/RNA complex, while it was not active on RNA. DNase I digested the formed DNA/miRNA duplexes and released miRNA to bind another probe DNA on GO, which formed a cyclic reaction and resulted in fluorescent signal amplification [103]. Adopting polyethyleneimine-grafted graphene nanoribbon (PEI-g-GNR) as an effective gene vector and MB, the fluorescent miRNA detection in Hela cells was developed [104]. Recently, an electrochemical miRNA detection manner was reported [105]. Using graphene-dendritic Au nanostructure, multifunctional enco-ded Au with biotin, and streptavidin-HRP as the tri-amplifications, a detection limit toward miRNA of 0.06 pM (S/N = 3) was realized.

References

1. He, S., Song, B., Li, D., Zhu, C., Qi, W., Wen, Y., Wang, L., Song, S., Fang, H., Fan, C.: A graphene nanoprobe for rapid, sensitive, and multicolor fluorescent DNA analysis. Adv. Funct. Mater. **20**, 453–459 (2010)
2. Liu, F., Choi, J.Y., Seo, T.S.: Graphene oxide arrays for detecting specific DNA hybridization by fluorescence resonance energy transfer. Biosens. Bioelectron. **25**, 2361–2365 (2010)
3. Bonanni, A., Pumera, M.: Graphene Platform for Hairpin-DNA-Based Impedimetric Genosensing. ACS Nano **5**, 2356–2361 (2011)
4. Lu, C.H., Yang, H.H., Zhu, C.L., Chen, X., Chen, G.N.: A graphene platform for sensing biomolecules. Angew. Chem. Int. Ed. **48**, 4785–4787 (2009)
5. Li, F., Huang, Y., Yang, Q., Zhong, Z., Li, D., Wang, L., Song, S., Fan, C.: A graphene-enhanced molecular beacon for homogeneous DNA detection. Nanoscale **2**, 1021–1026 (2010)
6. Lu, C.H., Li, J., Liu, J.J., Yang, H.H., Chen, X., Chen, G.N.: Increasing the sensitivity and single-base mismatch selectivity of the molecular beacon using graphene oxide as the "nanoquencher". Chem.-Eur. J. **16**, 4889–4894 (2010)
7. Hu, Y., Li, F., Bai, X., Li, D., Hua, S., Wang, K., Niu, L.: Label-free electrochemical impedance sensing of DNA hybridization based on functionalized graphene sheets. Chem. Commun. **47**, 1743–1745 (2011)
8. Dubuisson, E., Yang, Z., Loh, K.P.: Optimizing label-free DNA electrical detection on graphene platform. Anal. Chem. **83**, 2452–2460 (2011)
9. Hu, Y., Li, F., Han, D., Wu, T., Zhang, Q., Niu, L., Bao, Y.: Simple and label-free electrochemical assay for signal-on DNA hybridization directly at undecorated graphene oxide. Anal. Chim. Acta **753**, 82–89 (2012)
10. Tang, Z., Wu, H., Cort, J.R., Buchko, G.W., Zhang, Y., Shao, Y., Aksay, I.A., Liu, J., Lin, Y.: Constraint of DNA on functionalized graphene improves its biostability and specificity. Small **6**, 1205–1209 (2010)

11. Star, A., Tu, E., Niemann, J., Gabriel, J.C., Joiner, C.S., Valcke, C.: Label-free detection of DNA hybridization using carbon nanotube network field-effect transistors. Proc. Natl. Acad. Sci. U.S.A. **103**, 921–926 (2006)

12. Tang, X., Bansaruntip, S., Nakayama, N., Yenilmez, E., Chang, Y.-L., Wang, Q.: Carbon nanotube DNA sensor and sensing mechanism. Nano Lett. **6**, 1632–1636 (2006)

13. Zheng, M., Jagota, A., Strano, M.S., Santos, A.P., Barone, P., Chou, S.G., Diner, B.A., Dresselhaus, M.S., McLean, R.S., Onoa, G.B., Samsonidze, G.G., Semke, E.D., Usrey, M., Walls, D.J.: Structure-based carbon nanotube sorting by sequence-dependent DNA assembly. Science **302**, 1545–1548 (2003)

14. Jiang, X., Lin, X.: Atomic force microscopy of DNA self-assembled on a highly oriented pyrolytic graphite electrode surface. Electrochem. Commun. **6**, 873–879 (2004)

15. Kabelac, M., Kroutil, O., Predota, M., Lankas, F., Sip, M.: Influence of a charged graphene surface on the orientation and conformation of covalently attached oligonucleotides: a molecular dynamics study. Phys. Chem. Chem. Phys. **14**, 4217–4229 (2012)

16. Varghese, N., Mogera, U., Govindaraj, A., Das, A., Maiti, P.K., Sood, A.K., Rao, C.N.: Binding of DNA nucleobases and nucleosides with graphene. ChemPhysChem **10**, 206–210 (2009)

17. Gowtham, S., Scheicher, R., Ahuja, R., Pandey, R., Karna, S.: Physisorption of nucleobases on graphene: density-functional calculations. Phys. Rev. B **76**, 033401 (2007)

18. Das, A., Sood, A.K., Maiti, P.K., Das, M., Varadarajan, R., Rao, C.N.R.: Binding of nucleobases with single-walled carbon nanotubes: theory and experiment. Chem. Phys. Lett. **453**, 266–273 (2008)

19. Akca, S., Foroughi, A., Frochtzwajg, D., Postma, H.W.: Competing interactions in DNA assembly on graphene. PLoS ONE **6**, e18442 (2011)

20. Song, B., Li, D., Qi, W., Elstner, M., Fan, C., Fang, H.: Graphene on Au(111): a highly conductive material with excellent adsorption properties for high-resolution bio/nanodetection and identification. ChemPhysChem **11**, 585–589 (2010)

21. Ahmed, T., Kilina, S., Das, T., Haraldsen, J.T., Rehr, J.J., Balatsky, A.V.: Electronic fingerprints of DNA bases on graphene. Nano Lett. **12**, 927–931 (2012)

22. Wu, C., Zhou, Y., Miao, X., Ling, L.: A novel fluorescent biosensor for sequence-specific recognition of double-stranded DNA with the platform of graphene oxide. Analyst **136**, 2106–2110 (2011)

23. Hong, B.J., Compton, O.C., An, Z., Eryazici, I., Nguyen, S.T.: Successful stabilization of graphene oxide in electrolyte solutions enhancement of biofunctionalization and cellular uptake. ACS Nano **6**, 63–73 (2012)

24. Hong, B.J., An, Z., Compton, O.C., Nguyen, S.T.: Tunable biomolecular interaction and fluorescence quenching ability of graphene oxide: application to "turn-on" DNA sensing in biological media. Small **8**, 2469–2476 (2012)

25. Wu, M., Kempaiah, R., Huang, P.J., Maheshwari, V., Liu, J.: Adsorption and desorption of DNA on graphene oxide studied by fluorescently labeled oligonucleotides. Langmuir **27**, 2731–2738 (2011)

26. Liu, M., Zhao, H., Chen, S., Yu, H., Quan, X.: Capture of double-stranded DNA in stacked-graphene: giving new insight into the graphene/DNA interaction. Chem. Commun. **48**, 564–566 (2012)

27. Liu, M., Zhao, H., Chen, S., Yu, H., Quan, X.: Salt-controlled assembly of stacked-graphene for capturing fluorescence and its application in chemical genotoxicity screening. J. Mater. Chem. **21**, 15266–15272 (2011)

28. Dong, H., Gao, W., Yan, F., Ji, H., Ju, H.: Fluorescence resonance energy transfer between quantum dots and graphene oxide for sensing biomolecules. Anal. Chem. **82**, 5511–5517 (2010)

29. Shang, L., Dong, S., Nienhaus, G.U.: Ultra-small fluorescent metal nanoclusters: synthesis and biological applications. Nano Today **6**, 401–418 (2011)

30. Yeh, H.C., Sharma, J., Han, J.J., Martinez, J.S., Werner, J.H.: A DNA–silver nanocluster probe that fluoresces upon hybridization. Nano Lett. **10**, 3106–3110 (2010)

31. Tao, Y., Lin, Y., Huang, Z., Ren, J., Qu, X.: DNA-templated silver nanoclusters-graphene oxide nanohybrid materials: a platform for label-free and sensitive fluorescence turn-on detection of multiple nucleic acid targets. Analyst **137**, 2588–2592 (2012)
32. Batchelor-McAuley, C., Wildgoose, G.G., Compton, R.G.: The physicochemical aspects of DNA sensing using electrochemical methods. Biosens. Bioelectron. **24**, 3183–3190 (2009)
33. Balapanuru, J., Yang, J.X., Xiao, S., Bao, Q., Jahan, M., Polavarapu, L., Wei, J., Xu, Q.H., Loh, K.P.: A graphene oxide-organic dye ionic complex with DNA-sensing and optical-limiting properties. Angew. Chem. Int. Ed. **49**, 6549–6553 (2010)
34. Liu, M., Zhao, H., Chen, S., Yu, H., Zhang, Y., Quan, X.: A graphene-based platform for single nucleotide polymorphism (SNP) genotyping. Biosens. Bioelectron. **26**, 4213–4216 (2011)
35. Liu, M., Zhang, Q., Zhao, H., Chen, S., Yu, H., Zhang, Y., Quan, X.: Controllable oxidative DNA cleavage-dependent regulation of graphene/DNA interaction. Chem. Commun. **47**, 4084–4086 (2011)
36. Barsoukov, E., Macdonald, J.R.: Impedance Spectroscopy Theory, Experiment, and Applications. Wiley, London (2005)
37. Pänke, O., Balkenhohl, T., Kafka, J., Schäfer, D., Lisdat, F.: Impedance spectroscopy and biosensing. Adv. Biochem. Eng./Biotechnol. **109**, 195–237 (2008)
38. Guan, J.-G., Miao, Y.-Q., Zhang, Q.-J.: Impedimetric biosensors. J. Biosci. Bioeng. **97**, 219–226 (2004)
39. Daniels, J.S., Pourmand, N.: Label-Free impedance biosensors: opportunities and challenges. Electroanalysis **19**, 1239–1257 (2007)
40. Lisdat, F., Schäfer, D.: The use of electrochemical impedance spectroscopy for biosensing. Anal. Bioanal. Chem. **391**, 1555–1567 (2008)
41. Bonanni, A., Loo, A.H., Pumera, M.: Graphene for impedimetric biosensing. TrAC Trends Anal. Chem. **37**, 12–21 (2012)
42. Giovanni, M., Bonanni, A., Pumera, M.: Detection of DNA hybridization on chemically modified graphene platforms. Analyst **137**, 580–583 (2012)
43. Bonanni, A., Ambrosi, A., Pumera, M.: Nucleic acid functionalized graphene for biosensing. Chem.-Eur. J. **18**, 1668–1673 (2012)
44. Fujii, S., Enoki, T.: Cutting of oxidized graphene into nanosized pieces. J. Am. Chem. Soc. **132**, 10034–10041 (2010)
45. Hu, Y., Hua, S., Li, F., Jiang, Y., Bai, X., Li, D., Niu, L.: Green-synthesized gold nanoparticles decorated graphene sheets for label-free electrochemical impedance DNA hybridization biosensing. Biosens. Bioelectron. **26**, 4355–4361 (2011)
46. Hu, Y., Wang, K., Zhang, Q., Li, F., Wu, T., Niu, L.: Decorated graphene sheets for label-free DNA impedance biosensing. Biomaterials **33**, 1097–1106 (2012)
47. Wang, Z., Zhang, J., Chen, P., Zhou, X., Yang, Y., Wu, S., Niu, L., Han, Y., Wang, L., Boey, F., Zhang, Q., Liedberg, B., Zhang, H.: Label-free, electrochemical detection of methicillin-resistant staphylococcus aureus DNA with reduced graphene oxide-modified electrodes. Biosens. Bioelectron. **26**, 3881–3886 (2011)
48. Niwa, O., Jia, J., Sato, Y., Kato, D., Kurita, R., Maruyama, K., Suzuki, K., Hirono, S.: Electrochemical performance of angstrom level flat sputtered carbon film consisting of sp2 and sp3 mixed bonds. J. Am. Chem. Soc. **128**, 7144–7145 (2006)
49. Ivandini, T.A., Sarada, B.V., Rao, T.N., Fujishima, A.: Electrochemical oxidation of underivatized-nucleic acids at highly boron-doped diamond electrodes. Analyst **128**, 924–929 (2003)
50. Cui, X., Rivas, G., Farias, P.A.M., Shiraishi, H., Wang, J., Palecek, E.: Evaluation of different carbon electrodes for adsorptive stripping analysis of nucleic acids. Electroanalysis **8**, 753–758 (1996)
51. Kato, D., Sekioka, N., Ueda, A., Kurita, R., Hirono, S., Suzuki, K., Niwa, O.: Nanohybrid carbon film for electrochemical detection of SNPs without hybridization or labeling. Angew. Chem. Int. Ed. **47**, 6681–6684 (2008)

52. Zhou, M., Zhai, Y., Dong, S.: Electrochemical sensing and biosensing platform based on chemically reduced graphene oxide. Anal. Chem. **81**, 5603–5613 (2009)
53. Ambrosi, A., Pumera, M.: Stacked graphene nanofibers for electrochemical oxidation of DNA bases. Phys. Chem. Chem. Phys. **12**, 8943–8947 (2010)
54. Lim, C.X., Hoh, H.Y., Ang, P.K., Loh, K.P.: Direct voltammetric detection of DNA and pH sensing on epitaxial graphene: an insight into the role of oxygenated defects. Anal. Chem. **82**, 7387–7393 (2010)
55. Akhavan, O., Ghaderi, E., Rahighi, R.: Toward single-DNA electrochemical biosensing by graphene nanowalls. ACS Nano **6**, 2904–2916 (2012)
56. Qiu, Y., Qu, X., Dong, J., Ai, S., Han, R.: Electrochemical detection of DNA damage induced by acrylamide and its metabolite at the graphene-ionic liquid-Nafion modified pyrolytic graphite electrode. J. Hazard. Mater. **190**, 480–485 (2011)
57. Zhou, M., Wang, Y., Zhai, Y., Zhai, J., Ren, W., Wang, F., Dong, S.: Controlled synthesis of large-area and patterned electrochemically reduced graphene oxide films. Chem.-Eur. J. **15**, 6116–6120 (2009)
58. Guo, H.-L., Wang, X.-F., Qian, Q.-Y., Wang, F.-B., Xia, X.-H.: A green approach to the synthesis of graphene nanosheets. ACS Nano **3**, 2653–2659 (2009)
59. Chng, E.L., Pumera, M.: Solid-state electrochemistry of graphene oxides: absolute quantification of reducible groups using voltammetry. Chem. Asian J. **6**, 2899–2901 (2011)
60. Bonanni, A., Ambrosi, A., Pumera, M.: On oxygen-containing groups in chemically modified graphenes. Chem.-Eur. J. **18**, 4541–4548 (2012)
61. Bonanni, A., Chua, C.K., Zhao, G., Sofer, Z., Pumera, M.: Inherently electroactive graphene oxide nanoplatelets as labels for single nucleotide polymorphism detection. ACS Nano **6**, 8546–8551 (2012)
62. Liao, K.H., Mittal, A., Bose, S., Leighton, C., Mkhoyan, K.A., Macosko, C.W.: Aqueous only route toward graphene from graphite oxide. ACS Nano **5**, 1253–1258 (2011)
63. Zhang, Y., Jiang, W.: Decorating graphene sheets with gold nanoparticles for the detection of sequence-specific DNA. Electrochim. Acta **71**, 239–245 (2012)
64. Bo, Y., Wang, W., Qi, J., Huang, S.: A DNA biosensor based on graphene paste electrode modified with Prussian blue and chitosan. Analyst **136**, 1946–1951 (2011)
65. Zhu, L., Luo, L., Wang, Z.: DNA electrochemical biosensor based on thionine-graphene nanocomposite. Biosens. Bioelectron. **35**, 507–511 (2012)
66. Jayakumar, K., Rajesh, R., Dharuman, V., Venkatasan, R., Hahn, J.H., Pandian, S.K.: Gold nano particle decorated graphene core first generation PAMAM dendrimer for label free electrochemical DNA hybridization sensing. Biosens. Bioelectron. **31**, 406–412 (2012)
67. Lin, L., Liu, Y., Tang, L., Li, J.: Electrochemical DNA sensor by the assembly of graphene and DNA-conjugated gold nanoparticles with silver enhancement strategy. Analyst **136**, 4732–4737 (2011)
68. Du, Y., Guo, S., Dong, S., Wang, E.: An integrated sensing system for detection of DNA using new parallel-motif DNA triplex system and graphene–mesoporous silica–gold nanoparticle hybrids. Biomaterials **32**, 8584–8592 (2011)
69. Dong, X., Shi, Y., Huang, W., Chen, P., Li, L.J.: Electrical detection of DNA hybridization with single-base specificity using transistors based on CVD-grown graphene sheets. Adv. Mater. **22**, 1649–1653 (2010)
70. Choi, B.G., Park, H., Yang, M.H., Jung, Y.M., Lee, S.Y., Hong, W.H., Park, T.J.: Microwave-assisted synthesis of highly water-soluble graphene towards electrical DNA sensor. Nanoscale **2**, 2692–2697 (2010)
71. Lin, J., Teweldebrhan, D., Ashraf, K., Liu, G., Jing, X., Yan, Z., Li, R., Ozkan, M., Lake, R. K., Balandin, A.A., Ozkan, C.S.: Gating of single-layer graphene with single-stranded deoxyribonucleic acids. Small **6**, 1150–1155 (2010)
72. Yin, Z., He, Q., Huang, X., Zhang, J., Wu, S., Chen, P., Lu, G., Zhang, Q., Yan, Q., Zhang, H.: Real-time DNA detection using Pt nanoparticle-decorated reduced graphene oxide field-effect transistors. Nanoscale **4**, 293–297 (2012)

73. Stine, R., Robinson, J.T., Sheehan, P.E., Tamanaha, C.R.: Real-time DNA detection using reduced graphene oxide field effect transistors. Adv. Mater. **22**, 5297–5300 (2010)

74. Mohanty, N., Berry, V.: Graphene-based single-bacterium resolution biodevice and DNA transistor interfacing graphene derivatives with nanoscale and microscale biocomponents. Nano Lett. **8**, 4469–4476 (2008)

75. Xiang, X., Luo, M., Shi, L., Ji, X., He, Z.: Droplet-based microscale colorimetric biosensor for multiplexed DNA analysis via a graphene nanoprobe. Anal. Chim. Acta **751**, 155–160 (2012)

76. Guo, Y., Deng, L., Li, J., Guo, S., Wang, E., Dong, S.: Hemin graphene hybrid nanosheets with intrinsic peroxidase-like activity for label-free colorimetric detection of single-nucleotide polymorphism. ACS Nano **5**, 1282–1290 (2011)

77. Liu, M., Zhao, H., Chen, S., Yu, H., Quan, X.: Interface engineering catalytic graphene for smart colorimetric biosensing. ACS Nano **6**, 3142–3151 (2012)

78. He, S., Liu, K.K., Su, S., Yan, J., Mao, X., Wang, D., He, Y., Li, L.J., Song, S., Fan, C.: Graphene-based high-efficiency surface-enhanced Raman scattering-active platform for sensitive and multiplex DNA detection. Anal. Chem. **84**, 4622–4627 (2012)

79. Luo, M., Chen, X., Zhou, G., Xiang, X., Chen, L., Ji, X., He, Z.: Chemiluminescence biosensors for DNA detection using graphene oxide and a horseradish peroxidase-mimicking DNAzyme. Chem. Commun. **48**, 1126–1128 (2012)

80. Tang, L.A.L., Wang, J., Loh, K.P.: Graphene-Based SELDI Probe with ultrahigh extraction and sensitivity for DNA oligomer. J. Am. Chem. Soc. **132**, 10976–10977 (2010)

81. Ferrari, A.C., Meyer, J.C., Scardaci, V., Casiraghi, C., Lazzeri, M., Mauri, F., Piscanec, S., Jiang, D., Novoselov, K.S., Roth, S., Geim, A.K.: Raman spectrum of graphene and graphene layers. Phys. Rev. Lett. **97**, 187401 (2006)

82. Dresselhaus, M.S., Jorio, A., Hofmann, M., Dresselhaus, G., Saito, R.: Perspectives on carbon nanotubes and graphene Raman spectroscopy. Nano Lett. **10**, 751–758 (2010)

83. Ling, X., Xie, L., Fang, Y., Xu, H., Zhang, H., Kong, J., Dresselhaus, M.S., Zhang, J., Liu, Z.: Can graphene be used as a substrate for Raman enhancement? Nano Lett. **10**, 553–561 (2010)

84. Tang, L., Wang, Y., Liu, Y., Li, J.: DNA-directed self-assembly of graphene oxide with applications to ultrasensitive oligonucleotide assay. ACS Nano **5**, 3817–3822 (2011)

85. Venkatesan, B.M., Bashir, R.: Nanopore sensors for nucleic acid analysis. Nat. Nanotechnol. **6**, 615–624 (2011)

86. Healy, K.: Nanopore-based single-molecule DNA analysis. Nanomedicine **2**, 459–481 (2007)

87. Wanunu, M., Dadosh, T., Ray, V., Jin, J., McReynolds, L., Drndic, M.: Rapid electronic detection of probe-specific microRNAs using thin nanopore sensors. Nat. Nanotechnol. **5**, 807–814 (2010)

88. Clarke, J., Wu, H.C., Jayasinghe, L., Patel, A., Reid, S., Bayley, H.: Continuous base identification for single-molecule nanopore DNA sequencing. Nat. Nanotechnol. **4**, 265–270 (2009)

89. Siwy, Z.S., Davenport, M.: Graphene opens up to DNA. Nat. Nanotechnol. **5**, 697–698 (2010)

90. Garaj, S., Hubbard, W., Reina, A., Kong, J., Branton, D., Golovchenko, J.A.: Graphene as a subnanometre trans-electrode membrane. Nature **467**, 190–193 (2010)

91. Branton, D., Deamer, D.W., Marziali, A., Bayley, H., Benner, S.A., Butler, T., Di Ventra, M., Garaj, S., Hibbs, A., Huang, X., Jovanovich, S.B., Krstic, P.S., Lindsay, S., Ling, X.S., Mastrangelo, C.H., Meller, A., Oliver, J.S., Pershin, Y.V., Ramsey, J.M., Riehn, R., Soni, G. V., Tabard-Cossa, V., Wanunu, M., Wiggin, M., Schloss, J.A.: The potential and challenges of nanopore sequencing. Nat. Biotechnol. **26**, 1146–1153 (2008)

92. Schneider, G.F., Kowalczyk, S.W., Calado, V.E., Pandraud, G., Zandbergen, H.W., Vandersypen, L.M., Dekker, C.: DNA translocation through graphene nanopores. Nano Lett. **10**, 3163–3167 (2010)

93. Postma, H.W.: Rapid sequencing of individual DNA molecules in graphene nanogaps. Nano Lett. **10**, 420–425 (2010)
94. Merchant, C.A., Healy, K., Wanunu, M., Ray, V., Peterman, N., Bartel, J., Fischbein, M.D., Venta, K., Luo, Z., Johnson, A.T., Drndic, M.: DNA translocation through graphene nanopores. Nano Lett. **10**, 2915–2921 (2010)
95. Nelson, T., Zhang, B., Prezhdo, O.V.: Detection of nucleic acids with graphene nanopores: ab initio characterization of a novel sequencing device. Nano Lett. **10**, 3237–3242 (2010)
96. Venkatesan, B.M., Estrada, D., Banerjee, S., Jin, X., Dorgan, V.E., Bae, M.-H., Aluru, N.R., Pop, E., Bashir, R.: Stacked graphene-Al_2O_3 nanopore sensors for sensitive detection of DNA and DNA–protein complexes. ACS Nano **6**, 441–450 (2012)
97. He, Y., Scheicher, R.H., Grigoriev, A., Ahuja, R., Long, S., Huo, Z., Liu, M.: Enhanced DNA sequencing performance through edge-hydrogenation of graphene electrodes. Adv. Funct. Mater. **21**, 2674–2679 (2011)
98. Prasongkit, J., Grigoriev, A., Pathak, B., Ahuja, R., Scheicher, R.H.: Transverse conductance of DNA nucleotides in a graphene nanogap from first principles. Nano Lett. **11**, 1941–1945 (2011)
99. Min, S.K., Kim, W.Y., Cho, Y., Kim, K.S.: Fast DNA sequencing with a graphene-based nanochannel device. Nat. Nanotechnol. **6**, 162–165 (2011)
100. Ren, H., Wang, C., Zhang, J., Zhou, X., Xu, D., Zheng, J., Guo, S.: DNA cleavage system of nanosized graphene oxide sheets and copper ions. ACS Nano **4**, 7169–7174 (2010)
101. Zhou, X., Zhang, Y., Wang, C., Wu, X., Yang, Y., Zheng, B., Wu, H., Guo, S., Zhang, J.: Photo-Fenton reaction of graphene oxide: a new strategy to prepare graphene quantum dots for DNA cleavage. ACS Nano **6**, 6592–6599 (2012)
102. Dong, H., Zhang, J., Ju, H., Lu, H., Wang, S., Jin, S., Hao, K., Du, H., Zhang, X.: Highly sensitive multiple microRNA detection based on fluorescence quenching of graphene oxide and isothermal strand-displacement polymerase reaction. Anal. Chem. **84**, 4587–4593 (2012)
103. Cui, L., Lin, X., Lin, N., Song, Y., Zhu, Z., Chen, X., Yang, C.J.: Graphene oxide-protected DNA probes for multiplex microRNA analysis in complex biological samples based on a cyclic enzymatic amplification method. Chem. Commun. **48**, 194–196 (2012)
104. Dong, H., Ding, L., Yan, F., Ji, H., Ju, H.: The use of polyethylenimine-grafted graphene nanoribbon for cellular delivery of locked nucleic acid modified molecular beacon for recognition of microRNA. Biomaterials **32**, 3875–3882 (2011)
105. Yin, H., Zhou, Y., Zhang, H., Meng, X., Ai, S.: Electrochemical determination of microRNA-21 based on graphene, LNA integrated molecular beacon, AuNPs and biotin multifunctional bio bar codes and enzymatic assay system. Biosens. Bioelectron. **33**, 247–253 (2012)

Chapter 3
Graphene for Amino Acid, Peptide, Protein, and Enzyme Detection

Abstract The excellent biocompatibility, unique structure, and properties of graphene make it suitable for various biomolecules detection. Theoretical and experimental studies were carried out to illustrate the interaction of graphene with aromatic amino acids, amino acids of peptide, protein, and enzyme. The aromatic rings of these amino acids prefer to orient in parallel with respect to the graphene basal plane, which bears the signature of weak π–π stacking. The polarizability of amino acids may play a critical role in the binding strength with graphene, which has implications toward developing biosensors. For example, immunosensors have gained much attention in many biomedical research and clinical diagnostics, as a promising approach for selective and sensitive analysis. Immunosensors based on specific antigen–antibody recognition show great potentials with above merits and highly designable property in practical applications. In a word, graphene shows its great potentials in simplicity, sensitivity, and selectivity, etc., as the substrate for anchoring other materials or the platform for direct biomolecular detection.

Keywords Graphene · Amino acids · Peptide · Protein · Enzyme · Biomolecular detection · Immunosensor

3.1 Amino Acid

Because of their biological significance, amino acids are important in nutrition and maintenance of human health and are commonly used in nutritional supplements, fertilizers, and food technology. The sensitive and selective determination of amino acids is of great importance for biological studies. A theoretical study was carried out to illustrate the interaction of graphene with aromatic amino acids, such as phenylalanine (Phe), histidine (His), tyrosine (Tyr), and tryptophan (Tryp) [1]. Using density functional theory, Møller–Plesset second-order perturbation theory and linear combination of atomic orbitals–molecular orbital approach, it was found that the binding strength with graphene followed in the trend: His < Phe < Tyr < Tryp.

The aromatic rings of these amino acids preferred to orient in parallel with respect to the graphene basal plane, which bears the signature of weak π–π stacking. The polarizability of amino acids may play a critical role in the binding strength with graphene, which has implications toward developing biosensors. An electrochemical aptasensor was devised for His detection, based on the Au NPs-decorated graphene sheets [2]. His could induce self-cleavage of DNAzyme and the ferrocene approached the electrode surface, producing electrochemical signals. However, the non-specific adsorption of DNAzyme on graphene sheet might also happen due to the π–π interactions between the un-hybridized nucleobases and graphene. A flow injection chemiluminescence system based on GO–magnetite–molecularly imprinted polymer (GM–MIP) was proposed for Tryp detection with detection limit of 2.11×10^{-8} M (3σ) [3]. As for other non-aromatic amino acids, cysteine has attracted much attention due to its role in cross-linking of proteins and neurotoxicity, etc. In a fluorescent approach, the dye-labeled ssDNA showed weak fluorescence in the presence of GO, while it exhibited strong fluorescence upon the formation of double helix through the 'activated' metalized DNA by cysteine via robust Ag–S bonds [4]. High selectivity and sensitivity were obtained toward cysteine over other amino acids. Besides, 'OR' and 'INHIBIT' logic gates were designed based on the GO–DNA interactions and thiol-mediated DNA hybridization. Combining graphene with nanoparticles, such as Fe_3O_4 [5], Co [6], and Au [7], direct electrochemical oxidation of cysteine was observed at these nanomaterials-modified electrodes. Having the advantages of simple synthesis, fast response, excellent catalytic activity, and high reproducibility, electrochemical method shows its great promise in bioanalysis.

3.2 Peptide

Peptides are short polymers of amino acid monomers linked by peptide (covalent) bonds, which are formed between two monomers when the carboxyl group of one monomer reacts with the amino group of the other monomer. Peptides are distinguished from proteins based on the size, which contain fewer than 50 monomers. Using MD simulations, Kim et al. [8] demonstrated that the selected peptides bind to the planar or edge of graphene via π–π stacking or electrostatic interactions, respectively. Electronic measurements using mechanically ablated graphene field-effect transistors (GFETs) suggested that the edge- and plane-binding peptides both affected the electronic properties of graphene. Later, Katoch et al. [9] revealed the structure of graphene-binding peptide (GBP) on graphene by using AFM, Raman, ATR–FTIR, and MD. They found that GBP bound non-covalently to graphene, forming secondary structures, and caused no chemical perturbation to graphene. Within a 15–200-ns timescale, a detailed dynamics of adsorption-induced secondary structure transformation and dimerization of an α-helical peptide on graphene surface were illustrated [10]. Subsequently, a coarse-grained approach with an all-atom to all-residue description was used in hierarchy to investigate the binding of peptides to graphene sheet in asymptotic (long time) equilibrium [11].

These results provide important insights into how peptides interact with graphene, which would benefit the chemical biosensors applications. For instance, exploring graphene or GO as the platform, glutathione [12], magainin 2 [13], concanavalin A (ConA) [14], D-vasopressin [15] have all been selectively and sensitively detected via electrogenerated chemiluminescence (ECL), FETs, FRET, and DPV, respectively. In a recent study, Li et al. [16] fabricated a novel GO–ThS–Aβ conjugate and then utilized the strong near-infrared (NIR) optical absorption ability of nano-GO to generate local heat to dissociate the Aβ fibrils following low-power NIR laser irradiation. The disaggregation of Aβ fibrils was monitored by the fluorescence change of the Aβ fibrils staining dye, thioflavin-S (ThS). Then, the photothermal treatment of Alzheimer's disease could be realized with the new multifunctional GO systems.

3.3   Protein

Proteins are large biological molecules consisting of one or more chains of amino acids. They perform a vast array of functions within living organisms, such as catalyzing metabolic reactions, replicating DNA, responding to stimuli, and transporting molecules from one location to another. Recently, graphene sheets are found to serve as an effective platform for protein adsorptions with high loading capacity. For instance, Liu et al. [17] designed GO–streptavidin complexes via the biotin–streptavidin interaction for affinity purification of biotinylated protein complexes, which showed a versatile affinity scaffold. Adopting histidine as the linker, polyhistidine-tagged proteins were immobilized on GFETs [18]. This created a pathway for construction of bio/nanohybrids integrating desirable functionalities of both components, which benefited in the quantitative understanding of mechanical, chemical, and electronic interactions in bio/nanohybrids, monitoring and stimulating protein biological activity, and constructing hybrid devices for applications in optoelectronics and chemical detection. Recently, graphene-encapsulated SiO_2-based FET biosensor for selective and sensitive detection of key biomarker proteins for breast cancer was reported by Myung et al. [19]. The novel 3D structure of the composite significantly increased the surface-to-volume ratio in FET-type biosensors, and highly selective nature was observed to the target even in the presence of a highly concentrated BSA solution. Electrolyte-gated GFETs were also used for BSA detection. Results showed that the conductance of GFETs increased with exposure to BSA at several hundred picomolar [20]. Large adsorption capacity (181.8 mg/g) and fast adsorption kinetics for BSA were obtained at Fe_3O_4–GO core-shell structures [21]. The Fe_3O_4–GO composites offered the combined advantages of Fe_3O_4 (high magnetization and sensitive magnetic response) and GO (good dispersibility in aqueous solution and high binding capacity for proteins). Moreover, the presence of functional groups on GO surface allowed further functionalization with additional groups, offering the promise of selective biological separation and detection. Fe_3O_4–SiO_2–graphene

microspheres, in which SiO_2 shell further provided a good protection for Fe_3O_4 core, were also used for MALDI-TOF MS analysis of BSA [22]. Comparing to the direct formation of magnetic NPs on graphene surface, the performance of the core-shell nanostructure is much superior, which overcomes several drawbacks, such as less adsorption sites of graphene, unstability of magnetic NPs under harsh conditions and long-term use, and aggregation of graphene sheets. In a fluorescent way, squaraine (SQ) dye exhibited weak or no response to BSA without chemically converted graphene. Addition of BSA protein to SQ-graphene led to drastic fluorescence turn-on (by as much as 80 fold), attributing to the improved dye delivery by graphene, which illustrated the ability of graphene to modulate the aggregation structure and to tune the hydrophobicity of SQ dye [23]. Based on the synergetic effect, direct electrochemistry of hemoglobin was achieved at poly(diallyldimethylammonium chloride) functionalized graphene/RTIL film [24] and graphene-chitosan film [25]. Employing graphene platform, hemin was recently detected via fluorescence off strategy with detection limit of 50 nM [26]. In a very recently report, GO–aptamer hybrid was successfully used to photocatalyze viruses, proteins, and nucleic acids by electron and energy transfer in visible light irradiation [27]. It was the first report of GO–aptamer to photocatalyze proteins, which was critical to discover new applications of GO in environmental protection and biochemical engineering. Using layer-by-layer assembly, protein-loaded polyelectrolyte multilayer films with GO capping layers were fabricated for controlled release of ovalbumin [28]. It was found that ovalbumin release without GO layers took place in less than 1 h, while it could be tuned from 30 to 90 days by manipulating the number of GO deposition layers.

Peptide–protein interactions have critical roles in biology. Deep understanding of the nature, regulation, and function of these interactions would be central to human health [29]. Since most peptide–protein bindings do not produce an easily measurable output signal, this severely hinders homogeneous detection of protein using peptide as detection probe. To get into this object, a simple and general approach for investigating peptide–protein interactions was devised by Lu et al. [29]. In which, the fluorescence of pyrene-labeled peptide was quenched at GO surface due to the electron- or energy transfer processes. The competitive binding with target protein (α-bungarotoxin) or antibody (anti-HIV-1 gp 120) resulted in desorption of pyrene-labeled peptide from GO surface with the restoration of pyrene fluorescence. This manner was particularly similar to that they proposed for fluorescent DNA detection as mentioned in the previous DNA detection section. In a similar strategy, cyclin A_2, a prognostic indicator in early-stage cancers, was detected with GO as the fluorescence quencher [30]. The fluorescence of P1 (fluorescent-labeled $p21^{(WAF-1)}$ derived CBM peptide probe) was efficiently quenched when it was mixed with GO unless P1 bound to cyclin A_2. Therefore, the observed fluorescence after addition of GO into reaction solution of P1 and cyclin A_2 indicated that P1 bound to cyclin A_2 and emitted fluorescence. The assay based on preferential quenching of fluorescence from unbound P1 by GO could detect cyclin A_2 as low as 0.5 nM, 1200-fold better than 0.6 μM that using terbium-chelating peptide [31], and 10-fold better than that using SWNTs as the quencher.
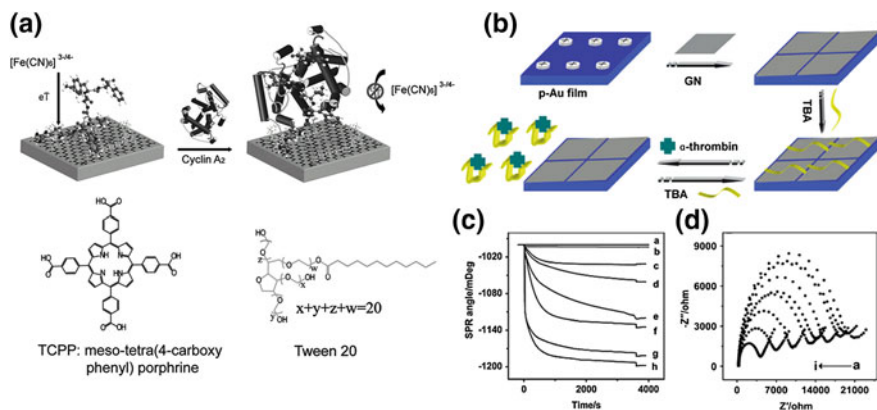
Fig. 3.1 a Schematic illustration of the porphyrin non-covalently functionalized graphene-based peptide sensor for cyclin A_2 detection. Reprinted from Ref. [32] by permission of John Wiley & Sons Ltd. **b** Fabrication of the sensing interface and the detection of thrombin on graphene sheets assembled Au film. Reprinted from Ref. [33] by permission of The Royal Society of Chemistry. **c** SPR angle–time curves for the detection process between the aptamer/graphene/Au sensing interface with different concentrations of thrombin [(*a*) 0 nM; (*b*) 0.08 nM; (*c*) 0.4 nM; (*d*) 1 nM; (*e*) 20 nM; (*f*) 25 nM; (*g*) 100 nM; (*h*) 150 nM]. **d** EIS response of the sensing interface to different concentrations of thrombin [(*a*) 0 nM; (*b*) 0.03 nM; (*c*) 0.08 nM; (*d*) 0.2 nM; (*e*) 1 nM; (*f*) 1.5 nM; (*g*) 5 nM; (*h*) 20 nM; (*i*) 100 nM]

Graphene can substantially suppress background fluorescence and shows much higher signal-to-background ratio. In their followed study, eliminating labeling steps, EIS detection of cyclin A_2 in cancer cells for the first time was recently proposed [32]. In their design, the specific hexapeptide P_0 (RWIMYF) and Tween 20 were immobilized on porphyrin/graphene surface as the detection probe for cyclin A_2 and protection agent for non-specific binding. P_0 bound to a surface pocket in cyclin A_2 with high affinity. The attachment of cyclin A_2 on electrode hampered $[Fe(CN)_6]^{3-/4-}$, which caused electrochemical impedance signal change (Fig. 3.1a). What more important was that this strategy could detect cyclin A_2 in cancer cells and evaluate the efficiency of anti-cancer drugs used in cancer therapy.

Thrombin, a trypsin-like serine protease, plays an important role in several physiological and pathological processes, such as thrombosis, hemostasis, incrustation, and inflammation. Therefore, detection of thrombin is critical to fundamental research as well as clinical diagnosis. Utilizing aptamer to selectively and specifically recognize thrombin has received much interest recently. Aptamer, selected from random sequence RNAs or DNAs combinatorial libraries by SELEX (systematic evolution of ligands by exponential enrichment), is a short and single-stranded artificial oligonucleotide receptor (40–100 bases) with a unique three-dimensional structure, which could bind the specific target molecules. Aptamers have been an ideal sensing element in the biochemical analysis for their remarkable target diversity, high binding affinity, convenient automated-synthesis, ease of labeling, and high stability. Due to the unique structure and interaction with

aptamer, graphene has been introduced into aptasensor for thrombin detection. Recently, Yuan and coworkers carried a series of researches using graphene platforms in sandwich-type [34–39] or label-free [40–42] aptasensors for highly sensitive thrombin determination. On the basis of signal amplification strategy of graphene-based conjugates, these aptasensors exhibited superior performance such as low limit of detection (LOD) (down to 0.33 fM), wide linear range, acceptable stability, and reproducibility. While the multiple fabrication and analysis steps make the process time consuming and less efficient, these might eventually restrict the practical applications. Comparatively simple and efficient manners have also been devised including label [43–45] and label-free [33, 46–49] manners. According to the FRET [43, 44] or chemiluminescence resonance energy transfer (CRET) [45], the fluorescence of fluorophore-labeled aptamer was quenched in the presence of graphene. After binding with thrombin, the aptamer–thrombin complex left graphene surface, resulting in the restoration of fluorescence, which elucidated the binding event. In a typical label-free manner, graphene sheets were assembled on positively charged Au film via electrostatic interaction (Fig. 3.1b) [33]. Then, thrombin aptamer was adsorbed onto the graphene layer through the strong non-covalent binding. The binding between the aptamer and thrombin greatly disturbed the interaction between the aptamer and graphene, resulting in the signal changes of both SPR (Fig. 3.1c) and EIS (Fig. 3.1d). This strategy represents an easy, label-free manner, which could be generalized to detect a spectrum of targets via SPR spectroscopy and EIS using different aptamers. Other strategies, such as incorporating nanomaterials including magnetic microbeads [50] and CdSe [51] into graphene sheets, have also been revealed for thrombin detection.

3.4 Enzyme

Enzymes are large biological molecules responsible for the thousands of chemical interconversions that sustain life. They are highly selective catalysts, greatly accelerating both the rate and specificity of metabolic reactions, from the digestion of food to DNA synthesis. Like proteins, enzymes are long, linear chains of amino acids that fold to 3D structure. To get a deep understanding and reveal the functions of enzymes, new substrate materials with appropriate structures, morphology, functionalities, and compositions are urgently needed and explored. Graphene or GO seems to be an ideal choice with the unique 2D structure, flat plane, tunable functionalities, oxygenic groups, and heterogeneous electron transfer, etc. As an example, horseradish peroxidase (HRP) was directly immobilized on GO surface through electrostatic interaction. With AFM and enzyme activity assays, it was found that full retention of the conformation of immobilized enzyme should be the key to improve its catalytic performance [52]. Enhanced direct electron transfer for the HRP–Fe(III)/Fe(II) redox center of HRP was obtained at sulfonated graphene [53], GO–MWNTs [54], and graphene–Fe_3O_4 [55] hybrid. Later, De et al. revealed GO as an inhibitor in modulating the activity of α-chymotrypsin (ChT) [56].

The properties, such as coexistence of anionic, hydrophobic, aromatic residues, and a large surface area-to-mass ratio, all contribute to GO's inhibition effect. In fact, it exhibits the highest inhibition dose response (by weight) for ChT inhibition compared with all other reported artificial inhibitors, e.g., CNT, dendrimer, Au NPs, polymeric micelles, ferric porphyrin, and cyclic peptide. By tuning the properties of GO or graphene, it is possible to strengthen its applicability to wider targets range with high specificity and selectivity. Recently, Jin et al. [57] reported an enzyme positive modulator, polyethylene glycol (PEG)–GO (PEGylated GO), to selectively and efficiently improve trypsin activity and thermostability, while showing barely any effect on chymotrypsin or proteinase K (as three well-characterized serine proteases). Investigation elucidated that the PEGylated GO-induced acceleration was substrate dependent and 43-fold increase could be achieved depending on the substrate concentration, which may be attributed to both the terminal amino groups on polymer coatings and 2D structure of GO. These researches demonstrate the novel potential of GO (or functionalized GO) in enzyme engineering and enzyme-based bioassays.

Recently, a label-free ECL biosensor for telomerase detection was constructed based on a cation porphyrin, meso-tetra(4-N,N,N-tri-methylanilinium) porphyrin (TAPP) functionalized chemically converted graphene (TAPP/CCG)-modified GCE, and Tween 20 for prevention of non-specific binding and $Ru(bpy)_3^{2+}$ as signal reporter [58]. This novel ECL assay could detect telomerase activity as low as 10 Hela cells/mL, which was 20,000-fold lower than that of the commonly used colorimetric analysis method. Due to the large surface area and excellent electrical conductivity of graphene, the porphyrin/graphene nanocomposite not only presented abundant positively charged domains for DNA capture but also played a role of signal amplification in electrochemical detection.

In a recent research, it was reported that GO could induce glucose oxidase (GOD) to undergo substantial conformation changes both at secondary and tertiary structure levels, inducing the exposure of flavin adenine dinucleotide (FAD) to solvent and transferring tryptophan (Trp) resides to a more hydrophobic environment [59]. These changes resulted in a significant decrease in the catalytic activity of GOD, which needs to be avoided in the glucose detection. By combining GO (graphene) with other materials, such as ionic liquid (IL) [60] or CdS [61], synergetic effects took place. The fabricated hybrids exhibited favorable microenvironment for GOD immobilization and promoted the direct electron transfer process. Also, they displayed high sensitivity and stability toward glucose detection. The specific illustration of the direct electrochemistry of GOD and its catalysis to glucose would be elucidated in the following glucose detection section. Other enzymes, such as microperoxidase-11 (MP-11) [62], α-chymotrypsin [63], deoxyribonuclease I [64], endonuclease/methyltransferase [65], and protease [66, 67], have all been successfully detected. The specific role of immobilized enzymes is their high catalytic behaviors toward the corresponding targets. Contrary to the previously mentioned dye fluorescence restoration strategy, a dye fluorescence quenching manner for helicase detection was developed by Jang et al. [68]. The design was based on the fact that dye-labeled dsDNA could not be adsorbed onto

graphene surface because of the efficient shielding of nucleobases within the negatively charged phosphate backbones of dsDNA, where strong fluorescence was observed. Upon the addition of helicase, the helicase-induced unwinding of dsDNA proceeded and the fluorescence was gradually quenched, because of the strong adsorption of unwound ssDNA on graphene. Hence, the helicase could be successfully detected via fluorescence decrease. Also, this method may be readily applicable to any research involving dsDNA unwinding and to the screening of helicase inhibitors as drug candidates in antivirus therapy.

3.5 Immunosensors

For antigen detection, enzyme-linked immunosorbent assays (ELISA) is the commercially available and routinely used method. However, it is time consuming and expensive, which inhibit its suitability for field applications. There is an urgent need to develop alternative methods with lower cost, higher sensitivity and selectivity, faster response, and point-of-care detection. Based on specific antigen–antibody recognition, immunosensors have gained much attention in many biomedical research and clinical diagnostics, as a promising approach for selective and sensitive analysis. Immunosensors show great potentials with above merits and highly designable property in practical applications. Various methods (EC, ECL, CL, FET, CRET, FRET, colorimetric, etc.) and coupling nanomaterials (CNT, QDs, NPs, etc.) have been used for immunosensors construction. Typically, a sandwich-type protocol is often adopted. Previously, the primary antibody (Ab1) is immobilized on a solid surface. Then, the specific antigen binds to the Ab1 site. Finally, the labeled secondary antibody (Ab2) binds to the antigen, which triggers the successive reactions of species in the solution or on the immunosensor platform. A signal is obtained to indicate the antigen–antibody recognition. Recently, graphene has been widely used in immunosensors construction. Examples of these researches have been illustrated in Table 3.1. Graphene nanomaterials play two main roles in immunosensors: the building blocks for platform construction (Ab1 immobilization) and the labels in bioconjugates with Ab2.

Using graphene as the substrate for Ab1 immobilization and an energy acceptor, Lee et al. reported an immunoassay based on CRET between graphene sheets and chemiluminescent donors [75]. CRET is a non-radiative dipole–dipole transfer of energy from a chemiluminescent donor to a suitable acceptor. Comparing with FRET, CRET occurs via the specific oxidation of a luminescent substrate during chemiluminescence (CL) reaction without an external excitation source. Therefore, it could avoid the drawbacks of FRET, such as the requirement of simultaneous external excitation of both donor and acceptor fluorophores. In their design, the target C-reactive protein (CRP) triggered the immunoreaction between graphene-Ab1 and HRP-Ab2 in buffer containing H_2O_2 and luminol (Fig. 3.2a). The reaction of luminol with ROS (i.e., reactive oxygen species, generated by H_2O_2 and HRP) resulted in the formation of a high-energy species that decomposed with loss of N_2

Table 3.1 Immunosensors based on graphene

Target	Recognition layer	Assay	Signal antibody	Electrolyte	Detection range	LOD	Reference
IgE	Graphene/Aptamer	FET	–	PBS	0.29–160 nM	$K_D = 47$ nM	[69]
IgG	TRGO-Au NP-anti-IgG	FET	–	PBS	0.2 ng/mL–0.2 mg/mL	0.2 ng/mL	[70]
	TRGO-Au NP-anti-IgG	FET	–	PBS	2 ng/mL–0.02 mg/mL	2 ng/mL	[71]
p53^{15}	CMG/anti-IgG	EIS	–	PBS + $Fe(CN)_6^{3-/4-}$	0.3–7 µg/mL	–	[72]
	Graphene-CHI/p53 Ab1	DPV	HRP-streptavidin-biotin-Ab2	PBS + thionine + H_2O_2	0.2–10 ng/mL	0.1 ng/mL	[73]
p53^{392}	Au NPs/NHS/p53 Ab1	SWV	HRP-p53^{392}/Ab2-GO	PBS + thionine + H_2O_2	0.02–2 nM	0.01 nM	[74]
CRP	Graphene/anti-CRP Ab1	CRET	HRP-anti-CRP Ab2	PBS + luminol + H_2O_2	1–1,000 ng/mL	0.93 ng/mL	[75]
HIgG	Graphene-PDDA/Au/Ab1	DPV	HRP-Ab2/Au/PDDA-EGO	PBS + o-PD + H_2O_2	0.1–200 ng/mL	0.05 ng/mL	[76]
	GR-MWCT/Ab1	CV	HRP-Ab2	PBS + H_2Q + H_2O_2	1–500 ng/mL	0.2 ng/mL	[77]
	P-GR-CdSe/Au NPs/Ab	ECL	–	PBS + $K_2S_2O_8$	0.02–2,000 pg/mL	5 fg/mL	[78]
	GN-Au NPs/Ab1	ECL	SiO$_2$-(CdTe/CdS)-Ab2	PBS + $K_2S_2O_8$	0.1 pg/mL–10 ng/mL	87 fg/mL	[79]
AFP	PTH/GDCS/Au/HRP-anti-AFP	DPV	–	ABS + H_2O_2	1.0–10 ng/mL	0.7 ng/mL	[80]
	Thi/AuAgGP/anti-AFP	DPV	HRP-anti-AFP-AuTi	ABS + H_2O_2	0.001–200 ng/mL	0.5 pg/mL	[81]
	GMGP/HRP-anti-AFP	DPV	–	PBS + $Fe(CN)_6^{3-/4}$+H_2O_2	0.01–200 ng/mL	1.0 pg/mL	[82]
	GS-TH/anti-AFP	CV	–	PBS	0.05–2 ng/mL	5.77 pg/mL	[83]
	GS-CHI/Ab1	SWV	HRP-Ab2-CNSs	PBS + o-PD + H_2O_2	0.05–6 ng/mL	0.02 ng/mL	[84]
	MGO/anti-AFP	DPV	HRP-Fc-GHS-anti-AFP	PBS + H_2O_2	0.01–200 ng/mL	1.0 ng/mL	[85]
	G-CdS-agarose/anti-AFP	ECL	–	PBS + $K_2S_2O_8$	0.0005–50 pg/mL	0.2 fg/mL	[86]
	HCG-Ab1	FRET	CdTe QDs-Ab5	PBS	–	0.15 ng/mL	[87]

(continued)

Table 3.1 (continued)

Target	Recognition layer	Assay	Signal antibody	Electrolyte	Detection range	LOD	Reference
β-Lactoglobulin	Graphene/Ab	DPV	–	PBS + Fe(CN)$_6^{3-/4-}$	1 pg/mL–100 ng/mL	0.85 pg/mL	[88]
Norethisterone	GS-TH/Ab1	CV	Au-MSN-HRP-Ab2	PBS + H$_2$O$_2$	0.01–10 ng/mL	3.58 pg/mL	[89]
CEA	MB/PPD/AgNP/anti-CEA	DPV	HRP-anti-CEA/Au NP-GO	ABS + H$_2$O$_2$	0.01–40 ng/mL	0.001 ng/mL	[90]
	Gp-Ni/MB/Au NP/anti-CEA	DPV	–	ABS	0.5–120 ng/mL	0.17 ng/mL	[91]
	MGO/anti-CEA	DPV	HRP-Thi-GHS-anti-CEA	PBS + H$_2$O$_2$	0.01–80 ng/mL	1.0 pg/mL	[85]
	RGO-CdS/Ab1	CL	HRP-Ab2-luminol-Au NPs	Tris-HCl + PIP + H$_2$O$_2$	0.05–20 ng/mL	0.01 ng/mL	[92]
	Gra/Au NP/Ab1	ECL	ZnO–Gra-GOD-Ab2	PBS + luminol + GOD	10 pg/mL–80 ng/mL	3.3 pg/mL	[93]
PDGF-BB	Au/SAM/Ab1	SWV	GO-Ab2-Ag	Fe(CN)$_6^{3-}$	0.01–100 ng/mL	5.0 pg/mL	[94]
ALV-J	GR-Au NP-PTBA/Ab	EIS	–	Fe(CN)$_6^{3-/4-}$	527–3162 TCID$_{50}$/mL	210 TCID$_{50}$/mL	[95]
OA	GSPE/Ab	SWV	OVA	PBS + Fe(CN)$_6^{3-/4-}$	~5,000 ng/L	19 ng/L	[96]
PSA	GS/Ab1	SWV	GS-QD-Ab2	PBS	0.005–10 ng/mL	3 pg/mL	[97]
	GS/Ab1	i-t	GS-TH-HRP-Ab2	PBS + H$_2$O$_2$	0.002–10 ng/mL	1 pg/mL	[98]
	GS-MB-CS/Ab	CV	–	PBS	0.05–5.0 ng/mL	13 pg/mL	[99]
	G-Fe$_3$O$_4$/TH/Ab1	ECL	Si/QDs-Ab2	PBS + Na$_2$SO$_3$	0.003–50 ng/mL	0.72 pg/mL	[100]
	GR-CHIT/Ab1	ECL	GOx-GNR-Ab2	PBS + luminol + glucose	10 pg/mL–8 ng/mL	8 pg/mL	[101]
	Graphene/PBSE/Ab	R	–	–	0.1–100 ng/mL	0.08 ng/mL	[102]
	GS-CoNP-PBSE/Ab	CV	–	PBS	0.02–2 ng/mL	0.01 ng/mL	[103]
	Fe$_3$O$_4$–Ab1	color	GO-Ab2	HQ + H$_2$O$_2$	–	–	[104]
fPSA	PEI-PTCA/Au NPs	DPV	Bio-AP/Ab/Au–NiNPs/O-GS	PBS + AA − P	0.01–50 ng/mL	3.4 pg/mL	[105]
fPSA	PEI-PTCA/Au NPs	DPV	Bio-AP/Ab/Au–PBNPs/O-GS	PBS + AA − P	0.02–10 ng/mL	6.7 pg/mL	[105]
SKOV-3	GO/Ab	DPV	ssDNA-Ab/cDNA	PBS + daunorubicin	6.5–65,000 cells/mL	5.2 cells/mL	[106]

(continued)

Table 3.1 (continued)

| Target	Recognition layer	Assay	Signal antibody	Electrolyte	Detection range	LOD	Reference
BTX-2	MB-Ab	SWV	BGGNR	PBS + Ru(bpy)$_3$Cl$_2$	1.0 pg/mL–10 ng/mL	1.0 pg/mL	[107]
MC-LR	G-CdS/Ab	PEC	–	PBS + AA	0.1–25 µg/L	0.021 µg/L	[108]
CLB	MWNTs/Ab/Ag–GO–CLB	DPV	–	KCl	0.01–10 ng/mL	6.8 pg/mL	[109]
BRCA1	PVP-GS/TH/Ab1	i-t	SBA-15/HRP/Ab2/ BMIM·BF4	PBS + H$_2$O$_2$	0.01–15 ng/mL	4.86 pg/mL	[110]
CA 15-3	GN-NPG-TH/Ab	DPV	HRP–liposome/Ab	PBS + H$_2$O$_2$	2 × 10^{-5}–40 U/mL	5 × 10^{-6} U/mL	[111]
hCG	GS/MWCNTs/Au/Ab1	DPV	HRP-Ab2/Au/TH/MCM-41	PBS + H$_2$O$_2$	0.005–500 mIU/mL	0.0026 mIU/mL	[112]
	GS/NPG/Ab	CV	–	PBS + HQ	0.5–40 ng/mL	0.034 ng/mL	[113]
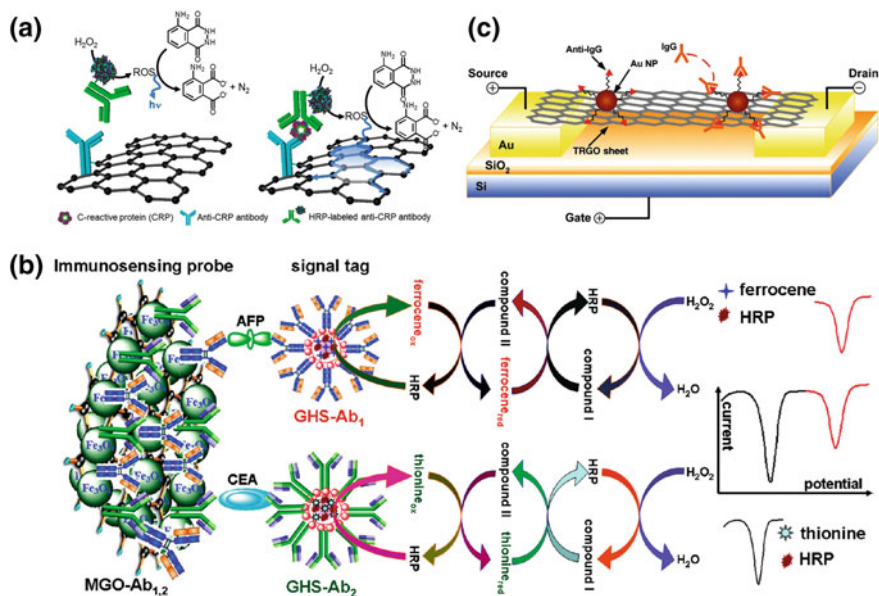
Fig. 3.2 a Schematic illustration of a graphene-based chemiluminescence resonance energy transfer platform for the detection of CRP. Anti-CRP antibody-conjugated graphene and luminol that is excited by HRP-catalyzed oxidation are used as an acceptor and a donor, respectively. Reprinted with permission from Ref. [75] Copyright 2012 American Chemical Society. **b** Schematic illustration of the multiplexed electrochemical immunoassay protocol and the measurement principle of the sandwich immunoassay. Reprinted with permission from Ref. [85] Copyright 2011 American Chemical Society. **c** Schematic of a TRGO FET. Anti-IgG is anchored to the TRGO sheet surface through Au NPs and functions as a specific recognition group for the IgG binding. The electrical detection of protein binding (IgG to anti-IgG) is accomplished by FET and direct current measurements. Reprinted from Ref. [71] by permission of John Wiley & Sons Ltd.

to give an excited molecule with a strong blue emission at 430 nm. LOD was found to be 0.93 ng/mL, and the performance was comparable to that of ELISA-based assay. One advantage of this graphene-based CRET might be that it allowed the homogeneous immunoassay of specific target without washing out unbound antibody or phase separation. Because most sandwich-type immunoassays require the removal of unbound probes before signal readout to determine analyte concentration present in clinical and biological samples [75]. It also revealed that the electrons transfer from excited state of luminol to conductive graphene was much easier than that to GO, an insulator or semiconductor. Other graphene-based platforms were also fabricated and used in various targets detection with a sandwich-type [73, 77, 79, 81, 84, 87, 89, 92, 96, 100, 104, 106, 110–112]. The large surface area and oxygenic groups of graphene provide a good candidate for nanomaterials anchoring, and then the increment the immobilization amount of probe and target. And its good electrical conductivity improves the electron transfer. These properties all contribute to improve the detection sensitivity.

In sandwich-type immunoassays, the detectable signal derives mainly from the labels in Ab2-bioconjugates. Research demonstrated that the loading ratio (the weight ratio of loaded drug to carriers) of GO could reach 200 %, much higher than that of other nanocarriers such as nanoparticles that usually have a loading ratio less than 100 % [114]. This could be attributed to the advantages of graphene, such as large surface area, good biocompatibility, and physiological stability. Besides, the functional groups of GO facilitate biomolecules binding. Based on these, Du and coworkers exploited functional GO as a nanocarrier to link enzyme and signal antibody at high ratio, which greatly increased the detection sensitivity toward phosphor-p53^{392} [74]. To increase the immobilization amount of biomolecules and accelerate electron transfer, GO and graphene have also been decorated with Au NPs [90], Ag [94], and guanine [107]. The immunoassays signals are greatly enhanced by incorporating graphene in Ab2-bioconjugates.

Taking the merits of graphene, it has been exploited as both the platform and label [76, 93, 97, 98, 101]. For instance, Liu et al. [76] designed a graphene-assisted dual amplification strategy for immunosensor application. Graphene–PDDA/Au NPs hybrids served as an effective matrix for antibody anchoring with good stability and bioactivity. Graphene-based nanoprobe (HRP-Ab2/Au/PDDA-EGO) was designed for constructing a sandwich-type immunosensor. Enhanced sensitivity was achieved by combining the advantages of high binding capacity and excellent electrical conductivity of graphene platform with the multilabel nanoprobe signal amplification. The application of this immunosensor to real clinical serum samples showed comparable detection results to that obtained by ELISA with the relative deviations ranging from −3.50 to 7.89 %. Biocompatible graphene sheets as an immunosensor platform or a label in bioconjugates not only present an abundant domain for bimolecular binding but also play a role in fast electron transfer kinetics and further signal amplification. Sensitive, selective, and simultaneous detection of multianalytes may be the trend in the future clinical diagnostics. Recently, Tang et al. [85] presented the simultaneous electrochemical determination of AFP and CEA in biological fluids. Anti-AFP (Ab1) and anti-CEA (Ab2) were coimmobilized on Fe_3O_4 NPs-coated graphene sheets to obtain MGO-Ab1,2 substrate. HRP-ferrocene and HRP-thionine were encapsulated into nanogold hollow microspheres (GHS) to form the signal tags as GHS-Ab1 and GHS-Ab2, respectively. Then, a sandwich-type immunoassay format was employed for the online detection of AFP and CEA by coupling a flow-through detection cell with an external magnet (Fig. 3.2b). The detection ranges of 0.01–200 ng/mL and 0.01–80 ng/mL were observed for AFP and CEA, respectively. The LODs for both analytes were down to 1.0 pg/mL. Results showed that this multiplexed immunoassay manner fulfilled the needs of clinical diagnosis. Later, a novel multiple-label method and dual catalysis amplification for simultaneous detection of PSA and fPSA were proposed by Han et al. [105]. In their design, Au NPs-modified nanoparticles were decorated on onion-like mesoporous graphene sheets, (Au–PBNPs/O-GS and Au–NiNPs/O-GS), as distinguishable signal tags. Subsequently, streptavidin and biotinylated alkaline phosphatase (bio-AP) were employed to block the possible remaining active sites. With the bio-AP, the amplification signals could be achieved by

catalysis of the ascorbic acid 2-phosphate to produce AA in situ. Then, AA was further catalyzed by Au–PBNPs/O-GS and Au–NiNPs/O-GS nanocomposites, respectively, to obtain the high signal responses.

To gain distinguishable detection signals, sandwich-type immunoassay, as above mentioned, is often used, in which labels of Ab2-bioconjugates trigger the reactions. This manner possesses high sensitivity and selectivity. Meanwhile, the multiple attaching and washing steps make the procedures complex and time consuming and also cause the loss of samples. Direct or label-free monitoring the antigen–antibody recognition may be of highly important and demanded. In this manner, the second Ab2-bioconjugates are not necessary as in a sandwich-type assay. Examples are illustrated in the following. By incorporating redox species into graphene platform, both DPV [80, 91, 109] and CV [83, 99, 103] are used to monitor the redox behaviors of the electroactive species before and after antigen recognition. This could also be realized by the redox indicators in the electrolytes [82, 88, 113]. Sensitive ECL immunosensing by incorporating QDs in graphene platform is also demonstrated [78, 86]. Comparing to CV or DPV with large stimulating potentials, EIS is less destructive and invasive to the biological interactions due to the low amplitude of applied potential or current. Besides, it is highly sensitive to the electrode interfacial property changes when high molecular weight or electrically charged biomolecules are binding to the platform. Recently, EIS has been successfully applied to immunoassay [72, 95]. For example, Loo et al. [72] designed an impedimetric immunosensor for IgG based on chemically modified graphene (CMG). Low impedance value was obtained at CMG-modified electrode due to the total accessibility of $Fe(CN)_6^{3-/4-}$ to electrode. When anti-IgG was immobilized on CMG electrode, impedance value increased due to the decrease of accessibility. Finally, IgG bound to CMG/anti-IgG and a further increase of impedance value was observed due to the additional steric hindrance caused by the bulky IgG molecules or the electrostatic interaction between IgG and $Fe(CN)_6^{3-/4-}$. The linear detection range was from 0.3 to 7 μg/mL. This impedimetric strategy is comparatively simple due to the elimination of the second Ab-conjugates reaction step. However, the performances (LOD, sensitivity, selectivity, etc.) are still not comparable to other electrochemical strategies. Further efforts are needed to improve the platform's performance with high sensitivity and selectivity to interfacial property changes.

The unique properties of graphene, such as single layer, extremely large surface area and high carrier mobility, make it suitable for FET applications as revealed in the previous DNA electrical detection segment. Graphene-based FETs (G-FETs) have also been constructed and used for immunosensors [69–71]. The recognition event could induce significant changes in the electrical characteristics of G-FETs, which represents it as a label-free manner with simplicity and sensitivity. Using G-FET for biological assay, there are two main considerations. One is the recognition reaction must occur within the Debye length, which is simply defined as the typical distance required for screening the surplus charge by the mobile carriers present in a material. The other is that no defects are introduced on single-layer graphene surface to enable specific detection and minimize non-specific binding [69]. Based on this,

Ohno et al. [69] succeeded in label-free IgE detection using an aptamer-modified G-FET with a dissociation constant of 47 nM. As artificial oligonucleotides produced in vitro, aptamer may bind graphene with high affinity. However, the directly immobilized antibody on graphene may be unstable and readily removed through simple washing processes. This introduces undesirable effects, such as poor device reproducibility and non-specificity. To overcome this, Mao et al. [70, 71] designed Au NP–antibody conjugates to modify G-FET with high affinity (Fig. 3.2c). Very low LOD of 0.2 ng/mL was reached, which was among the best of reported carbon nanomaterial-based biosensors. Besides, the performance might be improved by a large piece of single-layer graphene sheet with high antibody density.

Toward various antigens detection, electrochemical methods, such as DPV, CV, and SWV, are mostly adopted (Table 3.1) due to the features of simple pretreatment procedures, fast response, precise measurement, cost-effectiveness, high sensitivity and selectivity, and feasible miniaturization. However, the performances are largely dependent on the labels of Ab2-conjugates, which make the procedures complex. EIS and FET techniques represent as the simple, direct, and label-free manner, while high-quality, cost-efficient graphene platforms exhibiting high sensitivity and selectivity toward biomolecules binding events are still highly required. Simultaneous multiplexed immunoassay using EIS and FET is hardly realized due to their restriction of simple readout signal. Immunosensors adopting ECL, CL, CRET, and FRET show comparable performances to electrochemical methods, but share with the similar problem. A versatile detection method with all merits seems impossible. Choosing the most suitable one for specific target detection seems to be particularly important. Furthermore, there is room for improving the quality and property of graphene-based platforms or antibody bioconjugates.

References

1. Rajesh, C., Majumder, C., Mizuseki, H., Kawazoe, Y.: A theoretical study on the interaction of aromatic amino acids with graphene and single walled carbon nanotube. J. Chem. Phys. **130**, 124911 (2009)
2. Liang, J., Chen, Z., Guo, L., Li, L.: Electrochemical sensing of L-histidine based on structure-switching DNAzymes and gold nanoparticle–graphene nanosheet composites. Chem. Commun. **47**, 5476–5478 (2011)
3. Qiu, H., Luo, C., Sun, M., Lu, F., Fan, L., Li, X.: Determination of L-tryptophan based on graphene oxide-magnetite-molecularly imprinted polymers and chemiluminescence. Talanta **98**, 226–230 (2012)
4. Lin, Y., Tao, Y., Pu, F., Ren, J., Qu, X.: Combination of graphene oxide and thiol-activated DNA metallization for sensitive fluorescence turn-on detection of cysteine and their use for logic gate operations. Adv. Funct. Mater. **21**, 4565–4572 (2011)
5. Song, Y., He, Z., Hou, H., Wang, X., Wang, L.: Architecture of Fe_3O_4–graphene oxide nanocomposite and its application as a platform for amino acid biosensing. Electrochim. Acta **71**, 58–65 (2012)
6. Song, Y., He, Z., Zhu, H., Hou, H., Wang, L.: Electrochemical and electrocatalytic properties of cobalt nanoparticles deposited on graphene modified glassy carbon electrode: application to some amino acids detection. Electrochim. Acta **58**, 757–763 (2011)

7. Ge, S., Yan, M., Lu, J., Zhang, M., Yu, F., Yu, J., Song, X., Yu, S.: Electrochemical biosensor based on graphene oxide-Au nanoclusters composites for L-cysteine analysis. Biosens. Bioelectron. **31**, 49–54 (2012)

8. Kim, S.N., Kuang, Z., Slocik, J.M., Jones, S.E., Cui, Y., Farmer, B.L., McAlpine, M.C., Naik, R.R.: Preferential binding of peptides to graphene edges and planes. J. Am. Chem. Soc. **133**, 14480–14483 (2011)

9. Katoch, J., Kim, S.N., Kuang, Z., Farmer, B.L., Naik, R.R., Tatulian, S.A., Ishigami, M.: Structure of a peptide adsorbed on graphene and graphite. Nano Lett. **12**, 2342–2346 (2012)

10. Ou, L., Luo, Y., Wei, G.: Atomic-level study of adsorption, conformational change, and dimerization of an alpha-helical peptide at graphene surface. J. Phys. Chem. B **115**, 9813–9822 (2011)

11. Pandey, R.B., Kuang, Z., Farmer, B.L., Kim, S.S., Naik, R.R.: Stability of peptide (P1 and P2) binding to a graphene sheet via an all-atom to all-residue coarse-grained approach. Soft Matter **8**, 9101−9109 (2012)

12. Wang, Y., Lu, J., Tang, L., Chang, H., Li, J.: Graphene oxide amplified electrogenerated chemiluminescence of quantum dots and its selective sensing for glutathione from thiol-containing compounds. Anal. Chem. **81**, 9710–9715 (2009)

13. Ang, P.K., Jaiswal, M., Lim, C.H.Y.X., Wang, Y., Sankaran, J., Li, A., Lim, C.T., Wohland, T., Barbaros, O., Loh, K.P.: A bioelectronic platform using a graphene-lipid bilayer interface. ACS Nano **4**, 7387–7394 (2010)

14. Chen, Q., Wei, W., Lin, J.M.: Homogeneous detection of concanavalin A using pyrene-conjugated maltose assembled graphene based on fluorescence resonance energy transfer. Biosens. Bioelectron. **26**, 4497–4502 (2011)

15. Qin, H., Liu, J., Chen, C., Wang, J., Wang, E.: An electrochemical aptasensor for chiral peptide detection using layer-by-layer assembly of polyelectrolyte-methylene blue/polyelectrolyte-graphene multilayer. Anal. Chim. Acta **712**, 127–131 (2012)

16. Li, M., Yang, X., Ren, J., Qu, K., Qu, X.: Using graphene oxide high near-infrared absorbance for photothermal treatment of Alzheimer's disease. Adv. Mater. **24**, 1722–1728 (2012)

17. Liu, Z., Jiang, L., Galli, F., Nederlof, I., Olsthoorn, R.C.L., Lamers, G.E.M., Oosterkamp, T.H., Abrahams, J.P.: A graphene Oxide·Streptavidin complex for biorecognition—towards affinity purification. Adv. Funct. Mater. **20**, 2857–2865 (2010)

18. Lu, Y., Lerner, M.B., Qi, Z.J., Mitala, J.J., Lim, J.H., Discher, B.M., Johnson, A.T.C.: Graphene-protein bioelectronic devices with wavelength-dependent photoresponse. Appl. Phys. Lett. **100**, 033110 (2012)

19. Myung, S., Solanki, A., Kim, C., Park, J., Kim, K.S., Lee, K.B.: Graphene-encapsulated nanoparticle-based biosensor for the selective detection of cancer biomarkers. Adv. Mater. **23**, 2221–2225 (2011)

20. Ohno, Y., Maehashi, K., Yamashiro, Y., Matsumoto, K.: Electrolyte-gated graphene field-effect transistors for detecting pH and protein adsorption. Nano Lett. **9**, 3318–3322 (2009)

21. Wei, H., Yang, W., Xi, Q., Chen, X.: Preparation of Fe_3O_4@graphene oxide core–shell magnetic particles for use in protein adsorption. Mater. Lett. **82**, 224–226 (2012)

22. Liu, Q., Shi, J., Cheng, M., Li, G., Cao, D., Jiang, G.: Preparation of graphene-encapsulated magnetic microspheres for protein/peptide enrichment and MALDI-TOF MS analysis. Chem. Commun. **48**, 1874–1876 (2012)

23. Xu, Y., Malkovskiy, A., Pang, Y.: A graphene binding-promoted fluorescence enhancement for bovine serum albumin recognition. Chem. Commun. **47**, 6662–6664 (2011)

24. Liu, K., Zhang, J., Yang, G., Wang, C., Zhu, J.-J.: Direct electrochemistry and electrocatalysis of hemoglobin based on poly(diallyldimethylammonium chloride) functionalized graphene sheets/room temperature ionic liquid composite film. Electrochem. Commun. **12**, 402–405 (2010)

25. Xu, H., Dai, H., Chen, G.: Direct electrochemistry and electrocatalysis of hemoglobin protein entrapped in graphene and chitosan composite film. Talanta **81**, 334–338 (2010)

26. Shi, Y., Huang, W.T., Luo, H.Q., Li, N.B.: A label-free DNA reduced graphene oxide-based fluorescent sensor for highly sensitive and selective detection of hemin. Chem. Commun. **47**, 4676–4678 (2011)

27. Hu, X., Mu, L., Wen, J., Zhou, Q.: Covalently synthesized graphene oxide-aptamer nanosheets for efficient visible-light photocatalysis of nucleic acids and proteins of viruses. Carbon **50**, 2772–2781 (2012)

28. Hong, J., Shah, N.J., Drake, A.C., DeMuth, P.C., Lee, J.B., Chen, J.Z., Hammond, P.T.: Graphene multilayers as gates for multi-week sequential release of proteins from surfaces. ACS Nano **6**, 81–88 (2012)

29. Lu, C.H., Li, J., Zhang, X.L., Zheng, A.X., Yang, H.H., Chen, X., Chen, G.N.: General approach for monitoring peptide-protein interactions based on graphene–peptide complex. Anal. Chem. **83**, 7276–7282 (2011)

30. Wang, X., Wang, C., Qu, K., Song, Y., Ren, J., Miyoshi, D., Sugimoto, N., Qu, X.: Ultrasensitive and selective detection of a prognostic indicator in early-stage cancer using graphene oxide and carbon nanotubes. Adv. Funct. Mater. **20**, 3967–3971 (2010)

31. Pazos, E., Torrecilla, D., Vazquez Lopez, M., Castedo, L., Mascarenas, J.L., Vidal, A., Vazquez, M.E.: Cyclin A probes by means of intermolecular sensitization of terbium-chelating peptides. J. Am. Chem. Soc. **130**, 9652–9653 (2008)

32. Feng, L., Wu, L., Wang, J., Ren, J., Miyoshi, D., Sugimoto, N., Qu, X.: Detection of a prognostic indicator in early-stage cancer using functionalized graphene-based peptide sensors. Adv. Mater. **24**, 125–131 (2012)

33. Wang, L., Zhu, C., Han, L., Jin, L., Zhou, M., Dong, S.: Label-free, regenerative and sensitive surface plasmon resonance and electrochemical aptasensors based on graphene. Chem. Commun. **47**, 7794–7796 (2011)

34. Gan, X., Yuan, R., Chai, Y., Yuan, Y., Cao, Y., Liao, Y., Liu, H.: 3,4,9,10-Perylenetetracarboxylic dianhydride functionalized graphene sheet as labels for ultrasensitive electrochemiluminescent detection of thrombin. Anal. Chim. Acta **726**, 67–72 (2012)

35. Bai, L., Yuan, R., Chai, Y., Zhuo, Y., Yuan, Y., Wang, Y.: Simultaneous electrochemical detection of multiple analytes based on dual signal amplification of single-walled carbon nanotubes and multi-labeled graphene sheets. Biomaterials **33**, 1090–1096 (2012)

36. Wang, Y., Yuan, R., Chai, Y., Yuan, Y., Bai, L.: In situ enzymatic silver enhancement based on functionalized graphene oxide and layer-by-layer assembled gold nanoparticles for ultrasensitive detection of thrombin. Biosens. Bioelectron. **38**, 50–54 (2012)

37. Wang, Y., Yuan, R., Chai, Y., Yuan, Y., Bai, L., Liao, Y.: A multi-amplification aptasensor for highly sensitive detection of thrombin based on high-quality hollow CoPt nanoparticles decorated graphene. Biosens. Bioelectron. **30**, 61–66 (2011)

38. Peng, K., Zhao, H., Wu, X., Yuan, Y., Yuan, R.: Ultrasensitive aptasensor based on graphene-3,4,9,10-perylenetetracarboxylic dianhydride as platform and functionalized hollow PtCo nanochains as enhancers. Sens. Actuators B-Chem. **169**, 88–95 (2012)

39. Xie, S., Chai, Y., Yuan, R., Bai, L., Yuan, Y., Wang, Y.: A dual-amplification aptasensor for highly sensitive detection of thrombin based on the functionalized graphene-Pd nanoparticles composites and the hemin/G-quadruplex. Anal. Chim. Acta **755**, 46–53 (2012)

40. Jiang, L., Yuan, R., Chai, Y., Yuan, Y., Bai, L., Wang, Y.: Aptamer-based highly sensitive electrochemical detection of thrombin via the amplification of graphene. Analyst **137**, 2415–2420 (2012)

41. Yuan, Y., Gou, X., Yuan, R., Chai, Y., Zhuo, Y., Ye, X., Gan, X.: Graphene-promoted 3,4,9,10-perylenetetracarboxylic acid nanocomposite as redox probe in label-free electrochemical aptasensor. Biosens. Bioelectron. **30**, 123–127 (2011)

42. Xie, S., Yuan, R., Chai, Y., Bai, L., Yuan, Y., Wang, Y.: Label-free electrochemical aptasensor for sensitive thrombin detection using layer-by-layer self-assembled multilayers with toluidine blue-graphene composites and gold nanoparticles. Talanta **98**, 7–13 (2012)

43. Wang, L., Zhu, J.B., Han, L., Jin, L.H., Zhu, C.Z., Wang, E.K., Dong, S.J.: Graphene-based aptamer logic gates and their application to multiplex detection. ACS Nano **6**, 6659–6666 (2012)
44. Chang, H., Tang, L., Wang, Y., Jiang, J., Li, J.: Graphene fluorescence resonance energy transfer aptasensor for the thrombin detection. Anal. Chem. **82**, 2341–2346 (2010)
45. Bi, S., Zhao, T., Luo, B.: A graphene oxide platform for the assay of biomolecules based on chemiluminescence resonance energy transfer. Chem. Commun. **48**, 106–108 (2012)
46. Sun, T., Wang, L., Li, N., Gan, X.: Label-free electrochemical aptasensor for thrombin detection based on the nafion@graphene as platform. Bioprocess Biosyst. Eng. **34**, 1081–1085 (2011)
47. Wang, Y., Xiao, Y., Ma, X., Li, N., Yang, X.: Label-free and sensitive thrombin sensing on a molecularly grafted aptamer on graphene. Chem. Commun. **48**, 738–740 (2012)
48. Zhao, J., Chen, G., Zhu, L., Li, G.: Graphene quantum dots-based platform for the fabrication of electrochemical biosensors. Electrochem. Commun. **13**, 31–33 (2011)
49. Du, M., Yang, T., Zhao, C., Jiao, K.: Electrochemical logic aptasensor based on graphene. Sens. Actuators B-Chem. **169**, 255–260 (2012)
50. Guo, Y., Jia, X., Zhang, S.: DNA cycle amplification device on magnetic microbeads for determination of thrombin based on graphene oxide enhancing signal-on electrochemiluminescence. Chem. Commun. **47**, 725–727 (2011)
51. Zhang, X., Li, S., Jin, X., Zhang, S.: A new photoelectrochemical aptasensor for the detection of thrombin based on functionalized graphene and CdSe nanoparticles multilayers. Chem. Commun. **47**, 4929–4931 (2011)
52. Zhang, J., Zhang, F., Yang, H., Huang, X., Liu, H., Guo, S.: Graphene oxide as a matrix for enzyme immobilization. Langmuir **26**, 6083–6085 (2010)
53. Zhang, Q., Qiao, Y., Zhang, L., Wu, S., Zhou, H., Xu, J., Song, X.-M.: Direct electrochemistry and electrocatalysis of horseradish peroxidase immobilized on water soluble sulfonated graphene film via self-assembly. Electroanalysis **23**, 900–906 (2011)
54. Zhang, Q., Yang, S., Zhang, J., Zhang, L., Kang, P., Li, J., Xu, J., Zhou, H., Song, X.-M.: Fabrication of an electrochemical platform based on the self-assembly of graphene oxide–multiwall carbon nanotube nanocomposite and horseradish peroxidase: direct electrochemistry and electrocatalysis. Nanotechnology **22**, 494010 (2011)
55. Zhou, K., Zhu, Y., Yang, X., Li, C.: Preparation and application of mediator-free H_2O_2 biosensors of graphene-Fe_3O_4 composites. Electroanalysis **23**, 862–869 (2011)
56. De, M., Chou, S.S., Dravid, V.P.: Graphene oxide as an enzyme inhibitor: modulation of activity of alpha-chymotrypsin. J. Am. Chem. Soc. **133**, 17524–17527 (2011)
57. Jin, L., Yang, K., Yao, K., Zhang, S., Tao, H., Lee, S.T., Liu, Z., Peng, R.: Functionalized graphene oxide in enzyme engineering: a selective modulator for enzyme activity and thermostability. ACS Nano **6**, 4864–4875 (2012)
58. Wu, L., Wang, J., Feng, L., Ren, J., Wei, W., Qu, X.: Label-free ultrasensitive detection of human telomerase activity using porphyrin-functionalized graphene and electrochemiluminescence technique. Adv. Mater. **24**, 2447–2452 (2012)
59. Shao, Q., Wu, P., Xu, X., Zhang, H., Cai, C.: Insight into the effects of graphene oxide sheets on the conformation and activity of glucose oxidase: towards developing a nanomaterial-based protein conformation assay. Phys. Chem. Chem. Phys. **14**, 9076–9085 (2012)
60. Zhang, Q., Wu, S., Zhang, L., Lu, J., Verproot, F., Liu, Y., Xing, Z., Li, J., Song, X.M.: Fabrication of polymeric ionic liquid/graphene nanocomposite for glucose oxidase immobilization and direct electrochemistry. Biosens. Bioelectron. **26**, 2632–2637 (2011)
61. Wang, K., Liu, Q., Guan, Q.M., Wu, J., Li, H.N., Yan, J.J.: Enhanced direct electrochemistry of glucose oxidase and biosensing for glucose via synergy effect of graphene and CdS nanocrystals. Biosens. Bioelectron. **26**, 2252–2257 (2011)
62. Zhou, Y., Liu, S., Jiang, H.-J., Yang, H., Chen, H.-Y.: Direct electrochemistry and bioelectrocatalysis of microperoxidase-11 immobilized on chitosan-graphene nanocomposite. Electroanalysis **22**, 1323–1328 (2010)

63. Bhunia, S.K., Jana, N.R.: Peptide-functionalized colloidal graphene via interdigited bilayer coating and fluorescence turn-on detection of enzyme. ACS Appl. Mater. Interfaces **3**, 3335–3341 (2011)

64. Zhou, Z., Zhu, C., Ren, J., Dong, S.: A graphene-based real-time fluorescent assay of deoxyribonuclease I activity and inhibition. Anal. Chim. Acta **740**, 88–92 (2012)

65. Lee, J., Kim, Y.K., Min, D.H.: A new assay for endonuclease/methyltransferase activities based on graphene oxide. Anal. Chem. **83**, 8906–8912 (2011)

66. Li, J., Lu, C.H., Yao, Q.H., Zhang, X.L., Liu, J.J., Yang, H.H., Chen, G.N.: A graphene oxide platform for energy transfer-based detection of protease activity. Biosens. Bioelectron. **26**, 3894–3899 (2011)

67. Zhang, M., Yin, B.C., Wang, X.F., Ye, B.C.: Interaction of peptides with graphene oxide and its application for real-time monitoring of protease activity. Chem. Commun. **47**, 2399–2401 (2011)

68. Jang, H., Kim, Y.K., Kwon, H.M., Yeo, W.S., Kim, D.E., Min, D.H.: A graphene-based platform for the assay of duplex-DNA unwinding by helicase. Angew. Chem. Int. Ed. **49**, 5703–5707 (2010)

69. Ohno, Y., Maehashi, K., Matsumoto, K.: Label-free biosensors based on aptamer-modified graphene field-effect transistors. J. Am. Chem. Soc. **132**, 18012–18013 (2010)

70. Mao, S., Yu, K., Lu, G., Chen, J.: Highly sensitive protein sensor based on thermally-reduced graphene oxide field-effect transistor. Nano Res. **4**, 921–930 (2011)

71. Mao, S., Lu, G., Yu, K., Bo, Z., Chen, J.: Specific protein detection using thermally reduced graphene oxide sheet decorated with gold nanoparticle-antibody conjugates. Adv. Mater. **22**, 3521–3526 (2010)

72. Loo, A.H., Bonanni, A., Ambrosi, A., Poh, H.L., Pumera, M.: Impedimetric immunoglobulin G immunosensor based on chemically modified graphenes. Nanoscale **4**, 921–925 (2012)

73. Xie, Y., Chen, A., Du, D., Lin, Y.: Graphene-based immunosensor for electrochemical quantification of phosphorylated p53 (S15). Anal. Chim. Acta **699**, 44–48 (2011)

74. Du, D., Wang, L., Shao, Y., Wang, J., Engelhard, M.H., Lin, Y.: Functionalized graphene oxide as a nanocarrier in a multienzyme labeling amplification strategy for ultrasensitive electrochemical immunoassay of phosphorylated p53 (S392). Anal. Chem. **83**, 746–752 (2011)

75. Lee, J.S., Joung, H.A., Kim, M.G., Park, C.B.: Graphene-based chemiluminescence resonance energy transfer for homogeneous immunoassay. ACS Nano **6**, 2978–2983 (2012)

76. Liu, K., Zhang, J.J., Wang, C., Zhu, J.J.: Graphene-assisted dual amplification strategy for the fabrication of sensitive amperometric immunosensor. Biosens. Bioelectron. **26**, 3627–3632 (2011)

77. Liu, Y., Feng, H., Wu, Y., Joshi, L., Zeng, X., Li, J.: Layer-by-layer assembly of chemical reduced graphene and carbon nanotubes for sensitive electrochemical immunoassay. Biosens. Bioelectron. **35**, 63–68 (2012)

78. Li, L.-L., Liu, K.-P., Yang, G.-H., Wang, C.-M., Zhang, J.-R., Zhu, J.-J.: Fabrication of graphene-quantum dots composites for sensitive electrogenerated chemiluminescence immunosensing. Adv. Funct. Mater. **21**, 869–878 (2011)

79. Wang, J., Han, H., Jiang, X., Huang, L., Chen, L., Li, N.: Quantum dot-based near-infrared electrochemiluminescent immunosensor with gold nanoparticle-graphene nanosheet hybrids and silica nanospheres double-assisted signal amplification. Anal. Chem. **84**, 4893–4899 (2012)

80. Su, B., Tang, J., Huang, J., Yang, H., Qiu, B., Chen, G., Tang, D.: Graphene and nanogold-functionalized immunosensing interface with enhanced sensitivity for one-step electrochemical immunoassay of alpha-fetoprotein in human serum. Electroanalysis **22**, 2720–2728 (2010)

81. Su, B., Tang, D., Li, Q., Tang, J., Chen, G.: Gold-silver-graphene hybrid nanosheets-based sensors for sensitive amperometric immunoassay of alpha-fetoprotein using nanogold-enclosed titania nanoparticles as labels. Anal. Chim. Acta **692**, 116–124 (2011)

82. Zhang, B., Tang, D., Liu, B., Chen, H., Cui, Y., Chen, G.: GoldMag nanocomposite-functionalized graphene sensing platform for one-step electrochemical immunoassay of alpha-fetoprotein. Biosens. Bioelectron. **28**, 174–180 (2011)

83. Wei, Q., Mao, K., Wu, D., Dai, Y., Yang, J., Du, B., Yang, M., Li, H.: A novel label-free electrochemical immunosensor based on graphene and thionine nanocomposite. Sens. Actuators B-Chem. **149**, 314–318 (2010)

84. Du, D., Zou, Z., Shin, Y., Wang, J., Wu, H., Engelhard, M.H., Liu, J., Aksay, I.A., Lin, Y.: Sensitive immunosensor for cancer biomarker based on dual signal amplification strategy of graphene sheets and multienzyme functionalized carbon nanospheres. Anal. Chem. **82**, 2989–2995 (2010)

85. Tang, J., Tang, D., Niessner, R., Chen, G., Knopp, D.: Magneto-controlled graphene immunosensing platform for simultaneous multiplexed electrochemical immunoassay using distinguishable signal tags. Anal. Chem. **83**, 5407–5414 (2011)

86. Guo, Z., Hao, T., Duan, J., Wang, S., Wei, D.: Electrochemiluminescence immunosensor based on graphene-CdS quantum dots-agarose composite for the ultrasensitive detection of alpha fetoprotein. Talanta **89**, 27–32 (2012)

87. Liu, M., Zhao, H., Quan, X., Chen, S., Fan, X.: Distance-independent quenching of quantum dots by nanoscale-graphene in self-assembled sandwich immunoassay. Chem. Commun. **46**, 7909–7911 (2010)

88. Eissa, S., Tlili, C., L'Hocine, L., Zourob, M.: Electrochemical immunosensor for the milk allergen beta-lactoglobulin based on electrografting of organic film on graphene modified screen-printed carbon electrodes. Biosens. Bioelectron. **38**, 308–313 (2012)

89. Wei, Q., Xin, X., Du, B., Wu, D., Han, Y., Zhao, Y., Cai, Y., Li, R., Yang, M., Li, H.: Electrochemical immunosensor for norethisterone based on signal amplification strategy of graphene sheets and multienzyme functionalized mesoporous silica nanoparticles. Biosens. Bioelectron. **26**, 723–729 (2010)

90. Chen, H., Tang, D., Zhang, B., Liu, B., Cui, Y., Chen, G.: Electrochemical immunosensor for carcinoembryonic antigen based on nanosilver-coated magnetic beads and gold-graphene nanolabels. Talanta **91**, 95–102 (2012)

91. Li, Y., Yang, W.K., Fan, M.Q., Liu, A.: A sensitive label-free amperometric CEA immunosensor based on graphene-nafion nanocomposite film as an enhanced sensing platform. Anal. Sci. **27**, 727–731 (2011)

92. Tu, W., Wang, W., Lei, J., Deng, S., Ju, H.: Chemiluminescence excited photoelectrochemistry using graphene-quantum dots nanocomposite for biosensing. Chem. Commun. **48**, 6535–6537 (2012)

93. Cheng, Y., Yuan, R., Chai, Y., Niu, H., Cao, Y., Liu, H., Bai, L., Yuan, Y.: Highly sensitive luminol electrochemiluminescence immunosensor based on ZnO nanoparticles and glucose oxidase decorated graphene for cancer biomarker detection. Anal. Chim. Acta **745**, 137–142 (2012)

94. Qu, F., Lu, H., Yang, M., Deng, C.: Electrochemical immunosensor based on electron transfer mediated by graphene oxide initiated silver enhancement. Biosens. Bioelectron. **26**, 4810–4814 (2011)

95. Wang, Z., Shang, K., Dong, J., Cheng, Z., Ai, S.: Electrochemical immunoassay for subgroup J of avian leukosis viruses using a glassy carbon electrode modified with a film of poly (3-thiophene boronic acid), gold nanoparticles, graphene and immobilized antibody. Microchim. Acta **179**, 227–234 (2012)

96. Eissa, S., Zourob, M.: A graphene-based electrochemical competitive immunosensor for the sensitive detection of okadaic acid in shellfish. Nanoscale **4**, 7593–7599 (2012)

97. Yang, M., Javadi, A., Gong, S.: Sensitive electrochemical immunosensor for the detection of cancer biomarker using quantum dot functionalized graphene sheets as labels. Sens. Actuators B-Chem. **155**, 357–360 (2011)

98. Yang, M., Javadi, A., Li, H., Gong, S.: Ultrasensitive immunosensor for the detection of cancer biomarker based on graphene sheet. Biosens. Bioelectron. **26**, 560–565 (2010)

99. Mao, K., Wu, D., Li, Y., Ma, H., Ni, Z., Yu, H., Luo, C., Wei, Q., Du, B.: Label-free electrochemical immunosensor based on graphene/methylene blue nanocomposite. Anal. Biochem. **422**, 22–27 (2012)

100. Liu, F., Zhang, Y., Ge, S., Lu, J., Yu, J., Song, X., Liu, S.: Magnetic graphene nanosheets based electrochemiluminescence immunoassay of cancer biomarker using CdTe quantum dots coated silica nanospheres as labels. Talanta **99**, 512–519 (2012)

101. Xu, S., Liu, Y., Wang, T., Li, J.: Positive potential operation of a cathodic electrogenerated chemiluminescence immunosensor based on luminol and graphene for cancer biomarker detection. Anal. Chem. **83**, 3817–3823 (2011)

102. Yang, M., Gong, S.: Immunosensor for the detection of cancer biomarker based on percolated graphene thin film. Chem. Commun. **46**, 5796–5798 (2010)

103. Li, T., Yang, M., Li, H.: Label-free electrochemical detection of cancer marker based on graphene–cobalt hexacyanoferrate nanocomposite. J. Electroanal. Chem. **655**, 50–55 (2011)

104. Qu, F., Li, T., Yang, M.: Colorimetric platform for visual detection of cancer biomarker based on intrinsic peroxidase activity of graphene oxide. Biosens. Bioelectron. **26**, 3927−3931 (2011)

105. Han, J., Zhuo, Y., Chai, Y., Yuan, R., Zhang, W., Zhu, Q.: Simultaneous electrochemical detection of multiple tumor markers based on dual catalysis amplification of multi-functionalized onion-like mesoporous graphene sheets. Anal. Chim. Acta **746**, 70–76 (2012)

106. Xia, Y., Gao, P., Bo, Y., Wang, W., Huang, S.: Immunoassay for SKOV-3 human ovarian carcinoma cells using a graphene oxide-modified electrode. Microchim. Acta **179**, 201–207 (2012)

107. Tang, J., Hou, L., Tang, D., Zhou, J., Wang, Z., Li, J., Chen, G.: Magneto-controlled electrochemical immunoassay of brevetoxin B in seafood based on guanine-functionalized graphene nanoribbons. Biosens. Bioelectron. **38**, 86–93 (2012)

108. Tian, J., Zhao, H., Zhao, H., Quan, X.: Photoelectrochemical immunoassay for microcystin-LR based on a fluorine-doped tin oxide glass electrode modified with a CdS-graphene composite. Microchim. Acta **179**, 163–170 (2012)

109. Bai, J., Lai, Y., Jiang, D., Zeng, Y., Xian, Y., Xiao, F., Zhang, N., Hou, J., Jin, L.: Ultrasensitive electrochemical immunoassay based on graphene oxide-Ag composites for rapid determination of clenbuterol. Analyst **137**, 4349–4355 (2012)

110. Cai, Y., Li, H., Du, B., Yang, M., Li, Y., Wu, D., Zhao, Y., Dai, Y., Wei, Q.: Ultrasensitive electrochemical immunoassay for BRCA1 using BMIM.BF(4)-coated SBA-15 as labels and functionalized graphene as enhancer. Biomaterials **32**, 2117–2123 (2011)

111. Ge, S., Jiao, X., Chen, D.: Ultrasensitive electrochemical immunosensor for CA 15-3 using thionine-nanoporous gold-graphene as a platform and horseradish peroxidase-encapsulated liposomes as signal amplification. Analyst **137**, 4440–4447 (2012)

112. Lu, J., Liu, S., Ge, S., Yan, M., Yu, J., Hu, X.: Ultrasensitive electrochemical immunosensor based on Au nanoparticles dotted carbon nanotube-graphene composite and functionalized mesoporous materials. Biosens. Bioelectron. **33**, 29–35 (2012)

113. Li, R., Wu, D., Li, H., Xu, C., Wang, H., Zhao, Y., Cai, Y., Wei, Q., Du, B.: Label-free amperometric immunosensor for the detection of human serum chorionic gonadotropin based on nanoporous gold and graphene. Anal. Biochem. **414**, 196–201 (2011)

114. Yang, X.Y., Zhang, X.Y., Liu, Z.F., Ma, Y.F., Huang, Y., Chen, Y.: High-efficiency loading and controlled release of doxorubicin hydrochloride on graphene oxide. J. Phys. Chem. C **112**, 17554–17558 (2008)

Chapter 4
Graphene for Glucose, Dopamine, Ascorbic Acid, and Uric Acid Detection

Abstract Since every atom in graphene single sheet is a surface atom, molecular interaction and electron transport through graphene can be highly sensitive to adsorbed biomolecules. Graphene materials act as good candidates for glucose sensing due to the high surface area, excellent conductivity, and small band gap, which are favorable for biomolecules loading and electrons conducting. Generally, graphene-based platforms for glucose determination could be categorized into two kinds, namely enzyme catalysis and non-enzyme catalysis. The enzyme catalysis shows high sensitivity and selectivity. However, the inevitable drawbacks of instability originating from the intrinsic nature of the enzyme, as well as the critical operational conditions and complicated immobilization procedure, may limit the analytical applications. These drawbacks could be overcome in non-enzyme catalytic biosensors, which are stable, simple, reliable, and cost-effective. Detailed descriptions are illustrated in the following. The concentrations of dopamine (DA), ascorbic acid (AA), and uric acid (UA) in human body are important in the diagnosis, monitoring, prevention, and treatments of some certain diseases, such as HIV infections, schizophrenia, Parkinson, hyperuricemia, and a type of arthritis. Then various graphene platforms for the detection and quantification of DA, AA, and UA are also demonstrated.

Keywords Graphene · Glucose · Enzyme · Dopamine · Ascorbic acid · Uric acid

4.1 Glucose Detection

4.1.1 Catalysis by Enzymes

Glucose detection plays an important role in biotechnology, life science, food industry, and clinical diagnostics. Diabetes is a worldwide public health problem and one of the leading causes of death and disability in the world. In 2000, it was estimated that 2.8 % of the world population was affected by diabetes mellitus, a disease with hyperglycemia (i.e., elevated blood glucose level) as the major symptom

[27]. The diagnosis and management of this disease requires a tight monitoring of blood glucose level [28]. Back in 1962, Clark and Lyons [29] first illustrated the enzyme-based determination of glucose using a Cuprophane–GOD–Cuprophane membrane and a pH electrode. Glucose diffusing through the membrane was converted to gluconic acid, which then diffused both toward the pH sensitive glass and back into the donor solution. This caused a drop in pH, the magnitude of which was largely determined by the concentration of glucose, the rate of the flow and buffering capacity of the glucose-containing solution, temperature, and pH. Ever since then, great efforts have been devoted to the design and fabrication of glucose biosensors for sensitive, selective, and precise glucose determination. In most of the enzyme-based glucose biosensors, glucose oxidase (GOD) has received considerable attention and is used as the model enzyme, due to its high catalytic ability and selectivity to glucose. It could catalyze glucose to gluconolactone in the presence of molecular oxygen, simultaneously producing hydrogen peroxide (flowing equations). Then glucose is generally quantified by electrochemical oxidation of the liberated hydrogen peroxide or less commonly by the electrochemical reduction of consumed oxygen [27].

$$\text{Glucose} + \text{GOD-FAD} \rightarrow \text{gluconolactone} + \text{GOD-FADH}_2$$

$$\text{GOD-FAD} + 2\text{H}^+ + 2\text{e}^- \leftrightarrow \text{GOD-FADH}_2$$

$$\text{GOD-FADH}_2 + \text{O}_2 \rightarrow \text{GOD-FAD} + \text{H}_2\text{O}_2$$

$$\text{H}_2\text{O}_2 \rightarrow 2\text{H}^+ + \text{O}_2 + 2\text{e}^-$$
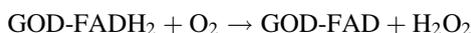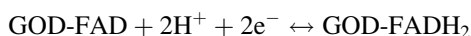
Two major limitations in immobilizing GOD on electrode surface still remain challenging, including the poor direct electron transfer (DET) between the active site of the enzyme and the electrode and the enzyme leaching. As the active redox center of GOD, flavin adenine dinucleotide (FAD) is deeply embedded in a protective protein shell, which makes the DET with electrodes difficult. Realizing the DET between the redox enzyme and electrode seems to be extremely important and urgent in electrochemical glucose detection. Various materials, such as CNT, AuNPs, ILs, and metal oxides [30–34], have been developed as the substrates for GOD immobilization and glucose detection. Recently, graphene materials act as good candidates for glucose sensing due to the high surface area, excellent conductivity, and small band gap, which are favorable for biomolecules loading and electrons conducting. Since every atom in graphene single sheet is a surface atom, molecular interaction and electron transport through graphene can be highly sensitive to adsorbed biomolecules. Various graphene-based materials have been used in constructing glucose biosensors (Table 4.1).

Exploiting their intrinsic properties, graphene and GO have been utilized as the matrixes for GOD immobilization and glucose detection [1–4]. It is found that graphene can remarkably enhance the DET kinetics of GOD, which may be ascribed to graphene's unique electronic structure and the surface defects. These defects result in high density of electronic states near the Fermi level, leading to the

Table 4.1 Enzyme-based graphene biosensors for glucose detection

Material	Potential (V)	Response time (s)	Linear range	Sensitivity	LOD	K_m (mM)	K_s (s^{-1})	Reference
CRGO/GOD	−0.2	–	0.01–10 mM	20.21 μA mM^{-1} cm^{-2}	2 μM	–	–	[1]
RGO-GOD	−0.44	<5	0.1–27 mM	1.85 μA mM^{-1} cm^{-2}	–	–	4.8	[2]
GO-GOD	0.4	–	∼22 mM	8.045 mA M^{-1} cm^{-2}	–	–	–	[3]
Graphene–GOD	−0.47	–	0.1–10 mM	110 ± 3 μA mM^{-1} cm^{-2}	10 ± 2 μM	–	2.68	[4]
N-doped graphene/GOD	−0.15	–	0.1–1.1 mM	–	–	–	–	[5]
Graphene–PFIL–GOD	−0.49	–	2–14 mM		–	–	–	[6]
Graphene–IL–GOD	−0.48	–	2–16 mM		–	–	–	[7]
Graphene/AuNP/CS/GOD	−0.2	–	2–10 mM		180 μM	–	–	[8]
G-AuNP/CdTe-CdS/AuNP/GOD	−0.2	0.045	0.01–10 nM	5,762.8 nA nM^{-1} cm^{-2}	3 pM	5.24 × 10^{-6}	–	[9]
Graphene–CdS/GOD	–	–	2–16 mM	1.76 μA mM^{-1} cm^{-2}	0.7 mM	1.6	–	[10]
Graphene–CS/PdNPs/GOD	0.7	10	0.001–1 mM	31.2 μA mM^{-1} cm^{-2}	0.2 μM	1.2	–	[11]
CS/FGS/Pt/GOD	0.4	–	∼5 mM		0.6 μM	–	–	[12]
Graphene–AuNP/GOD	−0.2	–	0.1–10 mM		35 μM	4.73	7.74 ± 0.16	[13]
ERGO–AuPdNP-GOD	–	–	∼3.5 mM	266.6 μA mM^{-1} cm^{-2}	6.9 μM	10.5	–	[14]
Graphene–DNA/GOD/AuNP	–	–	0.8–50 μM	24 mA mM^{-1}	0.3 μM	–	–	[15]
RGO-PAMAM-Ag/GOD	−0.25	–	0.032–1.89 mM	75.72 μA mM^{-1} cm^{-2}	4.5 μM	9.64	8.59	[16]
GO/SiO$_2$/AgNP/GOD	–	–	2–12 mM		310 μM	–	–	[17]

(continued)

Table 4.1 (continued)

Material	Potential (V)	Response time (s)	Linear range	Sensitivity	LOD	K_m (mM)	K_s (s^{-1})	Reference
Nafion/RGO-GOD	−0.2	3	0–20 mM	3.8 μA mM^{-1} cm^{-2}	170 μM	–	3.78	[18]
(IL-RGO/S-RGO)$_n$/GOD/nafion	–	–	10–500 μM	–	3.33 μM	0.325	–	[19]
CS/Graphene/GOD	–	–	0.08–12 mM	37.93 μA mM^{-1} cm^{-2}	0.02 mM	4.4	2.83	[20]
Graphene–CS–GOD	–	–	2–22 mM	–	20 μM	–	–	[21]
GNS-CNS/GOD	–	–	0.4–20 mM	–	0.1 mM	0.12	2.64	[22]
APTES-RGO-GOD	–	–	0–24 mM	–	–	–	–	[23]
Ppy/Graphene–GOD	0.2	11 ± 1	2–40 μM	–	3 ± 0.5 μM	–	–	[24]
(PEI/PAA-graphene)$_3$(PEI/GOD)$_5$	0.9		0–10 mM	0.261 μA mM^{-1} cm^{-2}	0.168 mM	–	–	[25]
TiO$_2$-graphene/GOD	−0.6	–	0–8 mM	6.2 μA mM^{-1} cm^{-2}	–	–	–	[26]

enhancement of DET kinetics. A study was intended to intrinsically change the density of electronic states of graphene by nitrogen doping [5]. Using nitrogen plasma treatment, the Fermi potential of graphene was changed and the electron transfer efficiency was enhanced. Higher redox peak currents and faster electron transfer kinetics of GOD were obtained on *N*-doped graphene than on graphene.

There are two main important parameters to evaluate the performance of GOD on modified electrode surface. The DET constant (K_s) of GOD on modified electrode can be estimated by using the Laviron model [35] at high scan rates:

$$\text{Log}\, K_s = \alpha \text{Log}(1-\alpha) + (1-\alpha)\text{Log}\,\alpha - \text{Log}\frac{RT}{nFv} - \frac{\alpha(1-\alpha)nF\Delta E_p}{2.3RT}$$

where K_s is the electron transfer rate constant, α is the charge transfer coefficient, which could be estimated from the plots of E_{pa} and E_{pc} versus the logarithm of the scan rates with the line slopes of $2.3RT/(1-\alpha)nF$ and $-2.3RT/\alpha nF$ at high scan rates, R is the universal gas constant, T is the temperature, n is the number of electrons transferred, F is the Faraday constant, v is the scan rate, ΔE_p is the peak separation of the FAD/FADH$_2$ redox couple.

The apparent Michalis–Menten constant—K_m, an indicator of enzyme–substrate reaction kinetics, is often used to evaluate the biological activity of the immobilized enzyme, which can be calculated from the Lineweaver-Burk equation [36]:

$$\frac{1}{i_{ss}} = \frac{K_m}{i_{max}}\frac{1}{C} + \frac{1}{i_{max}}$$

where i_{ss} is the steady-state current after the addition of substrate, i_{max} is the maximum current measured under saturated condition, C is the bulk concentration of substrate. The smaller K_m value indicates that the immobilized enzyme possesses higher enzymatic activity.

As in the sensing of other biomolecules, the aggregation of graphene sheets needs to be perfectly resolved prior to glucose detection. Our group is among the first ones to carry out well-dispersed graphene for constructing glucose biosensors [6–8]. To solve this issue, we firstly used polyvinylpyrrolidone (PVP) to protect graphene, and then polyethylenimine-functionalized ionic liquid (PFIL) to disperse PVP/graphene. PFIL had good film stability and high ionic conductivity for enhanced electrochemical response. Besides, the high biocompatibility and exchangeability of the counterions in PFIL were much favorable for further immobilization of biomolecules, such as negatively charged GOD. A novel PVP-protected graphene/PFIL/GOD electrochemical biosensor was constructed for the DET of GOD and glucose biosensing [6]. The direct electrochemistry of GOD at PFIL-graphene electrode was investigated with CV (Fig. 4.1a), which exhibited a pair of well-defined redox peaks with formal potential ($E^{o\prime}$) −0.43 V (vs. Ag/AgCl in saturated KCl) and cathodic to anodic current intensity ratio ∼1. This was the characteristic reversible electron transfer process of FAD in GOD, which underwent
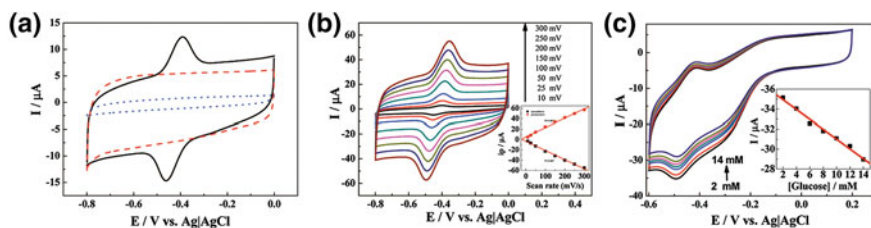
Fig. 4.1 a CVs of graphene–PFIL (*dashed*), graphite–GOD-PFIL (*dotted*), and graphene–GOD-PFIL (*solid*)-modified electrodes in 0.05 M PBS solution (pH = 7.4) saturated with N_2 at a scan rate of 0.05 V/s. **b** CVs at various scan rates from 0.01, 0.025, 0.05, 0.10, 0.15, 0.20, and 0.25 to 0.3 V/s, respectively. *Inset* Plot of peak current (i_p) versus scan rate. **c** CV measurements at the graphene–GOD–PFIL modified GC electrode in various concentrations of glucose PBS solution saturated with O_2: 2, 4, 6, 8, 10, 12, and 14 mM from outer to inner. The *inset* is the calibration curve (R = 0.994) corresponding to amperometric responses at −0.49 V. Scan rate: 0.05 V/s. Reprinted with permission from Ref. [6] Copyright 2009 American Chemical Society

a redox reaction with two protons and two electrons exchanged. From the peak currents and scan rate, the redox process of GOD in the composite was a reversible and surface-confined process (Fig. 4.1b). Finally, the graphene–PFIL–GOD electrode was applied to glucose detection as shown in Fig. 4.1c. The linear glucose response from 2 to 14 mM on graphene–PFIL–GOD electrode was suitable for practical application in determining blood glucose level, which is maintained between about 4 and 6 mM. In the following studies, another IL, amine-terminated ionic liquid (NH_2-IL), was covalently anchored on GO *via* epoxide ring-opening reaction [7]. The graphene-IL provided a favorable microenvironment for the DET of GOD, which could be used as an amperometric biosensor for routine analysis of glucose in real blood serum samples. Later, based on the synergistic effect of graphene and AuNPs, both the reduction of H_2O_2 and O_2 were achieved at graphene/AuNP/CS/GOD electrode, which exhibited good response to glucose [8].

By incorporating nanoparticles, such as quantum dots [9, 10], Pd [11], Pt [12], Au [13–15], and Ag [16], into graphene sheets, the resulting hybrids possess excellent conductivity and ultrafast electron transfer rate. Using CdTe-CdS core–shell quantum dots as ultrafast electron transfer relay, Gu and coworkers fabricated an electrochemical glucose biosensor with low LOD of 3 pM and high sensitivity of 5,762.8 nA nM^{-1} cm^{-2} [9]. The K_m value reached as low as 5.24×10^{-6} mM, which was smaller than most of the graphene-based glucose biosensors. These metal nanoparticle-modified graphene exhibited high performance toward DET of GOD and glucose detection based on the high electrocatalytic ability of noble metals. However, the supply of these noble metals may be a restriction in the long run for their rare amount. Other biocompatible materials, such as nafion [18, 19], chitosan [20, 21], carbon nanospheres [22], silane [23], Ppy [24], PEI [25], and TiO_2 [26], have also been adopted as components in graphene-based glucose biosensors. For instance, Yin et al. [22] devised one-step green preparation of graphene nanosheets–carbon nanospheres mixture (GNS-CNS) method. They revealed that GNS-CNS could provide a unique microenvironment for GOD to maintain its bioactivity

and facilitate the electron transfer between GOD and electrode. The small K_m value of 0.12 mM indicated that the immobilized GOD possessed high enzymatic activity and high affinity to glucose. The K_s value of 2.64 s^{-1} indicated fast electron transfer kinetics process.

4.1.2 Non-enzymatic Catalysis

Enzyme-based glucose detection shows high sensitivity and selectivity. However, the inevitable drawbacks of instability originating from the intrinsic nature of the enzyme as well as the critical operational conditions and complicated immobilization procedure may limit their analytical applications. Moreover, the catalytic activity of enzyme is easily affected by environmental conditions, such as temperature, pH, humidity, ionic detergents, and toxic chemicals. These drawbacks of the enzyme-based biosensors and the growing need for a stable, simple, reliable, and cost-effective sensor for glucose, particularly in the biomedical field, have lead to the emergence of a new generation (also called the fourth generation) of amperometric glucose sensors, known as 'non-enzymatic' or 'enzyme-free' glucose sensors, that is, not involving any enzyme [27]. In the field of non-enzymatic glucose sensor, the pioneering work was done in 1909 by Walther Loeb, who electrocatalytically oxidized glucose in H_2SO_4 at a lead anode. In spite of decades of research in this field, the practical application of non-enzymatic glucose sensors was prevented due to the lack of selectivity, sluggish kinetics of glucose oxidation at many of the bare electrodes, and fouling of electrode surface by the constituents of real samples, such as chloride ions and proteins. With introducing of nanomaterials, modified electrodes have been widely used in non-enzymatic glucose sensing to alleviate the drawbacks as mentioned above. Majority of the non-enzymatic sensors rely on the current response of glucose oxidation directly at the electrode surface, the mechanism of which considerably depends on the electrode material used. Two models, namely activated chemisorptions model [37] and incipient hydrous oxide/adatom mediator model [38] have been proposed to explain the mechanism of electro-oxidation of glucose at various electrode materials.

As above mentioned, the unique properties of graphene make it an ideal platform for biosensor construction in non-enzymatic glucose detection field. As an example, Mallesha et al. [27] used concentrated HNO_3 to treat graphene, which resulted in graphene with carboxylic and phenolic groups. The functionalized graphene-modified graphite electrode exhibited good sensitivity, stability, and shelf life toward glucose in alkaline medium. Moreover, in the interference studies (applied potential + 0.4 V), this proposed biosensor exhibited good selectivity toward glucose in the presence of ascorbic acid (AA), uric acid (UA), and dopamine (DA), which are the most common and potentially important interferents for a glucose biosensor in a clinical setting because these substances are co-oxidized at similar potentials, producing noise anodic current and also reducing the sensitivity.
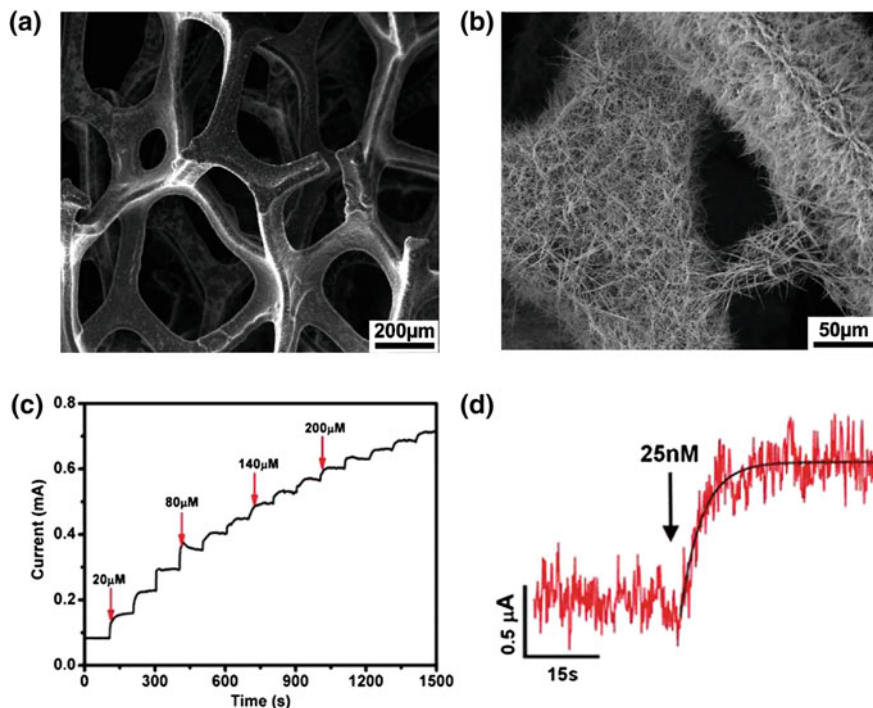
Fig. 4.2 SEM images of **a** 3D graphene foam and **b** 3D graphene/Co$_3$O$_4$ nanowire composite. **c** Amperometric response of the composite electrode (holding at 0.58 V) upon addition of glucose to increasing concentrations. **d** Amperometric response to 25 nM glucose. An exponential fitting with a time constant of ~3.7 s was shown. Reprinted with permission from Ref. [39] Copyright 2012 American Chemical Society

By using graphene as an excellent 2D support, graphene–metal (or metal oxide) nanocomposite materials have aroused tremendous attention in non-enzymatic glucose sensing for the property combination of two components. Various metal oxide and metal (or metal alloy), such as Co$_3$O$_4$ [39, 40], Ni(OH)$_2$ [41], NiO [28, 42], Ni [43], Pd [44, 45], Cu [46], PtNi [47], and Au–Pt [48], have been loaded on graphene for direct glucose detection based on the their electrochemical redox behaviors or the high electrocatalytic ability. For instance, Dong and coworkers fabricated 3D graphene/Co$_3$O$_4$ composite for electrochemical glucose detection (Fig. 4.2) [39]. In alkaline medium, Co$_3$O$_4$ underwent the following electrochemical reactions:

$$Co_3O_4 + OH^- + H_2O \leftrightarrow 3CoOOH + e^-$$

$$CoOOH + OH^- \leftrightarrow CoO_2 + H_2O + e^-$$
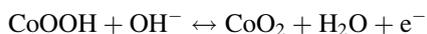
With the introduction of glucose, CoO_2 catalyzed glucose to gluconolactone by:

$$2CoO_2 + glucose \rightarrow 2CoOOH + gluconolactone$$

This composite showed an ultrahigh sensitivity of 3.39 mA mM^{-1} cm^{-2} and a remarkable low LOD of <25 nM (S/N = 8.5). The authors illustrated that, in the composite formation, graphene served as a 3D support with large capacity to uniformly anchor Co_3O_4. The rapid charge transfer of defect-free graphene foam, exceptionally electrochemical and electrocatalytic properties of Co_3O_4 nanowires, and the enormous accessible active area of the composite all contributed to the high performance toward electrochemical glucose detection. What's more, the synergistic co-operation between graphene and metal oxides promises many novel properties and performances. Using the abundant surface functional groups of GO as the reactive sites for the nucleation and binding of noble metal nanoparticles, Gao et al. [47] reported a facile one-step ultrasonication-assisted electrochemical method to synthesize graphene/PtNi composite. Well-dispersed PtNi alloy with high density was loaded on the effectively electrochemically reduced GO. Comparing to PtNi alloy, PtNi-chemically reduced GO, and PtNi-SWNT, the graphene/PtNi-modified electrode exhibited smaller electron transfer resistances and larger electrochemically active surface area. When used for non-enzymatic glucose detection, the graphene/PtNi composite exhibited high selectivity, superior resistance to poisoning, rapid response, and excellent stability, etc.

Besides the commonly used electrochemical methods, fluorescent [49], FET [50], and colorimetric [51, 52] strategies have also been adopted for glucose detection. In a fluorescent manner, Zhang and coworkers designed a new glucose detection platform based on the FRET between $NaYF_4$:Yb,Er upconverting phosphors (UCP) and GO [49]. Different from previously reported FRET models based on π–π stacking interaction, in their design, donor and acceptor were brought into FRET proximity through specific molecular recognition. ConA and chitosan (CS) were covalently attached to UCP and GO, respectively. The known tight binding of ConA with CS brought UCP and GO into appropriate proximity and hence induced energy transfer. Thereafter, the FRET process was inhibited (in part) because of competition between glucose and CS for ConA, which served as foundation of glucose sensing. Low LOD of 0.025 μM was calculated, and this strategy possessed high reproducibility and specificity. In a recent report, CVD-grown graphene was functionalized with the linker molecules to immobilize enzymes that induced the catalytic response of glucose [50]. Through measurements of the Dirac point shift and differential drain-source current, the graphene-based FET sensor could detect glucose levels in the range of 3.3–10.9 mM, which mostly covered the reference range of medical examination or screen test for diabetes diagnostic. Based on the intrinsic peroxidase catalytic activity, both GO–COOH [51] and GO–Fe_3O_4 [52] catalyzed the reduction of peroxidase substrate 3,3,5,5-tetramethylbenzidine (TMB) in the presence of H_2O_2 to produce a blue color. In the presence of GOD, colorimetric detection of glucose was sensitively and selectively detected. Kinetic analysis indicated that the catalysis followed typical Michaelis–Menten kinetics and a ping-pong mechanism.

4.2 DA, AA, and UA Detection

Dopamine, ascorbic acid, and uric acid are compounds of great biological and chemical interest and play a potential role in the metabolic system of human bodies. Dopamine (DA) is a monoamine neurotransmitter found in brain and is essential for the normal functions of the central nervous system. Ascorbic acid (AA) is important in health care of human beings. It is especially essential to the skin, connective tissues, and immune system. Uric acid (UA) is the final oxidation product of urine metabolism and is excreted in urine. Detection and quantification of DA, AA, and UA are important in diagnoses, monitoring, prevention, and treatments of some certain diseases such as HIV infections, schizophrenia, Parkinson, hyperuricemia, and a type of arthritis. Therefore, determination of these three species is of great significance not only in biomedical chemistry and neurochemistry but also for diagnostic and pathological investigations.

Back in 1976, Adams [53] described a number of electroanalytical techniques that were developed to investigate the role of neurotransmitters in the brain. It inspired many people to get involved in this research. Twelve years later, Wightman and coworker reported the use of in vivo probes, especially voltammetric microelectrodes, to monitor dynamics of neurochemical events in the extracellular space of the brain [54]. Especially, it represented that rapid, simple, and sensitive electrochemical methods have shown the great potential in neurotransmission detection. While, it is well known that at traditional bare electrodes, DA, AA, and UA exhibit oxidation peaks at potentials very close to each other, resulting in an overlapping voltammetric response. Moreover, high overpotentials are usually required for these analytes to undergo electrochemical oxidation at bare electrodes, and the electrode surface suffers fouling effect due to the accumulation of oxidation products. The sensitive and selective detection of one in the presence of the other two species or their simultaneous determination has been the major goal of many researches. Using nanomaterial-modified electrodes as platforms, electrochemical biosensors have been widely designed and used in these detections in recent years. It is always attractive to develop new nanomaterials or improve their properties to meet the demand.

To realize this, a new material, multilayer graphene nanoflake films (MGNFs) were fabricated on Si substrate using microwave-assisted plasma CVD without metal catalysts or any surface pretreatments [55]. The MGNFs were made of highly graphitized knife-edge nanoflakes with a 2–3-nm-thick sharp edge and had a preferentially vertical orientation relative to the Si substrate. It was found that the MGNFs possessed superior electron transfer kinetics, which could be ascribed to the abundance of edge planes and defects (such as kinks, steps, vacancies, and dangling bonds), unique electronic structure of graphene and the good electrical contact with Si. These edge defects could have different electrochemical interaction potential with the biomolecules of interest. They could also be locally negatively charged due to structural motifs, unpaired electrons, or surface polarizations, then repelled UA and AA anions and formed a molecular sieve permeable only to cationic DA. Therefore,

the MGNFs demonstrated well-resolved simultaneous discrimination of DA, AA, and UA as well as the sensing ability of DA with the detection limit of 0.17 μM. The biosensing performance was superior to all other untreated, unmodified carbon-based electrodes and was comparable only to the edge plane pyrolytic graphite (EPPG). Based on edge-plane defects, anodized epitaxial graphene (EG), consisting of oxygen-related defects, was also found to show enhanced electroanalytical performances toward DA ($pK_a = 8.87$), AA ($pK_a = 4.17$), and UA ($pK_a = 3.70$) in neutral condition [56]. Rich edge defects lead to sufficient density of states (DOS) near the Fermi level, which are responsible for the fast electron transfer process. As far as the possible effect of the surface oxygen functional groups on the simultaneous determination of such biomolecules was concerned very recently, it was found that the ratio of O to C (O/C) was very important in the determination of DA, AA, and UA. Since the type and quantity of oxygen groups of graphene play significant roles in determining its unique properties, the changes in composition and structure would inevitably affect the electrochemical behavior. Statistical results indicated that different oxygen functional groups play entirely distinct roles. Particularly, –C=O on the basal plane hindered AA oxidation more seriously and –COOH on the edges accelerated the electron transfer of DA faster than AA in the electrocatalytic oxidation process on electrochemically reduced graphene-modified electrode [57]. By adjusting the electrochemical reduction conditions and tuning the oxygen groups, sole and simultaneous DA and AA detection would be achieved. However, the exact function mechanism of these oxygen groups in analysis is still needed to be resolved. Results illustrated that with the O/C ratio up to 7 %, the electrochemically oxidized carbon electrodes have no ability to distinguish the three biomolecules [58].

4.2.1 DA

Employing graphene directly modified electrodes, electrochemical determination of DA has been achieved [59–62]. In these studies, it was revealed that the interaction between DA and graphene accelerated the electron transfer process and graphene-modified electrode exhibited excellent electrocatalytic activity toward the electrochemical oxidation of DA. While, in a recent research, it was suggested that the modification of graphite electrodes with graphene had no significant analytical advantage and exhibited reduced analytical performance toward DA and UA [63]. Using graphene, which was well characterized, completely free of surfactants and had not been purposely oxidized or treated, modified edge- and basal-plane pyrolytic graphite electrodes (EPPG and BPPG with fast and slow heterogeneous electron transfer kinetics, respectively), reduction in the sensitivity, and LOD was observed. These results were contradictory to most reports which claimed the application of graphene led to an enhancement in the electroanalytical response. The authors indicated that with the introduction of graphene, the global coverage of edge-plane-like sites/defects of the EPPG/BPPG electrode declined given that graphene was predominantly basal plane in nature and thus when immobilized upon
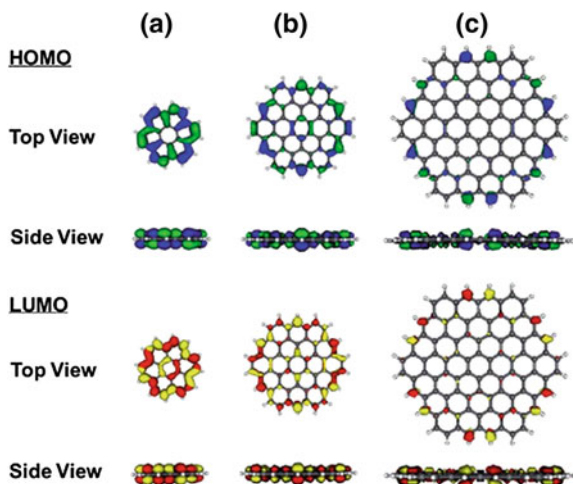
Fig. 4.3 Electron density distribution of electrons in the HOMO (highest-occupied molecular orbitals, shown in *blue* and *green*) and the LUMO (lowest-unoccupied molecular orbitals, shown in *red* and *yellow*) of a (*A*) 2 × 2 sheet (coronene), (*B*) 3 × 3 sheet, and (*C*) 4 × 4 sheet of graphene. Due to the symmetry of the sheets, the HOMO and HOMO − 1 are degenerate in energy and both are displayed simultaneously. Similarly, the LUMO and LUMO + 1 are degenerate in energy and both are displayed simultaneously in these figures. In each case, the 0.035 a.u. surface is shown. All molecular orbital diagrams were visualized using MOLEKEL 4.2. Reprinted from Ref. [64] by permission of The Royal Society of Chemistry

an electrode surface, these basal-plane sites effectively blocked the underlying edge-plane sites resulting in suppressed electron transfer. In their previous work, density functional theory (DFT) was conducted on symmetric graphene flakes of varying sizes indicating that the HOMO and LUMO energies were concentrated around the edge of the graphene sheet, at the edge plane sites, rather than the central basal plane region [64]. It was found that the probability that the electrons would be concentrated around the edge of the graphene flake increased as the size of the sheet increased (Fig. 4.3). The side view showed that any electron density concentrated in the basal region was less than that concentrated at the edges. Thus, in graphene, the electrons that have the highest energies and are, therefore, most likely to transfer, have a higher probability of being concentrated in the edge plane than in the central basal plane region, which is consistent with the experimental results and fundamental understanding regarding the electron transfer sites of graphitic materials. At graphene-modified EPPG, the authors divided two essential coverage regions for graphene, where in 'Zone I' graphene addition did not result in complete coverage of the underlying electrode and increased basal contribution from graphene modification leading to reduced electron transfer and electrochemical activity; in 'Zone II', once complete single-layer coverage was achieved, layered graphene *viz* graphite materializes with increased edge-plane content and thus an increase in heterogeneous electron transfer was observed with increased layering. While at

BPPG, no such Zones were observed. These were purely from the perspective of electrode kinetics, which gave insights into the electrochemical properties of graphene and guided the electrode design. Hence, the edge to basal ratio, coverage and orientation of graphene, and underlying supporting electrode are of great importance in the fabrication of sensing devices.

To best facilitate the performance of graphene in biosensing, one should particularly pay attention to the C/O ratio, edge defects, edge to basal ratio of graphene, and also the coverage and orientation on the underlying substrate. Specifically and precisely tuning the structure and intrinsic properties of graphene still remains as a great challenge. Other strategies, such as fabricating graphene with controllable architecture and morphology, incorporating graphene with other nanomaterials, have already been widely adopted for DA detection. For instance, a novel architecture, monolithic 3D graphene foam with high conductivity, was synthesized by CVD method and used for DA detection with remarkable sensitivity ($619.6 \ \mu A \ mM^{-1} \ cm^{-2}$) and low LOD (25 nM) [65]. The 3D multiplexed conductive pathways of graphene foam and the intimate interactions (hydrophobic and π–π interactions) between DA and graphene promoted the efficient electron transfer, in which the oxidation peak of DA could be easily distinguished from that of UA. Based on the synergistic effects, various nanomaterials have been incorporated into graphene sheets, including polystyrene [66], polyaniline [67], p-aminobenzoic acid [68], polypyrrole [69], poly(methylene blue) [70], polyoxometalate [71], MIPs [72, 73], Cyclodextrin [74, 75], layered double hydroxide film [76, 77], CNT [78], ferrocene [79], AuNPs [80–82], PdNPs [83], Cu_2O [84], and ZnO [85]. The main roles of these incorporators into graphene include preventing graphene sheets aggregation, improving solubility and stability in long term, enhancing the electrical conductivity and catalytic ability, increasing the specific surface area, and providing attachment points for molecules binding. Sensitive and selective electrochemical DA detection was realized on these nanocomposite-modified electrodes. Recently, our group fabricated a novel composite, graphene sheets/Congo red-molecular-imprinted polymer (GSCR-MIP), through free radical polymerization and applied it as a molecular recognition element to construct DA electrochemical sensor [72]. The template molecules (DA) were firstly adsorbed at the GSCR surface due to their excellent affinity, and subsequently, selective copolymerization of methacrylic acid and ethylene glycol dimethacrylate was further achieved at the GSCR surface. Potential scanning was presented to extract DA molecules from the imprinted polymers film, and as a result, DA could be rapidly and completely removed by this way. With regard to the traditional MIPs, the GSCR-MIPs not only possessed a faster desorption and adsorption dynamics, but also exhibited a higher selectivity and binding capacity toward DA molecule. Under experimental conditions, selective detection of DA in a linear concentration range of 0.1–830 μM was obtained, which revealed a low LOD and wide linear response.

By utilizing rGO as an enhancement, an ECL strategy for DA detection was recently proposed by Li et al. [86]. In their design, the electronic material RGO was mixed into the Nafion to improve its conductivity and facilitate the charge transfer in the electrochemical redox process of the RuNWs, because the RGO with the two-

dimensional planar structure had excellent conductivity. With the presence of tri-propylamine and DA, the ECL intensity of RuNWs was sensitively decreased with the increase of DA content. A near-linear detection range of 1 pM–10 μM was observed for DA with low LOD reaching 0.31 pM. The excellent performance was ascribed to the RuNWs that aggrandized the contacting surface area of the electrode and the rGO that made the charge transfer much easier on the solid-modified electrode surface. The super fluorescence quenching capacity of graphene and GO has been extensively employed to develop fluorescent sensors, as depicted in the above fluorescent DNA detection segment. Their own unique fluorescence and the potential for chemo- or biosensing are seldom explored. Recently, Chen and coworkers reported a GO-based photoinduced charge transfer (PCT) label-free NIR fluorescent biosensor for DA [87]. The multiple non-covalent interactions between GO and DA and the ultrafast decay at the picosecond range of the near-IR fluorescence of GO resulted in effective self-assembly of DA molecules on the surface of GO, and significant fluorescence quenching, allowing development of a PCT-based biosensor with direct readout of the near-IR fluorescence of GO for selective and sensitive detection of DA. The developed method gave a LOD of 94 nM and was successfully applied to the determination of DA in biological fluids with quantitative recovery (98–115 %).

4.2.2   AA

Direct oxidation of AA at bare electrodes is irreversible and the product, 2,3-diketogluconic acid, is readily adsorbed onto electrode surface resulting in the electrode fouling and a high overpotential for AA oxidation [88, 89]. To overcome these drawbacks, Wu and coworkers fabricated PdNPs-GO composites for the electrochemical oxidation of AA in neutral media [89]. PdNPs with a mean diameter of 2.6 nm were homogeneously deposited on GO sheets by the redox reaction between $PdCl_4^{2-}$ and GO. Based on the synergistic effect, the anodic peak potential of AA at PdNPs-GO-modified electrode was shifted negatively, and large anodic peak potential separation of AA and DA was observed comparing to bare GCE or Pd electrode. Sensitive and selective sensing of AA was achieved even in the presence of DA. Sensitive determination of AA is also obtained at graphene-doped carbon paste electrode [90] and graphene immobilized pyrolyzed photoresist film electrode [91]. In a comparative study, it was also reveled that the C/O atomic ratio appeared to be a critical parameter affecting GO's electrochemical characteristics and electrocatalytic potency [92]. Using AA as the analyte, GO with low oxygen content exhibited sufficiently high catalytic currents and fulfilled the criteria for construction chemical sensors for AA.

4.2.3 UA

Through electrostatic interaction, positively charged PDDA-AuNPs/graphene hybrids were prepared and used for attracting negatively charged UA molecules [93]. At the hybrid-modified electrode, the anodic peak current of UA obtained by CV increased 102-fold in comparison to bare GCE under optimizing conditions. Quantitative determination of UA had been successfully carried out in buffer solution, in urine samples and in the presence of adrenaline. Polymers, such as poly(acridine red) [94] and poly(acridine orange) [95], have also been incorporated into graphene sheets for sensing UA with satisfactory results. Recently, through the replacement of carboxyl acid groups at the edges of graphene sheets, neutral red (NR) was covalently anchored on graphene sheets with amine groups [96]. The introduction of NR improved the solubility and stability of graphene, also accelerated the electron transfer. The resultant hybrid exhibited good electrocatalytic activity toward the oxidation of UA, with linear range of 0.125–12.25 μM and LOD of 0.062 μM. The combination between dye molecule and graphene *via* covalent bond would open up new avenues to synthesize other multifunctional graphene materials with excellent photochemical or electrochemical properties, as the authors indicated.

4.2.4 Simultaneous Determination of DA, AA, and UA

Simultaneous determination of DA, AA, and UA has recently been achieved at graphene-modified electrodes. Our group is among the first ones to carry out this study utilizing graphene nanocomposite-modified electrodes [97–99]. For instance, chitosan–graphene composite was synthesized by direct blending of chitosan and GO followed by an in situ chemical reduction [97]. Chitosan molecules were intercalated among graphene layers and acted both as dispersant and stabilizer. The obtained chitosan–graphene hybrid could easily be purified, stored, and re-dispersed in water by adjusting the pH value of the solution (Fig. 4.4a). Furthermore, the re-dispersed acidic chitosan-graphene solution depicted excellent dispersion and stability even after aging for a week. Sensitive and selective simultaneous determination of DA, AA, and UA in mixtures was realized at the hybrid-modified electrode (Fig. 4.4b–d). The linear ranges for DA, AA, and UA were 1.0–24 μM, 50–1,200 μM, and 2.0–45 μM, respectively, and the LODs were 1.0, 50, and 2.0 μM, correspondingly. The chitosan–graphene composite showed good electrochemical catalytic activity to the oxidation reactions by considerably degreasing the overpotential. In a followed study, GO-templated polyaniline (GO-PAN) microsheets were prepared *via* oxidation polymerization of aniline with GO as template [98]. The resulted GO-PAN microsheet exhibited preferable electroactivity even in neutral media and displayed excellent electrocatalytic activity toward oxidation of DA, AA, and UA. In DA, AA, and UA ternary mixture, three well-defined peaks located at about 195, −55, and 385 mV were obtained. Over 200 mV

Fig. 4.4 **a** Synthesize of chitosan–graphene composite and snapshots of the outcomes at different stages of the procedure; DPVs at chitosan–graphene–glassy carbon electrode in 0.05 M PBS (pH 7.0). **b** 100 μM AA, 20 μM UA, and different concentrations of DA; **c** 5 μM DA, 20 μM UA, and different concentrations of AA; **d** 100 μM AA, 5 μM DA, and different concentrations of UA. Scan rate: 5 mV/s pulse amplitude 25 mV. *Inset* Plot of peak current versus sample concentrations. Reprinted from Ref. [97] by permission of John Wiley & Sons Ltd.

difference of oxidation peak potential between DA and AA was also obtained at Pt/PFIL/graphene sheet-modified electrode, leading to distinguishable signal of AA from DA [99]. The proposed sensor was also examined in real human urine samples with three independent oxidation peaks observed.

Tuning the composition, structure, and properties of graphene seems as an efficient way to adjust it for various applications. As one of the most effective strategies, chemical doping with heteroatoms, such as nitrogen or boron atoms, has been adopted to modulate the electronic properties and surface chemistry of graphene [100, 101]. A review on graphene doping could also be found [102]. Recently, Sheng et al. [103] reported nitrogen-doped graphene (NG) for simultaneous determination of DA, AA, and UA, where well-defined oxidation peaks with large peak separations and peak currents were observed. The authors indicated that the highly electrocatalytic activity of NG could be attributed to the fact that nitrogen atoms in NG layers interacted with these molecules *via* hydrogen bond, which activated the hydroxyl and amine groups and accelerated the charge transfer kinetics of these molecules at NG surface. Meanwhile, the π–π interactions between graphene layers and these molecules also promoted the charge transfer. It was found that oxidation peak currents of DA, AA, and UA were influenced by the nitrogen doping level, while the peak potentials remained nearly unchanged. A nitrogen content of 8.4 % was finally set in NG. NG nanosheets could be promising candidates for constructing biosensors, bioelectronics, and biofuel cells. Sensitive and selective DA, AA, and UA simultaneous determination has also been achieved on functionalized graphene [104], PTCA–graphene [105], graphene/IL/chitosan [106],

CD–graphene–MWCNTs [107], RGO–AuNPs–CSHMs (chitosan/silica sol–gel hybrid membranes) [108], RGO/AuNPs [109], AuNPs–β-CD–graphene [110], Cu-zeolite A/graphene [111], graphene/Pt [112], etc.

References

1. Zhou, M., Zhai, Y., Dong, S.: Electrochemical sensing and biosensing platform based on chemically reduced graphene oxide. Anal. Chem. **81**, 5603–5613 (2009)
2. Unnikrishnan, B., Palanisamy, S., Chen, S.M.: A simple electrochemical approach to fabricate a glucose biosensor based on graphene-glucose oxidase biocomposite. Biosens. Bioelectron. **39**, 70–75 (2013)
3. Liu, Y., Yu, D., Zeng, C., Miao, Z., Dai, L.: Biocompatible graphene oxide-based glucose biosensors. Langmuir **26**, 6158–6160 (2010)
4. Wu, P., Shao, Q., Hu, Y., Jin, J., Yin, Y., Zhang, H., Cai, C.: Direct electrochemistry of glucose oxidase assembled on graphene and application to glucose detection. Electrochim. Acta **55**, 8606–8614 (2010)
5. Wang, Y., Shao, Y., Matson, D.W., Li, J., Lin, Y.: Nitrogen-doped graphene and its application in electrochemical biosensing. ACS Nano **4**, 1790–1798 (2010)
6. Shan, C., Yang, H., Song, J., Han, D., Ivaska, A., Niu, L.: Direct electrochemistry of glucose oxidase and biosensing for glucose based on graphene. Anal. Chem. **81**, 2378–2382 (2009)
7. Jiang, Y., Zhang, Q., Li, F., Niu, L.: Glucose oxidase and graphene bionanocomposite bridged by ionic liquid unit for glucose biosensing application. Sens. Actuators B-Chem. **161**, 728–733 (2012)
8. Shan, C., Yang, H., Han, D., Zhang, Q., Ivaska, A., Niu, L.: Graphene/AuNPs/chitosan nanocomposites film for glucose biosensing. Biosens. Bioelectron. **25**, 1070–1074 (2010)
9. Zhiguo, G., Shuping, Y., Zaijun, L., Xiulan, S., Guangli, W., Yinjun, F., Junkang, L.: An ultrasensitive electrochemical biosensor for glucose using CdTe-CdS core–shell quantum dot as ultrafast electron transfer relay between graphene-gold nanocomposite and gold nanoparticle. Electrochim. Acta **56**, 9162–9167 (2011)
10. Wang, K., Liu, Q., Guan, Q.M., Wu, J., Li, H.N., Yan, J.J.: Enhanced direct electrochemistry of glucose oxidase and biosensing for glucose via synergy effect of graphene and CdS nanocrystals. Biosens. Bioelectron. **26**, 2252–2257 (2011)
11. Zeng, Q., Cheng, J.S., Liu, X.F., Bai, H.T., Jiang, J.H.: Palladium nanoparticle/chitosan-grafted graphene nanocomposites for construction of a glucose biosensor. Biosens. Bioelectron. **26**, 3456–3463 (2011)
12. Wu, H., Wang, J., Kang, X., Wang, C., Wang, D., Liu, J., Aksay, I.A., Lin, Y.: Glucose biosensor based on immobilization of glucose oxidase in platinum nanoparticles/graphene/chitosan nanocomposite film. Talanta **80**, 403–406 (2009)
13. Chen, Y., Li, Y., Sun, D., Tian, D., Zhang, J., Zhu, J.-J.: Fabrication of gold nanoparticles on bilayer graphene for glucose electrochemical biosensing. J. Mater. Chem. **21**, 7604–7611 (2011)
14. Yang, J., Deng, S., Lei, J., Ju, H., Gunasekaran, S.: Electrochemical synthesis of reduced graphene sheet-AuPd alloy nanoparticle composites for enzymatic biosensing. Biosens. Bioelectron. **29**, 159–166 (2011)
15. Zheng, J., He, Y., Sheng, Q., Zhang, H.: DNA as a linker for biocatalytic deposition of Au nanoparticles on graphene and its application in glucose detection. J. Mater. Chem. **21**, 12873–12879 (2011)
16. Luo, Z., Yuwen, L., Han, Y., Tian, J., Zhu, X., Weng, L., Wang, L.: Reduced graphene oxide/PAMAM-silver nanoparticles nanocomposite modified electrode for direct electrochemistry of glucose oxidase and glucose sensing. Biosens. Bioelectron. **36**, 179–185 (2012)

17. Lu, W., Luo, Y., Chang, G., Sun, X.: Synthesis of functional SiO_2-coated graphene oxide nanosheets decorated with Ag nanoparticles for H_2O_2 and glucose detection. Biosens. Bioelectron. **26**, 4791–4797 (2011)
18. Choi, B.G., Im, J., Kim, H.S., Park, H.: Flow-injection amperometric glucose biosensors based on graphene/Nafion hybrid electrodes. Electrochim. Acta **56**, 9721–9726 (2011)
19. Gu, H., Yu, Y., Liu, X., Ni, B., Zhou, T., Shi, G.: Layer-by-layer self-assembly of functionalized graphene nanoplates for glucose sensing in vivo integrated with on-line microdialysis system. Biosens. Bioelectron. **32**, 118–126 (2012)
20. Kang, X., Wang, J., Wu, H., Aksay, I.A., Liu, J., Lin, Y.: Glucose oxidase-graphene-chitosan modified electrode for direct electrochemistry and glucose sensing. Biosens. Bioelectron. **25**, 901–905 (2009)
21. Liu, S., Tian, J., Wang, L., Luo, Y., Lu, W., Sun, X.: Self-assembled graphene platelet-glucose oxidase nanostructures for glucose biosensing. Biosens. Bioelectron. **26**, 4491–4496 (2011)
22. Yin, H., Zhou, Y., Meng, X., Shang, K., Ai, S.: One-step "green" preparation of graphene nanosheets and carbon nanospheres mixture by electrolyzing graphite rob and its application for glucose biosensing. Biosens. Bioelectron. **30**, 112–117 (2011)
23. Wang, Z.J., Zhou, X.Z., Zhang, J., Boey, F., Zhang, H.: Direct electrochemical reduction of single-layer graphene oxide and subsequent functionalization with glucose oxidase. J. Phys. Chem. C **113**, 14071–14075 (2009)
24. Alwarappan, S., Liu, C., Kumar, A., Li, C.Z.: Enzyme-doped graphene nanosheets for enhanced glucose biosensing. J. Phys. Chem. C **114**, 12920–12924 (2010)
25. Zeng, G., Xing, Y., Gao, J., Wang, Z., Zhang, X.: Unconventional layer-by-layer assembly of graphene multilayer films for enzyme-based glucose and maltose biosensing. Langmuir **26**, 15022–15026 (2010)
26. Jang, H.D., Kim, S.K., Chang, H., Roh, K.M., Choi, J.W., Huang, J.: A glucose biosensor based on TiO_2-Graphene composite. Biosens. Bioelectron. **38**, 184–188 (2012)
27. Mallesha, M., Manjunatha, R., Suresh, G.S., Melo, J.S., D'Souza, S.F., Venkatesha, T.V.: Direct electrochemical non-enzymatic assay of glucose using functionalized graphene. J. Solid State Electrochem. **16**, 2675–2681 (2012)
28. Zhang, Y., Wang, Y., Jia, J., Wang, J.: Nonenzymatic glucose sensor based on graphene oxide and electrospun NiO nanofibers. Sens. Actuators B-Chem. **171–172**, 580–587 (2012)
29. Clark, L.C., Lyons, C.: Electrode systems for continuous monitoring in cardiovascular surgery. Ann. N.Y. Acad. Sci. **102**, 29–45 (1962)
30. Li, F., Wang, Z., Shan, C., Song, J., Han, D., Niu, L.: Preparation of gold nanoparticles/functionalized multiwalled carbon nanotube nanocomposites and its glucose biosensing application. Biosens. Bioelectron. **24**, 1765–1770 (2009)
31. Jia, F., Shan, C., Li, F., Niu, L.: Carbon nanotube/gold nanoparticles/polyethylenimine-functionalized ionic liquid thin film composites for glucose biosensing. Biosens. Bioelectron. **24**, 951–956 (2008)
32. Yang, F., Jiao, L., Shen, Y., Xu, X., Zhang, Y., Niu, L.: Enhanced response induced by polyelectrolyte-functionalized ionic liquid in glucose biosensor based on sol–gel organic–inorganic hybrid material. J. Electroanal. Chem. **608**, 78–83 (2007)
33. Zhang, Y., Shen, Y., Han, D., Wang, Z., Song, J., Li, F., Niu, L.: Carbon nanotubes and glucose oxidase bionanocomposite bridged by ionic liquid-like unit: preparation and electrochemical properties. Biosens. Bioelectron. **23**, 438–443 (2007)
34. Yang, Y., Yang, H., Yang, M., liu, Y., Shen, G., Yu, R.: Amperometric glucose biosensor based on a surface treated nanoporous ZrO_2/Chitosan composite film as immobilization matrix. Anal. Chim. Acta **525**, 213–220 (2004)
35. Laviron, E.: General expression of the linear potential sweep voltammogram in the case of diffusionless electrochemical systems. J. Electroanal. Chem. **101**, 19–28 (1979)
36. Kamin, R.A., Wilson, G.S.: Rotating ring-disk enzyme electrode for biocatalysis kinetic studies and characterization of the immobilized enzyme layer. Anal. Chem. **52**, 1198–1205 (1980)

37. Pletcher, D.: Electrocatalysis: present and future. J. Appl. Electrochem. **14**, 403–415 (1984)
38. Burke, L.D.: Premonolayer oxidation and its role in electrocatalysis. Electrochim. Acta **39**, 1841–1848 (1994)
39. Dong, X.C., Xu, H., Wang, X.W., Huang, Y.X., Chan-Park, M.B., Zhang, H., Wang, L.H., Huang, W., Chen, P.: 3D graphene-cobalt oxide electrode for high-performance supercapacitor and enzymeless glucose detection. ACS Nano **6**, 3206–3213 (2012)
40. Wang, X., Dong, X., Wen, Y., Li, C., Xiong, Q., Chen, P.: A graphene-cobalt oxide based needle electrode for non-enzymatic glucose detection in micro-droplets. Chem. Commun. **48**, 6490–6492 (2012)
41. Zhang, Y., Xu, F., Sun, Y., Shi, Y., Wen, Z., Li, Z.: Assembly of Ni(OH)$_2$ nanoplates on reduced graphene oxide: a two dimensional nanocomposite for enzyme-free glucose sensing. J. Mater. Chem. **21**, 16949–16954 (2011)
42. Lv, W., Jin, F.-M., Guo, Q., Yang, Q.-H., Kang, F.: DNA-dispersed graphene/NiO hybrid materials for highly sensitive non-enzymatic glucose sensor. Electrochim. Acta **73**, 129–135 (2012)
43. Sun, J.-Y., Huang, K.-J., Fan, Y., Wu, Z.-W., Li, D.-D.: Glassy carbon electrode modified with a film composed of Ni(II), quercetin and graphene for enzyme-less sensing of glucose. Microchim. Acta **174**, 289–294 (2011)
44. Lu, L.M., Li, H.B., Qu, F., Zhang, X.B., Shen, G.L., Yu, R.Q.: In situ synthesis of palladium nanoparticle-graphene nanohybrids and their application in nonenzymatic glucose biosensors. Biosens. Bioelectron. **26**, 3500–3504 (2011)
45. Wang, Q., Cui, X., Chen, J., Zheng, X., Liu, C., Xue, T., Wang, H., Jin, Z., Qiao, L., Zheng, W.: Well-dispersed palladium nanoparticles on graphene oxide as a non-enzymatic glucose sensor. RSC Adv. **2**, 6245–6249 (2012)
46. Luo, J., Jiang, S., Zhang, H., Jiang, J., Liu, X.: A novel non-enzymatic glucose sensor based on Cu nanoparticle modified graphene sheets electrode. Anal. Chim. Acta **709**, 47–53 (2012)
47. Gao, H., Xiao, F., Ching, C.B., Duan, H.: One-step electrochemical synthesis of PtNi nanoparticle-graphene nanocomposites for nonenzymatic amperometric glucose detection. ACS Appl. Mater. Interfaces **3**, 3049–3057 (2011)
48. Zhu, C., Fang, Y., Wen, D., Dong, S.: One-pot synthesis of functional two-dimensional graphene/SnO$_2$ composite nanosheets as a building block for self-assembly and an enhancing nanomaterial for biosensing. J. Mater. Chem. **21**, 16911–16917 (2011)
49. Zhang, C., Yuan, Y., Zhang, S., Wang, Y., Liu, Z.: Biosensing platform based on fluorescence resonance energy transfer from upconverting nanocrystals to graphene oxide. Angew. Chem. Int. Ed. **50**, 6851–6854 (2011)
50. Kwak, Y.H., Choi, D.S., Kim, Y.N., Kim, H., Yoon, D.H., Ahn, S.S., Yang, J.W., Yang, W.S., Seo, S.: Flexible glucose sensor using CVD-grown graphene-based field effect transistor. Biosens. Bioelectron. **37**, 82–87 (2012)
51. Song, Y., Qu, K., Zhao, C., Ren, J., Qu, X.: Graphene oxide: intrinsic peroxidase catalytic activity and its application to glucose detection. Adv. Mater. **22**, 2206–2210 (2010)
52. Dong, Y.L., Zhang, H.G., Rahman, Z.U., Su, L., Chen, X.J., Hu, J., Chen, X.G.: Graphene oxide-Fe$_3$O$_4$ magnetic nanocomposites with peroxidase-like activity for colorimetric detection of glucose. Nanoscale **4**, 3969–3976 (2012)
53. Adams, R.N.: Probing brain chemistry with electroanalytical techniques. Anal. Chem. **48**, 1126A–1138A (1976)
54. Wightman, R.M., May, L.J., Michael, A.C.: Detection of dopamine dynamics in the brain. Anal. Chem. **60**, 769A–793A (1988)
55. Shang, N.G., Papakonstantinou, P., McMullan, M., Chu, M., Stamboulis, A., Potenza, A., Dhesi, S.S., Marchetto, H.: Catalyst-free efficient growth, orientation and biosensing properties of multilayer graphene nanoflake films with sharp edge planes. Adv. Funct. Mater. **18**, 3506–3514 (2008)
56. Lim, C.X., Hoh, H.Y., Ang, P.K., Loh, K.P.: Direct voltammetric detection of DNA and pH sensing on epitaxial graphene: an insight into the role of oxygenated defects. Anal. Chem. **82**, 7387–7393 (2010)

57. Xiong, H., Jin, B.: The electrochemical behavior of AA and DA on graphene oxide modified electrodes containing various content of oxygen functional groups. J. Electroanal. Chem. **661**, 77–83 (2011)

58. Sudhakara Prasad, K., Muthuraman, G., Zen, J.-M.: The role of oxygen functionalities and edge plane sites on screen-printed carbon electrodes for simultaneous determination of dopamine, uric acid and ascorbic acid. Electrochem. Commun. **10**, 559–563 (2008)

59. Ma, X., Chao, M., Wang, Z.: Electrochemical detection of dopamine in the presence of epinephrine, uric acid and ascorbic acid using a graphene-modified electrode. Anal. Methods **4**, 1687–1692 (2012)

60. Kim, Y.R., Bong, S., Kang, Y.J., Yang, Y., Mahajan, R.K., Kim, J.S., Kim, H.: Electrochemical detection of dopamine in the presence of ascorbic acid using graphene modified electrodes. Biosens. Bioelectron. **25**, 2366–2369 (2010)

61. Zhu, M., Zeng, C., Ye, J.: Graphene-modified carbon fiber microelectrode for the detection of dopamine in mice hippocampus tissue. Electroanalysis **23**, 907–914 (2011)

62. Wang, Y., Li, Y., Tang, L., Lu, J., Li, J.: Application of graphene-modified electrode for selective detection of dopamine. Electrochem. Commun. **11**, 889–892 (2009)

63. Brownson, D.A., Foster, C.W., Banks, C.E.: The electrochemical performance of graphene modified electrodes: an analytical perspective. Analyst **137**, 1815–1823 (2012)

64. Brownson, D.A.C., Munro, L.J., Kampouris, D.K., Banks, C.E.: Electrochemistry of graphene: not such a beneficial electrode material? RSC Adv. **1**, 978–988 (2011)

65. Dong, X., Wang, X., Wang, L., Song, H., Zhang, H., Huang, W., Chen, P.: 3D graphene foam as a monolithic and macroporous carbon electrode for electrochemical sensing. ACS Appl. Mater. Interfaces **4**, 3129–3133 (2012)

66. Li, S., Qian, T., Wu, S., Shen, J.: A facile, controllable fabrication of polystyrene/graphene core-shell microspheres and its application in high-performance electrocatalysis. Chem. Commun. **48**, 7997–7999 (2012)

67. Liu, S., Xing, X., Yu, J., Lian, W., Li, J., Cui, M., Huang, J.: A novel label-free electrochemical aptasensor based on graphene-polyaniline composite film for dopamine determination. Biosens. Bioelectron. **36**, 186–191 (2012)

68. Huang, K.J., Jing, Q.S., Wu, Z.W., Wang, L., Wei, C.Y.: Enhanced sensing of dopamine in the present of ascorbic acid based on graphene/poly(p-aminobenzoic acid) composite film. Colloids Surf. B **88**, 310–314 (2011)

69. Si, P., Chen, H., Kannan, P., Kim, D.H.: Selective and sensitive determination of dopamine by composites of polypyrrole and graphene modified electrodes. Analyst **136**, 5134–5138 (2011)

70. Sun, W., Wang, Y., Zhang, Y., Ju, X., Li, G., Sun, Z.: Poly(methylene blue) functionalized graphene modified carbon ionic liquid electrode for the electrochemical detection of dopamine. Anal. Chim. Acta **751**, 59–65 (2012)

71. Zhang, H., Xie, A., Shen, Y., Qiu, L., Tian, X.: Layer-by-layer inkjet printing of fabricating reduced graphene-polyoxometalate composite film for chemical sensors. Phys. Chem. Chem. Phys. **14**, 12757–12763 (2012)

72. Mao, Y., Bao, Y., Gan, S., Li, F., Niu, L.: Electrochemical sensor for dopamine based on a novel graphene-molecular imprinted polymers composite recognition element. Biosens. Bioelectron. **28**, 291–297 (2011)

73. Liu, B., Lian, H.T., Yin, J.F., Sun, X.Y.: Dopamine molecularly imprinted electrochemical sensor based on graphene–chitosan composite. Electrochim. Acta **75**, 108–114 (2012)

74. Guo, Y., Guo, S., Ren, J., Zhai, Y., Dong, S., Wang, E.: Cyclodextrin functionalized graphene nanosheets with high supramolecular recognition capability: synthesis and host-guest inclusion for enhanced electrochemical performance. ACS Nano **4**, 4001–4010 (2010)

75. Tan, L., Zhou, K.-G., Zhang, Y.-H., Wang, H.-X., Wang, X.-D., Guo, Y.-F., Zhang, H.-L.: Nanomolar detection of dopamine in the presence of ascorbic acid at β-cyclodextrin/graphene nanocomposite platform. Electrochem. Commun. **12**, 557–560 (2010)

76. Wang, Y., Peng, W., Liu, L., Tang, M., Gao, F., Li, M.: Enhanced conductivity of a glassy carbon electrode modified with a graphene-doped film of layered double hydroxides for selectively sensing of dopamine. Microchim. Acta **174**, 41–46 (2011)

77. Li, M., Zhu, J.E., Zhang, L., Chen, X., Zhang, H., Zhang, F., Xu, S., Evans, D.G.: Facile synthesis of NiAl-layered double hydroxide/graphene hybrid with enhanced electrochemical properties for detection of dopamine. Nanoscale **3**, 4240–4246 (2011)

78. Dong, X., Ma, Y., Zhu, G., Huang, Y., Wang, J., Chan-Park, M.B., Wang, L., Huang, W., Chen, P.: Synthesis of graphene–carbon nanotube hybrid foam and its use as a novel three-dimensional electrode for electrochemical sensing. J. Mater. Chem. **22**, 17044–17048 (2012)

79. Liu, M., Wang, L., Deng, J., Chen, Q., Li, Y., Zhang, Y., Li, H., Yao, S.: Highly sensitive and selective dopamine biosensor based on a phenylethynyl ferrocene/graphene nanocomposite modified electrode. Analyst **137**, 4577–4583 (2012)

80. Li, J., Yang, J., Yang, Z., Li, Y., Yu, S., Xu, Q., Hu, X.: Graphene–Au nanoparticles nanocomposite film for selective electrochemical determination of dopamine. Anal. Methods **4**, 1725–1728 (2012)

81. Li, S.-J., Deng, D.-H., Shi, Q., Liu, S.-R.: Electrochemical synthesis of a graphene sheet and gold nanoparticle-based nanocomposite, and its application to amperometric sensing of dopamine. Microchim. Acta **177**, 325–331 (2012)

82. Yang, J., Strickler, J.R., Gunasekaran, S.: Indium tin oxide-coated glass modified with reduced graphene oxide sheets and gold nanoparticles as disposable working electrodes for dopamine sensing in meat samples. Nanoscale **4**, 4594–4602 (2012)

83. Wu, C.-H., Wang, C.-H., Lee, M.-T., Chang, J.-K.: Unique Pd/graphene nanocomposites constructed using supercritical fluid for superior electrochemical sensing performance. J. Mater. Chem. **22**, 21466–21471 (2012)

84. Zhang, F., Li, Y., Gu, Y.-E., Wang, Z., Wang, C.: One-pot solvothermal synthesis of a Cu_2O/ Graphene nanocomposite and its application in an electrochemical sensor for dopamine. Microchim. Acta **173**, 103–109 (2011)

85. Dong, X., Cao, Y., Wang, J., Chan-Park, M.B., Wang, L., Huang, W., Chen, P.: Hybrid structure of zinc oxide nanorods and three dimensional graphene foam for supercapacitor and electrochemical sensor applications. RSC Adv. **2**, 4364–4369 (2012)

86. Li, Q., Zheng, J.Y., Yan, Y., Zhao, Y.S., Yao, J.: Electrogenerated chemiluminescence of metal-organic complex nanowires: reduced graphene oxide enhancement and biosensing application. Adv. Mater. **24**, 4745–4749 (2012)

87. Chen, J.L., Yan, X.P., Meng, K., Wang, S.F.: Graphene oxide based photoinduced charge transfer label-free near-infrared fluorescent biosensor for dopamine. Anal. Chem. **83**, 8787–8793 (2011)

88. Raj, C.R., Tokuda, K., Ohsaka, T.: Electroanalytical applications of cationic self-assembled monolayers: square-wave voltammetric determination of dopamine and ascorbate. Bioelectrochemistry **53**, 183–191 (2001)

89. Wu, G.H., Wu, Y.F., Liu, X.W., Rong, M.C., Chen, X.M., Chen, X.: An electrochemical ascorbic acid sensor based on palladium nanoparticles supported on graphene oxide. Anal. Chim. Acta **745**, 33–37 (2012)

90. Li, F., Li, J., Feng, Y., Yang, L., Du, Z.: Electrochemical behavior of graphene doped carbon paste electrode and its application for sensitive determination of ascorbic acid. Sens. Actuators B-Chem. **157**, 110–114 (2011)

91. Keeley, G.P., O'Neill, A., McEvoy, N., Peltekis, N., Coleman, J.N., Duesberg, G.S.: Electrochemical ascorbic acid sensor based on DMF-exfoliated graphene. J. Mater. Chem. **20**, 7864–7869 (2010)

92. Stergiou, D.V., Diamanti, E.K., Gournis, D., Prodromidis, M.I.: Comparative study of different types of graphenes as electrocatalysts for ascorbic acid. Electrochem. Commun. **12**, 1307–1309 (2010)

93. Xue, Y., Zhao, H., Wu, Z., Li, X., He, Y., Yuan, Z.: The comparison of different gold nanoparticles/graphene nanosheets hybrid nanocomposites in electrochemical performance and the construction of a sensitive uric acid electrochemical sensor with novel hybrid nanocomposites. Biosens. Bioelectron. **29**, 102–108 (2011)

94. Li, Y., Ran, G., Yi, W.J., Luo, H.Q., Li, N.B.: A glassy carbon electrode modified with graphene and poly(acridine red) for sensing uric acid. Microchim. Acta **178**, 115–121 (2012)

95. Wang, Z., Xia, J., Zhu, L., Zhang, F., Guo, X., Li, Y., Xia, Y.: The fabrication of poly (acridine orange)/graphene modified electrode with electrolysis micelle disruption method for selective determination of uric acid. Sens. Actuators B-Chem. **161**, 131–136 (2012)

96. Song, J., Qiao, J., Shuang, S., Guo, Y., Dong, C.: Synthesis of neutral red covalently functionalized graphene nanocomposite and the electrocatalytic properties toward uric acid. J. Mater. Chem. **22**, 602–608 (2012)

97. Han, D., Han, T., Shan, C., Ivaska, A., Niu, L.: Simultaneous determination of ascorbic acid, dopamine and uric acid with chitosan-graphene modified electrode. Electroanalysis **22**, 2001–2008 (2010)

98. Bao, Y., Song, J., Mao, Y., Han, D., Yang, F., Niu, L., Ivaska, A.: Graphene oxide-templated polyaniline microsheets toward simultaneous electrochemical determination of AA/DA/UA. Electroanal. **23**, 878–884 (2011)

99. Li, F., Chai, J., Yang, H., Han, D., Niu, L.: Synthesis of Pt/ionic liquid/graphene nanocomposite and its simultaneous determination of ascorbic acid and dopamine. Talanta **81**, 1063–1068 (2010)

100. Panchakarla, L.S., Subrahmanyam, K.S., Saha, S.K., Govindaraj, A., Krishnamurthy, H.R., Waghmare, U.V., Rao, C.N.R.: Synthesis, structure, and properties of boron- and nitrogen-doped graphene. Adv. Mater. **21**, 4726–4730 (2009)

101. Wang, X., Li, X., Zhang, L., Yoon, Y., Weber, P.K., Wang, H., Guo, J., Dai, H.: N-doping of graphene through electrothermal reactions with ammonia. Science **324**, 768–771 (2009)

102. Guo, B., Fang, L., Zhang, B., Gong, J.R.: Graphene doping: a review. Insciences J. **1**, 80–89 (2011)

103. Sheng, Z.H., Zheng, X.Q., Xu, J.Y., Bao, W.J., Wang, F.B., Xia, X.H.: Electrochemical sensor based on nitrogen doped graphene: simultaneous determination of ascorbic acid, dopamine and uric acid. Biosens. Bioelectron. **34**, 125–131 (2012)

104. Mallesha, M., Manjunatha, R., Nethravathi, C., Suresh, G.S., Rajamathi, M., Melo, J.S., Venkatesha, T.V.: Functionalized-graphene modified graphite electrode for the selective determination of dopamine in presence of uric acid and ascorbic acid. Bioelectrochemistry **81**, 104–108 (2011)

105. Zhang, W., Chai, Y., Yuan, R., Chen, S., Han, J., Yuan, D.: Facile synthesis of graphene hybrid tube-like structure for simultaneous detection of ascorbic acid, dopamine, uric acid and tryptophan. Anal. Chim. Acta **756**, 7–12 (2012)

106. Niu, X., Yang, W., Guo, H., Ren, J., Yang, F., Gao, J.: A novel and simple strategy for simultaneous determination of dopamine, uric acid and ascorbic acid based on the stacked graphene platelet nanofibers/ionic liquids/chitosan modified electrode. Talanta **99**, 984–988 (2012)

107. Zhang, Y., Yuan, R., Chai, Y., Li, W., Zhong, X., Zhong, H.: Simultaneous voltammetric determination for DA, AA and NO_2^- based on graphene/poly-cyclodextrin/MWCNTs nanocomposite platform. Biosens. Bioelectron. **26**, 3977–3980 (2011)

108. Liu, X., Xie, L., Li, H.: Electrochemical biosensor based on reduced graphene oxide and Au nanoparticles entrapped in chitosan/silica sol–gel hybrid membranes for determination of dopamine and uric acid. J. Electroanal. Chem. **682**, 158–163 (2012)

109. Liu, S., Yan, J., He, G., Zhong, D., Chen, J., Shi, L., Zhou, X., Jiang, H.: Layer-by-layer assembled multilayer films of reduced graphene oxide/gold nanoparticles for the electrochemical detection of dopamine. J. Electroanal. Chem. **672**, 40–44 (2012)

110. Tian, X., Cheng, C., Yuan, H., Du, J., Xiao, D., Xie, S., Choi, M.M.: Simultaneous determination of L-ascorbic acid, dopamine and uric acid with gold nanoparticles-beta-cyclodextrin-graphene-modified electrode by square wave voltammetry. Talanta **93**, 79–85 (2012)
111. He, P., Wang, W., Du, L., Dong, F., Deng, Y., Zhang, T.: Zeolite A functionalized with copper nanoparticles and graphene oxide for simultaneous electrochemical determination of dopamine and ascorbic acid. Anal. Chim. Acta **739**, 25–30 (2012)
112. Sun, C.L., Lee, H.H., Yang, J.M., Wu, C.C.: The simultaneous electrochemical detection of ascorbic acid, dopamine, and uric acid using graphene/size-selected Pt nanocomposites. Biosens. Bioelectron. **26**, 3450–3455 (2011)

Chapter 5
Graphene for Detection of Adenosine Triphosphate, Nicotinamide Adenine Dinucleotide, Other Molecules, Gas, and Ions

Abstract Graphene-based electrochemical aptasensing platforms have been rapidly developed to detect different targets by combining various electrochemical techniques with aptamer-based signal conversion strategies. Electrochemical aptasensor for adenosine triphosphate (ATP) detection was recently realized by using functionalized graphene nanosheets. Nicotinamide adenine dinucleotide (NADH) is involved as a cofactor in hundreds of enzymatic reactions of NAD^+/NADH-dependent dehydrogenases. The mechanism of NADH oxidation was thoroughly studied on graphene platform. Graphene sheets also serve as good substrates for detection of various other molecules, including acetylcholine/choline, cholesterol, benzenediol isomers (hydroquinone, resorcinol, and catechol), and epinephrine. The unique structure and oxygenic functionalities of GO facilitate it to be easily turned into a potentially useful gas storage material and biological ionic and molecular channels. Functionalized nanopores in graphene monolayers were designed and used as ionic sieves with high selectivity and transparency. Some cations, such as Li^+, Na^+ and K^+ ions and anions, such as Cl^- and Br^- ions have been detected by graphene nanopores.

Keywords Graphene · Adenosine triphosphate · Nicotinamide adenine dinucleotide · Gas sensor · Ion-selective sensor

5.1 ATP

Adenosine triphosphate (ATP), as the major carrier of chemical energy in living species, is an important substrate in living organisms, which plays a critical role in the regulation and integration of cellular metabolism. In addition, it has also been used as an indicator for cell viability and cell injury [1]. Therefore, the detection of ATP is highly important in biochemical study and clinic diagnosis. Electrochemical aptasensor represents an attractive choice, which is simple, rapid, and allows device miniaturization. Until now, graphene-based electrochemical aptasensing platforms

have been rapidly developed to detect different targets by combining various electrochemical techniques with aptamer-based signal conversion strategies. For instance, Guo et al. [2] demonstrated a new kind of electrochemical label-free aptasensor based on graphene–mesoporous silica–gold NP hybrids (GSGHs) as an enhanced element of the sensing platform for detection of ATP using a parallel-motif DNA triplex system for amplification. The GSGH platform had good biocompatibility and large electrode surface area and provided suitable microenvironment for signal amplification. Based on 'enhanced three-step sensing platform,' a low LOD of 0.023 nM was obtained for ATP detection. This strategy provided some new avenues on the design of nanomaterial-based aptamer sensors to direct the development of nanoelectroanalytical chemistry. Another wisely designed electrochemical aptasensor for ATP detection was recently realized by using porphyrin-functionalized graphene nanosheets as the platform [3]. The ATP aptamer adsorption on the platform decreased the electrochemical signal of porphyrin. In the presence of ATP, the aptamer caught ATP on electrode surface, which made a barrier and inhibited electron transfer, resulting in further decrease of porphyrin signal. Besides, the electrochemical behavior of ATP, with an irreversible oxidation peak appearing at 1.369 V (vs. SCE), was achieved on graphene–chitosan-modified graphite electrode with diphenylacetylene, which showed a direct, simple detection manner [4]. Different from the commonly used manner in which graphene was the platform for aptamer anchoring, Wang et al. [5] reported that ATP aptamer-immobilized Au electrode could adsorb graphene, resulting in a large decrease of the R_{et} value. When aptamer bound with ATP, the adsorption of graphene was inhibited on the electrode surface and the R_{et} value would not decrease. The R_{et} value change served as the signal for ATP detection with label-free, sensitive, and simple features. Recently, graphene nanoribbons were prepared by oxidative unzipping of MWCNTs and used in FET for ATP sensing [6]. It was found that the graphene nanoribbons exhibited high on/off ratio of $\sim 52.0 \pm 8.6$ ($n = 10$ devices) and lower LOD with two orders of magnitude than that of SWCNTs.

Fluorescent aptasensors for ATP have also been constructed using graphene as the platform due to its fluorescence-quenching capability. Based on the strong π–π stacking interactions between aptamer and graphene, coupling the specific interaction between ATP and aptamer, ATP assays have been successfully realized via various strategies, such as logic gates [7], aptamer [8, 9], molecular aptamer beacon [10], hybridization inhibition [11], ATP-dependent enzymatic reaction [12], and upconversion nanophosphors [13]. Though high sensitivity and low LOD were achieved, attention still needs to be paid to the non-specific desorption of aptamer from graphene or GO surface. In particular, when the concentration of coexistent non-targets exceeds a certain level, non-specific desorption increases significantly, resulting in a strong false-positive signal. Hence, the non-specific effect cannot be ignored and it is necessary to reduce or eliminate the false-positive signal. To address this issue, an interesting imaging method for in situ ATP detection was recently developed by Tan et al. [14]. Instead of using aptamer, ATP aptamer
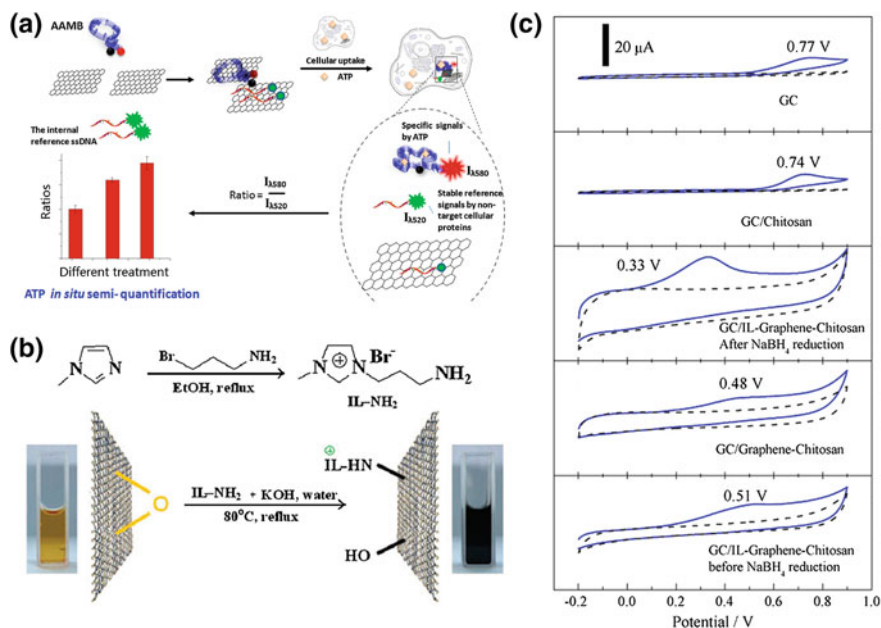
Fig. 5.1 a An ATP aptamer molecular beacon (*AAMB*) is adsorbed on GO to form a double-quenching platform. After the AAMB/GO complex spontaneously enters cells, the AAMB is released and then opened by intracellular ATP. The resulting fluorescence recovery ($\lambda_{em} = 580$ nm) is used to perform ATP live-cell imaging. Moreover, in the presence of an internal reference, i.e., FAM-labeled ssDNA ($\lambda_{em} = 520$ nm), which is released non-specifically from GO when inside cells, this system can also be used for ATP semi-quantification inside living cells. Reprinted with permission from Ref. [14] Copyright 2012 American Chemical Society. **b** Schematic illustration of the IL structure and synthesis of IL-graphene. Reprinted from Ref. [41] by permission of The Royal Society of Chemistry. **c** CVs of bare GC electrode, chitosan, chitosan/IL–graphene (after NaBH$_4$ reduction), chitosan/graphene (without any protection), and chitosan/IL–graphene (before NaBH$_4$ reduction)-modified GC electrodes (from *top to down*) in PBS (0.05 M, pH 7.4) in the absence (*dash line*) and presence (*straight line*) of 1 mM NADH. Scan rate: 0.05 V s^{-1}. Reprinted from Ref. [31] Copyright 2010, with permission from Elsevier

molecular beacon (AAMB) was utilized to form AAMB/GO system for cellular delivery (Fig. 5.1a). The AAMB/GO spontaneously entered cells, and AAMB was released and opened by intracellular ATP. The resulting fluorescence recovery was used to perform ATP live-cell imaging with greatly improved background and signaling. Using the non-specific desorption as the internal reference, a semi-quantitative assay for intracellular ATP imaging was also realized, which is currently a challenging task. This strategy holds great potential to detect other biomolecules inside living cells, especially proteins with known aptamers.

5.2 NADH

Nicotinamide adenine dinucleotide (NADH) is involved as a cofactor in several hundred enzymatic reactions of NAD$^+$/NADH-dependent dehydrogenases. The electrochemical oxidation of NADH has attracted considerable attention due to its significance both as a cofactor for dehydrogenase enzymes and its role in the electron transfer chain in biological system, and also due to the need to develop amperometric biosensors for substrates of NAD$^+$-dependent dehydrogenases. The electrochemical reaction of NADH involves an electron transfer followed by de-protonation and a second electron transfer. The mechanism of NADH oxidation is as follows.

$$NADH - e^- \rightarrow NADH^{\cdot +}$$

$$NADH^{\cdot +} \rightarrow NAD^{\cdot} + H^+$$

$$NAD^{\cdot} - e^- \rightarrow NAD^+$$
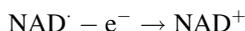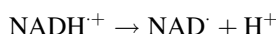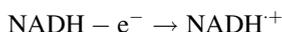
Problems inherent to such anodic detection are the large overvoltage encountered for NADH oxidation at commonly used electrodes and surface fouling associated with the accumulation of radical intermediates produced. In addition, the electrochemical oxidation becomes unselective at high overpotential, because other electroactive species present in the electrolyte would undergo oxidation. Oxidation of NADH at lower overpotential and avoiding the fouling effect can be achieved through electrode modification, which improves the reaction kinetics and decreases the effects of product adsorption and side reactions that happen at bare solid electrodes. Consequently, considerable effort has been devoted to identify new electrode materials and new methods that will reduce the overpotential for NADH oxidation and minimize surface passivation effects.

The discovery of graphene essentially offers an opportunity to the pursuit mentioned above. A comparative study was carried out to investigate the electrochemical activity of SWNTs, pristine GO, chemically reduced GO, and electrochemically reduced GO using NADH as the redox probes [15]. It was concluded that the fast electron transfer kinetics for the NADH oxidation at electrochemically reduced GO and SWNTs could be mainly associated with the presence of the quinone-like moieties. Other elements, such as C/O ratio, surface chemistry, and surface cleanness, are also considered to closely associate with the fast electron transfer kinetics. Recently, Brownson et al. [16, 17] explored the electroanalytical performance of CVD-grown graphene electrode and compared the response to EPPG and BPPG electrode, toward a selection of electrochemically active analytes. In the best case, similar electroanalytical performance (analytical sensitivity) was observed at EPPG and CVD-graphene electrode due to the similar DOS present at both electrodes, which for the CVD-graphene was as expected given the prevalence of graphitic island across its surface, which contributed to a large global coverage of edge plane

sites (an abundance of electron transfer sites leading to fast heterogeneous electron transfer) that would closely replicate the composition of a highly ordered pyrolytic graphite (HOPG) electrode. In other cases, the response of the CVD-graphene was worse than that of an EPPG electrode due to the lack of oxygenated species, where it appeared that the control of such oxygenated species (either their absence or presence) was of high importance in electroanalysis. Actually, the adsorption of NAD$^+$ at graphene was due to the presence of oxygenated species, namely carboxylic groups, formed at the edges and the edge-like defects of graphene sheets [18]. No relevant interactions were observed when the NADH and NAD$^+$ were on the basal plane of graphene or close to hydrogen-only substituted edges of graphene sheets, which revealed the role of oxygenated species of graphene in molecule interaction. This was evidenced by a recent research that functionalized graphene with low C/O ratio caused a decrease of the overpotential for the electrochemical oxidation of NADH [19]. The oxygen functional groups and lattice defects of graphene played a prominent role on the electrochemical activity. When using chemically fabricated graphene-modified EPPG for NADH oxidation, a substantial negative shift of the anodic peak potential was observed when compared with bare EPPG [20]. The ability of graphene-modified EPPG alleviating surface passivation during the oxidation of NADH might be attributed to the presence of oxygen groups and defects. Existing defects, such as kinks, steps, and vacancies, can produce localized edge states between the conduction and valence bands, resulting in the high DOS near the fermi level, which promote the electroanalytical reaction. The surface cleanness of graphene also makes a contribution to the electrochemical performance. For example, surfactants, routinely used in the production of graphene and additionally in the solubilization with the aim of reducing the likelihood of coalescing, may be detrimental in the electrochemical oxidation of NADH [21]. It was suggested that given the wide variety of ionic and nonionic surfactants, the use of control experiments in the form of surfactant-modified electrodes must be performed when claims of electrocatalysis for graphene was made to deconvolute the origin of the electrochemical response, which was usually (wrongly) attributed to graphene itself! Besides the surfactants, carbonaceous oxidative debris, derived from the disruption of graphene sheets owing to the harsh oxidative and strong acidic environment, also affects profoundly the electrochemical behaviors of graphene or GO. Carbonaceous debris is actually a mixture of polyaromatic derivatives rich in functional groups, which can strongly adhere to graphene sheets via π–π stacking and hydrogen bonds. Researchers found that the presence of the carbonaceous oxidative debris deteriorated the electrochemical catalysis of GO and greatly slowed down the heterogeneous electron rates, while when GO was in situ electrochemically reduced to graphene, the debris (reduced forms) favored the electrochemical catalysis of reduced GO and accelerated the heterogeneous electron kinetics [22]. These are only plausible explanations, and further efforts are still needed to undergo investigations for more rational explanations. When using graphene in electroanalytical performance, one should particularly pay attention to these factors to get more reliable and precise results.

Using graphene-modified electrodes for electrocatalysis, a summary was recently made by Valentini et al. [23] to elucidate that the electrochemical performance was related to (a) electrostatic interactions between the structural defects of the oxidized graphene and the electroactive probes; (b) π–π stacking-based interactions, between the graphene basal plane and the electroactive probes; (c) different electrochemical-based redox interactions occurring between the edge defects of graphene and the biomolecules; (d) the covalent-based interactions due to the presence of oxygen functional groups. They used graphene-modified screen-printed electrode (SPE) for NADH detection, and good results were obtained comparing to that of pristine SWCNT paste electrode. Various forms of graphene, such as chemically reduced GO [24, 25], acid-treated graphene [26], free-standing graphene [27], DMF-exfoliated graphene [28], and Q-graphene [29], have been adopted for electrochemical detection of NADH. Lower overpotential and better anti-fouling properties are mainly attributed to the dense edge-plane-like defective sites and valuable oxygen content of graphene. For instance, a newly synthesized type of graphene, Q-graphene, had been physically and electrochemically characterized and showed the potential as a new electrode material for future use in advanced electroanalytical applications, particularly where a high level of edge-plane-like sites/defects was required to tailor and optimize a specific response (i.e., where an intermediate level of basal plane content was also required) or through utilization of its valuable oxygen content for beneficial implementation where oxygenated electrocatalytic reactions were employed for electrocatalysis study [29].

Using graphene as a good substrate, various materials have been incorporated with graphene to form hybrids with tailoring and tunable properties for electrochemical NADH determination, including IL [30, 31], methylene blue [32, 33], methylene green [34], AuNPs [35, 36], metal–nitride [37], TiO_2 [38], MWCNTs [39], and PEDOT:PSS [40]. Our group firstly exploited IL-functionalized graphene (IL-graphene) [41] for low-potential NADH detection [31]. As shown in Fig. 5.1b, $-NH_2$-terminated IL was covalently anchored on GO through the epoxy ring opening reaction, and the resultant IL-graphene possessed excellent dispersibility and stability [41]. At IL-graphene/chitosan-modified GCE, a substantial decrease (440 mV) in the overvoltage of NADH oxidation was observed with oxidation starting at ca. 0 V (vs. Ag/AgCl) (Fig. 5.1c), which might be ascribed to the high specific surface area, electrical conductivity, and π-conjugation structure of graphene, coupling the unique properties of IL as high ionic conductivity and solubility toward various substrates. The NADH amperometric response at such a modified electrode was more stable (95.4 and 90 % of the initial activity remaining after 10 and 30 min at 1 mM NADH solution) than that at bare electrode (68 and 46 %). Furthermore, the IL-graphene/chitosan-modified electrode exhibited a good linearity from 0.25 to 2 mM and high sensitivity of 37.43 μA mM^{-1} cm^{-2}. Instead of covalent anchoring, GO was directly dispersed in IL to form a dispersion and then to modify SPE for NADH detection [30]. High peak currents and significant potential shift were detected, which were attributed to the large surface area, the disordering effect due to the dispersion in IL, and consequent exposure of the nanoribbons to electron transfer processes, the oxygen groups, and unsaturated

carbons also responsible for a more efficient electron transfer. The performances of the GO/IL-modified SPEs suggested that they might have great potential for the assembly of biosensors for various purposes.

Recently, graphene–MB film was formed in a simple immersion process and could be loaded on different substrates as electrode [33]. This strategy avoided the inconvenience of dispersion and chemical reduction, and problems of the low loading limit of electroactive dyes. The oxidation of NADH started from −0.08 V (vs. Ag/AgCl) at the graphene–MB thin film electrode, showing a decrease of 530 mV in overpotential compared to a Ti metal electrode. Later, a facile and versatile route to synthesize nanohybrids of titanium nitride (TiN) decorated on nitrogen-doped graphene (NG) was reported by Wen et al. [37]. In the investigation of NADH oxidation, the TiN/NG electrode led to a remarkable increase of the peak current in comparison with the bare GCE and the NG electrode. The peak potential markedly shifted from 760 mV for the bare GCE to 230 mV for the TiN/NG electrode, indicating a considerable decrease (by 530 mV) in the overpotential of NADH oxidation. Through the first-principle density functional theory (DFT) calculations, Ti atoms of TiN interacted with the graphene to form chemisorption interfaces via metal carbide bonding. The plane-averaged charge density difference along the z-axis likely pushed electrons into the middle region of graphene to contact TiN nanoparticles, which enabled the whole system to act metallically so that the electronic structure of graphene was disturbed. Consequently, the TiN–graphene hybrids could provide the channel of electron transfer through orbital hybridization and show catalytic properties for electrochemical oxidation and reduction of some electroactive substrates. It was believed that the electrocatalytic activity of TiN/NG mainly arose from the synergetic effects between TiN and NG. The uniform decoration and high surface area provided reactants with more active sites in TiN nanoparticles. The excellent conductivity of NG provided a path for transferring electrons back and forth between the electrode and the external circuit.

5.3   Other Molecules, Gas, and Ions Sensing

5.3.1   Other Molecules

Graphene sheets also serve as good substrates for various other molecule detection, including acetylcholine/choline [42], cholesterol [43], benzenediol isomers (hydroquinone, resorcinol, catechol) [44], epinephrine [45], aromatic molecules (crystal violet, amaranth, phosphorus triphenyl [46], and rhodamine 6G, rhodamine B, methyl violet, methylene blue [47]), folic acid [48], naphthalene and 1-naphthol [49], malachite green [50], microcystin-LR [51], cocaine/adenosine [52], pyrogallol [53, 54], nitric oxide [55], urea [56], hydrazine [57], nitrophenol [58], catechol [59], hypoxanthine [60], chlorite [61], paraoxon [62, 63], phenol [64], heparin [65, 66], trinitrotoluene (TNT) [67, 68], bleomycin [69], ochratoxin A, and fumonisin B_1 [70].

For instance, Deng and coworkers constructed a graphene-amplified solid-state ECL biosensing platform, in which CdTe QDs were anchored on electrochemically reduced GO (ERGO) [42]. Using O_2 as coreactant, the QDs/ERGO-modified electrode showed ECL intensity increase by 4.2 and 178.9 times as compared with intrinsic QDs and QDs/GO-modified electrodes due to the adsorption of dissolved O_2 on ERGO and facilitated electron transfer. The amplified ECL of QDs/ERGO was used to construct sensitive biosensors for choline and acetylcholine based on the consumption of dissolved O_2 in enzymatic reaction with LOD of 8.8 and 4.7 μM. Utilizing hemin–graphene nanosheets as an ECL amplification and sensing element, a cathodic electrogenerated ECL sensing platform was also developed for the detection of cholesterol with good specificity and excellent stability [43]. In luminol–NaOH–H_2O_2 system, graphene–magnetite–MIP (GM–MIP) was developed as a CL platform for determination of hydroquinone, resorcinol, catechol, and epinephrine [44, 45]. In the preparation of GM–MIP, graphene was used to improve the adsorption capacity, and Fe_3O_4 NPs were used for separation and immobilization. The obtained GM–MIP–CL sensor had shown to provide a sensitive and fast method for on-site determination of hydroquinone, resorcinol, catechol, and epinephrine.

The superior structure of GO, such as the large surface area, presence of oxygen functionalities, and π-conjugated basal planes, makes GO an ideal host material to adsorb aromatic compounds. Recently, GO (graphene) has been used in constructing SERS substrate [46–48]. For instance, Liu et al. [46] designed fGO/AgNPs substrate by combining the properties of fGO and AgNPs, including the high affinity of fGO toward aromatic molecules and the localized surface plasmon resonance (LSPR)-based SERS property of AgNPs. As a consequence of the proximity of fGO to AuNPs, more molecules were trapped in the enhancement region and resulted in better enhanced SERS signals than AgNPs alone. As a result, crystal violet, amaranth, and phosphorus triphenyl were ultrasensitively detected. The possible effect of fGO on the SERS intensities of these model molecules was attributed to the following: (a) fGO is a double-sided polyaromatic scaffold with an ultrahigh specific surface area and therefore is capable of adsorbing aromatic compounds and (b) fGO could chemically enhance the Raman signals of adsorbed molecules. Hence, the synergistic effects of more molecules near the metal surface and fGO-induced chemical enhancement endowed the fGO-modified AgNPs nanostructure film with better SERS performance. In a similar manner, versatile SERS determination of rhodamine 6G, methyl violet, rhodamine B, methylene blue, and folic acid was also achieved by using Ag- or Au NP-decorated single-layer rGO [47] and GO/PDDA/AgNP [48] substrates.

Adsorption technique represents one of the most simple and effective ways for aromatic pollutant elimination. However, the adsorption capacities of present materials are not high enough. The large surface area of graphene enables it to have potential application in this field. Unfortunately, two main aspects restrict its performance, namely the tendency to aggregate and poor dispersibility in aqueous solution. Recently, Zhao et al. [49] found an effective way to address this problem through the sulfonation of GO with the aryl diazonium salt of sulfanilic acid. The 3-nm-thick sulfonated graphene exhibited high dispersibility in aqueous solution and

high adsorption capability toward naphthalene and 1-naphthol approaching ~2.3–2.4 mM/g, which is one of the highest capabilities of today's nanomaterials. By incorporating magnetite into graphene sheets, Fe_3O_4/RGO was fabricated with one-step solvothermal strategy and used for adsorption of dye pollutants [50]. Excellent removal efficiency (over 91 % for rhodamine B and over 94 % for malachite green) was obtained, and the adsorption behavior fitted well with the Freundlich isothermal and the pseudo-second-order kinetic model. Moreover, Fe_3O_4/RGO adsorbent could be removed completely from aqueous solution by an external magnetic field and regenerated by simply washing with ethylene glycol. Besides nanoparticles, RNA had also been covalently anchored on GO sheets for adsorption of microcystin-LR [51]. Furthermore, aptamer covalently immobilized on GO nanosheets is a potentially useful tool in recognizing, enriching, and separating small molecules and biomacromolecules in the purification of contaminated water and the preparation of samples.

Aptamer-conjugated GO for selective enrichment and detection of cocaine and adenosine from plasma samples using MS was reported by Gulbakan et al. [52]. When combined with aptamer-based affinity capture, their results showed that GO provided an efficient platform for selective enrichment of target analytes and the attainment of direct MS readouts, even from very complex media. Using GO could eliminate the need for any additional energy-adsorbing matrix for ionization and background interference, which is the biggest problem when conventional MALDI matrices are employed. This graphene-based, aptamer-enhanced extraction MS could be extended to a more complex system and be used when analyzing different biological samples, including proteins, metabolites, and cell surface markers.

Employing graphene, both 3D GO/hemoglobin hydrogel [54] and 2D graphene/hemin [53] had been constructed for pyrogallol catalysis in organic and aqueous solvents, respectively. Based on the strong electrostatic attraction, GO and hemoglobin formed a hydrogel, where hemoglobin still kept its catalytic activity [54]. After addition of GO/hemoglobin hydrogel into the reaction system, a microinterface between the water phase and organic solvent formed. Since pyrogallol is hydrophilic and insoluble in organic solvent, they accumulated on the surface of the gel and then crossed the interface to enter the gel for reaction. The 3D network with pore sizes as large as 5–10 μm facilitated the diffusion or release of reactants. Though the hydrogel had a lower apparent activity in the initial stage of reaction, it maintained its activity for a much longer time, which resulted in a higher average activity in the whole reaction period. Different from the electrostatic attraction, the formation of 2D graphene/hemin was through π–π stacking interactions (Fig. 5.2a) [53]. The graphene/hemin conjugates also functioned as effective catalysts in the oxidation of pyrogallol with exceptionally high catalytic activity (k_{cat}) and substrate-binding affinity (K_M) approaching that of natural enzymes (Fig. 5.2b–d). An iron–porphyrin derivative, tetramethylpyridyl–porphyrin iron (FeTMPyP), was also immobilized on graphene with nearly enzyme-like activity, demonstrating the general applicability of graphene as a support for metalloporphyrin species. The authors illustrated that the enhanced performance may be attributed to several features. First, graphene-supported hemin or FeTMPyP could prevent molecules
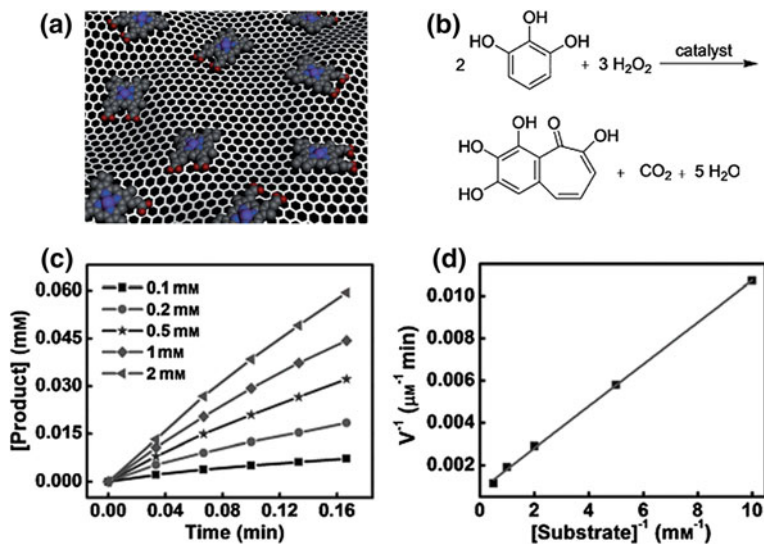
Fig. 5.2 a Formation of graphene/hemin conjugates through π–π stacking interactions.
b Oxidation reaction of pyrogallol, in which pyrogallol was oxidized to purpurogallin by
hydrogen peroxide. **c** The initial pyrogallol oxidation profile catalyzed by graphene/hemin
conjugates (5 μM hemin equivalent). The concentrations of pyrogallol ranged from 0.1 to 2 mM.
d Lineweaver–Burk plot of the pyrogallol oxidation catalyzed by the hemin–graphene conjugates.
Reprinted from Ref. [53] by permission of John Wiley & Sons Ltd.

from self-dimerization to form catalytically inactive species. Second, graphene as a
support could block one side of the porphyrin molecule which could prevent H_2O_2
attack from both sides, thus lowering the possibility of oxidative destruction of the
catalyst molecules themselves. Third, graphene provided a 2D support with a large
open and accessible surface area; therefore, the diffusion of the substrate and
product away from the catalytic centers was much easier, which could be beneficial
to the reaction turnover rate and the binding interactions. Moreover, graphene could
function as a π donor to the iron centers of hemin through cation–π interactions.

Exploring graphene-based composites as the platforms, various molecules have
been detected using electrochemical (CV [55–58], CA [59–64], and ASV [67]),
colorimetric [66], and fluorescent [65, 68–70] methods. For instance, Tu et al. [61]
introduced positively charged picket-fence porphyrin (FeTMAPP) to functionalize
rGO with good biocompatibility and dispersibility in aqueous solution. The planar
side of FeTMAPP reduced the distance between the porphyrin plane and flattened
rGO, thus resulting in a fast electronic communication between FeTMAPP and
flattened rGO. Due to the synergistic effect, the nanocomposite showed excellent
electrocatalytic activity toward the reduction of chlorite, leading to highly sensitive
amperometric biosensing at low applied potential. The biosensor for chlorite
showed a LOD of 24 nM at a signal-to-noise ratio of 3. Recently, a novel label-free
colorimetric strategy was developed for ultrasensitive detection of heparin based on

GO quenching the color of self-assembly Au nanorods [66]. They took full advantage of the strong electrostatic interaction between GO and CTAB-stabilized Au nanorods as well as high binding affinity of protamine with heparin, and attained the ultrasensitive detection of heparin with LOD of 5 ng/mL. A fluorescent assay was also developed for heparin detection by Cai et al. [65]. In their design, a water-soluble pyrene-based butterfly-shaped conjugated oligoelectrolyte (TFP) was synthesized and integrated with GO. Efficient fluorescence quenching of TFP by GO occurred due to the electrostatic and π–π interactions, leading to nearly dark emission in the absence of analytes. Addition of heparin minimized the fluorescence quenching of GO toward TFP, and strong yellow fluorescence was observed, which allowed to light up visual discrimination of heparin from its analogs. The LOD was estimated to be 0.046 U/mL, which was practical for heparin monitoring during postoperative and long-term care.

Theoretical and experimental studies of graphene have indicated that its band gap and optical properties could be manipulated by reducing its size to nanolevel, forming GQDs. When their sizes are down to 100 nm, GQDs possess strong quantum confinement and edge effects. If their sizes are reduced to ca. 10 nm, the two effects would become more pronounced and induce new physical, optical properties. Recently, researches have been carried out to illustrate the fabrication, property, and application of GQDs [71–78]. The new photoluminescence of GQDs expands the application of graphene-based materials especially in photovoltaics, bioimaging, and fluorescent assay. Based on this, our group, for the first time, reported that water-soluble and surface-unmodified GQDs served as a novel, effective, and simple fluorescent sensing platform for ultrasensitive detection of 2,4,6-trinitrotoluene (TNT) in solution by FRET quenching [68]. The fluorescent GQDs could specifically bind to TNT species via π–π stacking interaction between GQDs and aromatic rings. As a consequence, TNT molecules suppressed strongly the fluorescence emission by the FRET from GQDs donor to the irradiative TNT acceptor through intermolecular polar–polar interactions at spatial proximity. The unmodified GQDs sensitively detected down to ∼0.495 ppm (2.2 mM) TNT with the use of only 1 mL of GQDs solution. Eliminating further treatment or modification, this method simplified and shortened the experimental process. It possessed good assembly flexibility and could find new avenues in other analytes detection employing the own photoluminescence of GQDs.

5.3.2   Gas

The unique structure and oxygenic functionalities of GO facilitate it to be easily turned into a potentially useful gas storage material. Yildirim et al. showed that by using the well-known reactivity between boronic acids and hydroxyl groups, GO layers could be linked together to form a new layered structure, naming graphene oxide framework (GOF) [79, 80]. Such GOF structures had tunable pore widths, volumes, and binding sites depending on the linkers, and exhibited interesting gas
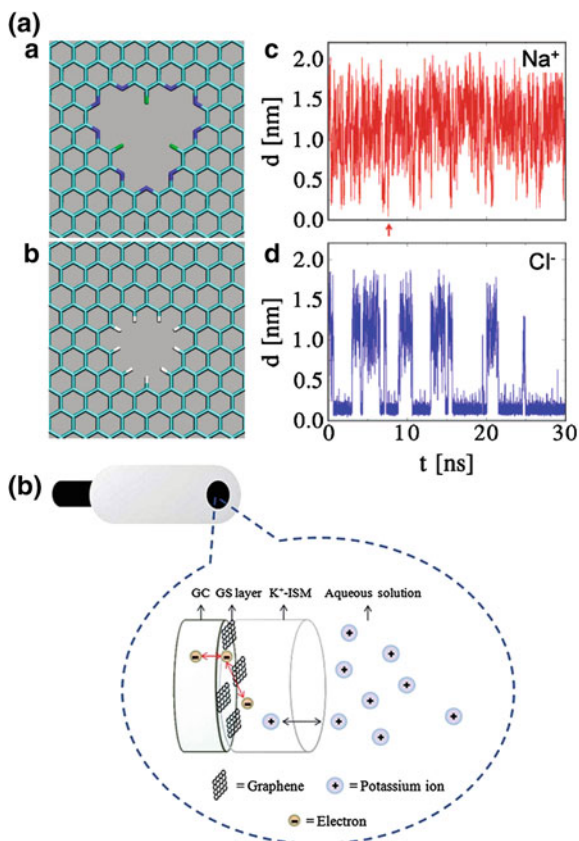
sorption properties. The GOF exhibited reasonably higher surface area about 470 m^2/g compared to the ca. 10 m^2/g for GO. Both isosteric heat of adsorption and the adsorbed hydrogen capacity per surface area were twice as large as typical porous carbon materials and comparable to metal–organic frameworks with open metal centers. They found that the pillaring unit was highly important in expanding GO layers and keeping some available room for hydrogen adsorption. Also, through theoretical calculations, the ideal GOF structures should have much higher surface area, which could be improved by chemical reduction to remove unreacted functional groups. Using graphene as the support, MoS$_2$/RGO [81] and Al$_2$O$_3$/graphene [82] were fabricated for hydrogen evolution reaction and ethanol gas sensing, respectively.

5.3.3 Ions

Biological ionic and molecular channels play a key role in many cellular transport phenomena, where channels with novel structures and recognition principles are in need. To achieve this goal, functionalized nanopores in graphene monolayers were designed and served as ionic sieves of high selectivity and transparency [83]. Nanopores were formed by ion etching and modified by local oxidation. The F–N-pore was terminated by negatively charged nitrogens and fluorines, favoring the passage of cations, such as Li$^+$, Na$^+$, and K$^+$ ions (Fig. 5.3a a). The H-pore was terminated by positively charged hydrogens, favoring the passage of anions, such as Cl$^-$ and Br$^-$ ions (Fig. 5.3a b). MD simulations were used to study the ions passing the nanopores, where ions were driven by an electric field E applied in the direction perpendicular to the graphene sheet. Different dynamics were revealed from the distance fluctuations. The Na$^+$ ion passed the F–N-pore fast, without significantly binding with it. The ion rarely got closer than 5 Å to the pore center and stayed most of the time in the water region ($d > 10$ Å) (Fig. 5.3a c). The Cl$^-$ ion had more stable binding to the symmetric H-pore, where it stayed for ~ 70 % of the time (Fig. 5.3a d). The ion selectivity and passage rates through these nanopores could be optimized by choosing the type of monolayer material, the size and shape of the nanopores, and the structure and number of functional ligands attached to their rim. Moreover, atomic monolayers with different types of nanopores might be arranged in dense arrays that would allow fast and efficient separation of different molecular species at the microscale and nanoscale. Recently, nanosized N-doped GO with visible fluorescence in water was prepared by cutting and unzipping of N-doped CNTs and used to distinguish between normal and transition metal ions [84]. It was found that the normal metal ions enhanced the fluorescence, whereas the transition metal ions caused the decrease of fluorescence intensity of N-doped GO when the concentration was high.

Because of their obvious advantages (e.g., maintenance-free, robustness, and cost-effective fabrication), solid contact ion-selective electrodes (SC-ISEs) have emerged as the most promising generation of potentiometric ion sensors. The main component

of SC-ISEs is a SC ion-to-electron transducer between the ion-selective membrane (ISM) and the conducting substrate (CS), whose intrinsic properties greatly determine the analytical performance of SC-ISEs, in particular the stability and reproducibility of potential readings. Various materials have been developed as the transducer layer, such as Au clusters [86], CNT [87, 88], conducting polymers [89, 90]. Recently, efforts have been devoted to exploring graphene as the potential transducer in SC-ISEs due to its specific capacitance. For instance, our group first fabricated a new type of K$^+$ SC-ISE using graphene as the intermediate layer between an ionophore-doped solvent polymeric membrane and a GCE (Fig. 5.3b) [85]. The obtained potentiometric sensors were characterized with a calibration line of slope close to Nernstian (59.2 mV/decade) within the activity from $10^{-4.5}$ to 0.1 M. A significant water layer was not detected in the ion-selective membrane or the transducer layer interface, preventing the adverse influence of gases. The high capacitance of the graphene SC resulted in a signal that was stable over 1 week. The short response time was less than 10 s for activities higher than 10^{-5} M. Almost at the same time, a K$^+$ SC-ISE with graphene as the SC was also fabricated, which exhibited a Nernstian response of 59.2 mV/decade and a detection limit of $10^{-6.2}$ M [91]. Actually, by

changing the components of the ISM, the SC-ISE could be switched to detect other ions. For instance, Ca^{2+} SC-ISE was developed also using RGO of different thicknesses as the ion-to-electron transducer materials [92]. RGO films acted as asymmetric capacitors, creating a capacitance due to the constant-phase elements present in the system. Highly reproducible sensing responses overtime with an outstanding increased signal-to-noise ratio with drifts of only 10 μV/h were obtained. These performance parameters were among the best compared to those of other ISE transducer materials so far. Screen-printed Ca^{2+} SC-ISE was also prepared by a one-step electrodeposition technique [93]. The disposable electrode exhibited a Nernstian slope (29.1 mV/decade), low detection limit ($10^{-5.8}$ M), and fast response time (less than 10 s). With its ease of fabrication and processing into reproducible films of controlled thickness and ease for further tailoring chemical composition and electrical properties, graphene offers great promise as a reliable high-performance transducer material for SC-ISE sensors.

By using an ion-selective crown ether and FRET from carbon dots to graphene, a metal ion sensor with high K^+ selectivity and tunable dynamic range was reported recently [94]. LOD was estimated to be 10 μM, and sufficient discrimination was obtained against other ions, especially Na^+ (37-fold). Moreover, the strategy could be readily extended to sensing of other cations by simply using other specific crown ethers.

Heavy metals are extremely harmful pollutants in the biosphere due to their toxicity, and even trace amounts of them pose a detrimental risk to human health. It is very important to detect them with high sensitivity, selectivity, and rapidness. Based on the specific formation of cytosine–Ag–cytosine and the super quenching ability of GO, a type of fluorescent assay for Ag^+ was recently reported [95]. In their design, fluorophore-labeled cytosine-rich oligonucleotide was adsorbed on GO in the absence of Ag^+, where the fluorescence was quenched. While with the addition of Ag^+, the oligonucleotide specifically interacted with Ag^+ and the resulted structure left from GO surface, leading to the restoration of the fluorescence. By modifying this procedure, a dual-output fluorescent DNA INHIBIT logic gate for detection of Ag^+ and cysteine was also developed with two separate cytosine-rich oligonucleotides [96].

Exploiting the optical property of GO (length or width <1 μm), a novel platform for effective 'turn-on' fluorescence sensing of Pb^{2+} in aqueous solution was developed [97]. The AuNP-functionalized graphene exhibited minimal background fluorescence, while fluorescence restoration and significant enhancement happened upon adding Pb^{2+}, which was attributed to the fact that Pb^{2+} could accelerate the leaching rate of AuNPs on graphene surface in the presence of both thiosulfate and 2-mercaptoethanol. Low LOD of 10 nM and high selectivity over common coexistent metal ions were achieved. Highly selective adsorption of Pb^{2+} was obtained at SiO_2/graphene with the maximum adsorption capacity of 113.6 mg/g [98]. This composite showed potential application in the removal of Pb^{2+} from agricultural and industrial wastewater. Recently, DNAzymes, which are in vitro-selected DNA molecules with enzyme-like catalytic activities, have been utilized in constructing Pb^{2+} sensors with graphene as the fluorescence quencher [99, 100]. Pb^{2+}-dependent

DNAzyme hybridized with fluorophore-labeled substrate strand and the single ribonucleotide served as the cleavage site. In the presence of Pb^{2+}, the substrate strand was specifically and irreversibly cleaved at this cleavage site, resulting in the disassembly of the duplex into three ss-DNA fragments and changes of the fluorescence intensity. Low LOD reached 0.3–0.5 nM. In a similar manner, Cu^{2+}-dependent DNAzymes have also been designed and used for sensitive Cu^{2+} detection with the LOD down to nM level [101, 102]. Furthermore, the controllable DNA cleavage reaction provides an original and alternative internal method to regulate the interaction between graphene and DNA relative to the previous external sequence-specific hybridization-dependent regulation, which will open new opportunities for nucleic acid studies and sensing applications in the future.

Due to the strong van der Waals interactions between long alkyl chains and hydrophobic graphene surfaces, 1-octadecanethiol molecules could self-assemble into large-scale highly ordered monolayers on single-layer graphene regardless of the roughness of graphene surfaces inherited from the underlying amorphous SiO_2 dielectric substrates [103]. AFM images showed that after contacting with Hg^{2+}, the height of graphene changed from 0.6 to 1.6 nm. Then, detection of 10 ppm Hg^{2+} ions with alkanethiol-modified graphene-FETs was achieved, which opens up new opportunities for graphene-based electronics as heavy metal sensors. Highly selective adsorption of Hg^{2+} by PPy–RGO composite was recently achieved with an adsorption capacity of 980 mg/g and desorption capacity of up to 92.3 %, showing practical utility for wastewater treatment [104]. The polymerization of pyrrole along graphene sheets resulted in an increased surface area and adsorption sites, which contributed to the enhanced adsorption capacity. Later, electrochemical detection of Hg^{2+} using PPy–RGO was also reported [105, 106]. The metal ion Hg^{2+} was believed to selectively coordinate with the nitrogens of the pyrrole unit in a 1:4 complexation mode from a mixed solution of Cu^{2+}, Pb^{2+}, Cd^{2+}, Zn^{2+}, and Hg^{2+} due to a greater binding affinity of PPy–RGO for Hg^{2+} than for the other four metal ions. When square-wave anodic stripping voltammetry (SWASV) was used, the adsorbed Hg^{2+} was then reduced to Hg^0 at a certain potential. The anodic stripping current (that is, Hg^0 was reoxidized to Hg^{2+}) was obtained in a potential range for the identification of Hg^{2+}. Excellent sensitivity (0.124 µA nM^{-1}) and low LOD (15 nM) results were achieved. Monodispersed AuNP-decorated graphene had also been used for voltammetric detection of Hg^{2+} [107].

Based on the interaction between mercapto group and Hg^{2+}, both fluorescent measurement [108] and voltammetric [109] measurement of Hg^{2+} were realized by using graphene as the substrate. Another well-known interaction is the thymine–Hg^{2+}–thymine complex, in which Hg^{2+} ions are sandwiched between the poly(T)-oligonucleotides (PTO). According to this, fluorescent detection of Hg^{2+} was achieved by using graphene as the fluorescence quencher [110, 111] or fluorescence donor [112]. Exploiting GO as an electrochemically active indicator, electrochemical detection of Hg^{2+} was recently reported by Park et al. [113]. In their design, thiol-functionalized PTO was anchored on gold electrode and used as the platform for trapping Hg^{2+} ions, taking advantage of forming thymine–Hg^{2+}–thymine complex and stronger π–π interactions of ssDNA with GO than dsDNA due to disclosed base

moiety of ssDNA. In the absence of Hg^{2+}, GO interacted with PTO and the electrochemical reduction peak of GO was observed. While, in the presence of Hg^{2+}, a little amount of GO could be adsorbed on dsDNA-modified electrode and very low intensity of the electrochemical reduction peak of GO was obtained. Using the thymine–Hg^{2+}–thymine system, very low LOD (lower than 1 nM) was achieved.

Simultaneous and selective electrochemical sensing of several metal ions seems to be extremely important and challenging. Recently, this was achieved by Wei et al. [114] using SnO_2/RGO composite. SnO_2 was used in combination with graphene to fabricate an electrochemical platform for the simultaneous analysis of Cd^{2+}, Pb^{2+}, Cu^{2+}, and Hg^{2+} in solution by SWASV. The SnO_2 nanoparticles not only prevented the graphene from gathering together but also acted as electrochemical catalyst in detecting these metal ions. LODs toward Cd^{2+}, Pb^{2+}, Cu^{2+}, and Hg^{2+} ions were 0.1015, 0.1839, 0.2269, and 0.2789 nM, respectively, which were very below the guideline value given by the World Health Organization (WHO).

References

1. Erecinska, M., Wilson, D.F.: Regulation of cellular energy metabolism. J. Membr. Biol. **70**, 1–14 (1982)
2. Guo, S., Du, Y., Yang, X., Dong, S., Wang, E.: Solid-state label-free integrated aptasensor based on graphene-mesoporous silica-gold nanoparticle hybrids and silver microspheres. Anal. Chem. **83**, 8035–8040 (2011)
3. Zhang, H., Han, Y., Guo, Y., Dong, C.: Porphyrin functionalized graphene nanosheets-based electrochemical aptasensor for label-free ATP detection. J. Mater. Chem. **22**, 23900–23905 (2012)
4. Ruan, C., Xu, L., Wang, X., Lou, J., Gao, W., Sun, W.: Graphene functionalized graphite electrode with diphenylacetylene for sensitive electrochemical determination of adenosine-5′-triphosphate. Electroanalysis **24**, 286–292 (2012)
5. Wang, L., Xu, M., Han, L., Zhou, M., Zhu, C., Dong, S.: Graphene enhanced electron transfer at aptamer modified electrode and its application in biosensing. Anal. Chem. **84**, 7301–7307 (2012)
6. Dong, X., Long, Q., Wang, J., Chan-Park, M.B., Huang, Y., Huang, W., Chen, P.: A graphene nanoribbon network and its biosensing application. Nanoscale **3**, 5156–5160 (2011)
7. Wang, L., Zhu, J.B., Han, L., Jin, L.H., Zhu, C.Z., Wang, E.K., Dong, S.J.: Graphene-based aptamer logic gates and their application to multiplex detection. ACS Nano **6**, 6659–6666 (2012)
8. Lu, C.H., Li, J., Lin, M.H., Wang, Y.W., Yang, H.H., Chen, X., Chen, G.N.: Amplified aptamer-based assay through catalytic recycling of the analyte. Angew. Chem. Int. Ed. **49**, 8454–8457 (2010)
9. Wang, Y., Li, Z., Hu, D., Lin, C.-T., Li, J., Lin, Y.: Aptamer graphene oxide nanocomplex for in situ molecular probing in living cells. J. Am. Chem. Soc. **132**, 9274–9276 (2010)
10. He, Y., Wang, Z.G., Tang, H.W., Pang, D.W.: Low background signal platform for the detection of ATP: when a molecular aptamer beacon meets graphene oxide. Biosens. Bioelectron. **29**, 76–81 (2011)
11. Pu, W.D., Zhang, L., Huang, C.Z.: Graphene oxide as a nano-platform for ATP detection based on aptamer chemistry. Anal. Methods **4**, 1662–1666 (2012)

12. Zhu, W., Zhao, Z., Li, Z., Jiang, J., Shen, G., Yu, R.: A ligation-triggered highly sensitive fluorescent assay of adenosine triphosphate based on graphene oxide. Analyst **137**, 5506–5509 (2012)

13. Liu, C., Wang, Z., Jia, H., Li, Z.: Efficient fluorescence resonance energy transfer between upconversion nanophosphors and graphene oxide: a highly sensitive biosensing platform. Chem. Commun. **47**, 4661–4663 (2011)

14. Tan, X., Chen, T., Xiong, X., Mao, Y., Zhu, G., Yasun, E., Li, C., Zhu, Z., Tan, W.: Semiquantification of ATP in live cells using nonspecific desorption of DNA from graphene oxide as the internal reference. Anal. Chem. **84**, 8622–8627 (2012)

15. Wang, J., Yang, S., Guo, D., Yu, P., Li, D., Ye, J., Mao, L.: Comparative studies on electrochemical activity of graphene nanosheets and carbon nanotubes. Electrochem. Commun. **11**, 1892–1895 (2009)

16. Brownson, D.A., Gorbachev, R.V., Haigh, S.J., Banks, C.E.: CVD graphene vs. highly ordered pyrolytic graphite for use in electroanalytical sensing. Analyst **137**, 833–839 (2012)

17. Brownson, D.A., Gomez-Mingot, M., Banks, C.E.: CVD graphene electrochemistry: biologically relevant molecules. Phys. Chem. Chem. Phys. **13**, 20284–20288 (2011)

18. Pumera, M., Scipioni, R., Iwai, H., Ohno, T., Miyahara, Y., Boero, M.: A mechanism of adsorption of beta-nicotinamide adenine dinucleotide on graphene sheets: experiment and theory. Chem.-Eur. J. **15**, 10851–10856 (2009)

19. Punckt, C., Pope, M.A., Liu, J., Lin, Y., Aksay, I.A.: Electrochemical performance of graphene as effected by electrode porosity and graphene functionalization. Electroanalysis **22**, 2834–2841 (2010)

20. Lin, W.-J., Liao, C.-S., Jhang, J.-H., Tsai, Y.-C.: Graphene modified basal and edge plane pyrolytic graphite electrodes for electrocatalytic oxidation of hydrogen peroxide and β-nicotinamide adenine dinucleotide. Electrochem. Commun. **11**, 2153–2156 (2009)

21. Brownson, D.A.C., Metters, J.P., Kampouris, D.K., Banks, C.E.: Graphene electrochemistry: surfactants inherent to graphene can dramatically effect electrochemical processes. Electroanalysis **23**, 894–899 (2011)

22. Li, X., Yang, X., Jia, L., Ma, X., Zhu, L.: Carbonaceous debris that resided in graphene oxide/reduced graphene oxide profoundly affect their electrochemical behaviors. Electrochem. Commun. **23**, 94–97 (2012)

23. Valentini, F., Romanazzo, D., Carbone, M., Palleschi, G.: Modified screen-printed electrodes based on oxidized graphene nanoribbons for the selective electrochemical detection of several molecules. Electroanalysis **24**, 872–881 (2012)

24. Zhou, M., Zhai, Y., Dong, S.: Electrochemical sensing and biosensing platform based on chemically reduced graphene oxide. Anal. Chem. **81**, 5603–5613 (2009)

25. Guo, K., Qian, K., Zhang, S., Kong, J., Yu, C., Liu, B.: Bio-electrocatalysis of NADH and ethanol based on graphene sheets modified electrodes. Talanta **85**, 1174–1179 (2011)

26. Kumar, S.P., Manjunatha, R., Nethravathi, C., Suresh, G.S., Rajamathi, M., Venkatesha, T.V.: Electrocatalytic oxidation of NADH on functionalized graphene modified graphite electrode. Electroanalysis **23**, 842–849 (2011)

27. Qi, B., He, L., Bo, X., Yang, H., Guo, L.: Electrochemical preparation of free-standing few-layer graphene through oxidation–reduction cycling. Chem. Eng. J. **171**, 340–344 (2011)

28. Keeley, G.P., O'Neill, A., Holzinger, M., Cosnier, S., Coleman, J.N., Duesberg, G.S.: DMF-exfoliated graphene for electrochemical NADH detection. Phys. Chem. Chem. Phys. **13**, 7747–7750 (2011)

29. Randviir, E.P., Brownson, D.A., Gomez-Mingot, M., Kampouris, D.K., Iniesta, J., Banks, C.E.: Electrochemistry of Q-graphene. Nanoscale **4**, 6470–6480 (2012)

30. Valentini, F., Roscioli, D., Carbone, M., Conte, V., Floris, B., Palleschi, G., Flammini, R., Bauer, E.M., Nasillo, G., Caponetti, E.: Oxidized graphene in ionic liquids for assembling chemically modified electrodes: a structural and electrochemical characterization study. Anal. Chem. **84**, 5823–5831 (2012)

31. Shan, C., Yang, H., Han, D., Zhang, Q., Ivaska, A., Niu, L.: Electrochemical determination of NADH and ethanol based on ionic liquid-functionalized graphene. Biosens. Bioelectron. **25**, 1504–1508 (2010)
32. Liu, Q., Li, Y., Zhang, L., Li, D., Fan, C., Long, Y.-T.: Comparative studies on electrocatalytic activities of chemically reduced graphene oxide and electrochemically reduced graphene oxide noncovalently functionalized with poly(methylene blue). Electroanalysis **22**, 2862–2870 (2010)
33. Wang, D., Li, Y., Hasin, P., Wu, Y.: Preparation, characterization, and electrocatalytic performance of graphene-methylene blue thin films. Nano Res. **4**, 124–130 (2010)
34. Liu, H., Gao, J., Xue, M., Zhu, N., Zhang, M., Cao, T.: Processing of graphene for electrochemical application: noncovalently functionalize graphene sheets with water-soluble electroactive methylene green. Langmuir **25**, 12006–12010 (2009)
35. Chang, H., Wu, X., Wu, C., Chen, Y., Jiang, H., Wang, X.: Catalytic oxidation and determination of beta-NADH using self-assembly hybrid of gold nanoparticles and graphene. Analyst **136**, 2735–2740 (2011)
36. Fan, Y., Yang, X., Yang, C., Liu, J.: Au-TiO$_2$/Graphene nanocomposite film for electrochemical sensing of hydrogen peroxide and NADH. Electroanalysis **24**, 1334–1339 (2012)
37. Wen, Z., Cui, S., Pu, H., Mao, S., Yu, K., Feng, X., Chen, J.: Metal nitride/graphene nanohybrids: general synthesis and multifunctional titanium nitride/graphene electrocatalyst. Adv. Mater. **23**, 5445–5450 (2011)
38. Wang, K., Wu, J., Liu, Q., Jin, Y., Yan, J., Cai, J.: Ultrasensitive photoelectrochemical sensing of nicotinamide adenine dinucleotide based on graphene-TiO$_2$ nanohybrids under visible irradiation. Anal. Chim. Acta **745**, 131–136 (2012)
39. Prasannakumar, S., Manjunatha, R., Nethravathi, C., Suresh, G.S., Rajamathi, M., Venkatesha, T.V.: Graphene-carbon nanotubes modified graphite electrode for the determination of nicotinamide adenine dinucleotide and fabrication of alcohol biosensor. J. Solid State Electrochem. **16**, 3189–3199 (2012)
40. Sriprachuabwong, C., Karuwan, C., Wisitsorrat, A., Phokharatkul, D., Lomas, T., Sritongkham, P., Tuantranont, A.: Inkjet-printed graphene-PEDOT:PSS modified screen printed carbon electrode for biochemical sensing. J. Mater. Chem. **22**, 5478–5485 (2012)
41. Yang, H., Shan, C., Li, F., Han, D., Zhang, Q., Niu, L.: Covalent functionalization of polydisperse chemically-converted graphene sheets with amine-terminated ionic liquid. Chem. Commun. 3880–3882 (2009)
42. Deng, S., Lei, J., Cheng, L., Zhang, Y., Ju, H.: Amplified electrochemiluminescence of quantum dots by electrochemically reduced graphene oxide for nanobiosensing of acetylcholine. Biosens. Bioelectron. **26**, 4552–4558 (2011)
43. Zhang, M., Yuan, R., Chai, Y., Chen, S., Zhong, X., Zhong, H., Wang, C.: A cathodic electrogenerated chemiluminescence biosensor based on luminol and hemin-graphene nanosheets for cholesterol detection. RSC Adv. **2**, 4639–4641 (2012)
44. Qiu, H., Luo, C., Sun, M., Lu, F., Fan, L., Li, X.: A chemiluminescence array sensor based on graphene-magnetite-molecularly imprinted polymers for determination of benzenediol isomers. Anal. Chim. Acta **744**, 75–81 (2012)
45. Qiu, H., Luo, C., Sun, M., Lu, F., Fan, L., Li, X.: A chemiluminescence sensor for determination of epinephrine using graphene oxide–magnetite-molecularly imprinted polymers. Carbon **50**, 4052–4060 (2012)
46. Liu, X., Cao, L., Song, W., Ai, K., Lu, L.: Functionalizing metal nanostructured film with graphene oxide for ultrasensitive detection of aromatic molecules by surface-enhanced Raman spectroscopy. ACS Appl. Mater. Interfaces **3**, 2944–2952 (2011)
47. Lu, G., Li, H., Liusman, C., Yin, Z., Wu, S., Zhang, H.: Surface enhanced Raman scattering of Ag or Au nanoparticle-decorated reduced graphene oxide for detection of aromatic molecules. Chem. Sci. **2**, 1817–1821 (2011)

48. Ren, W., Fang, Y.X., Wang, E.K.: A binary functional substrate for enrichment and ultrasensitive SERS spectroscopic detection of folic acid using graphene oxide/Ag nanoparticle hybrids. ACS Nano **5**, 6425–6433 (2011)

49. Zhao, G., Jiang, L., He, Y., Li, J., Dong, H., Wang, X., Hu, W.: Sulfonated graphene for persistent aromatic pollutant management. Adv. Mater. **23**, 3959–3963 (2011)

50. Sun, H., Cao, L., Lu, L.: Magnetite/reduced graphene oxide nanocomposites: one step solvothermal synthesis and use as a novel platform for removal of dye pollutants. Nano Res. **4**, 550–562 (2011)

51. Hu, X., Mu, L., Wen, J., Zhou, Q.: Immobilized smart RNA on graphene oxide nanosheets to specifically recognize and adsorb trace peptide toxins in drinking water. J. Hazard. Mater. **213–214**, 387–392 (2012)

52. Gulbakan, B., Yasun, E., Shukoor, M.I., Zhu, Z., You, M.X., Tan, X.H., Sanchez, H., Powell, D.H., Dai, H.J., Tan, W.H.: A dual platform for selective analyte enrichment and ionization in mass spectrometry using aptamer-conjugated graphene oxide. J. Am. Chem. Soc. **132**, 17408–17410 (2010)

53. Xue, T., Jiang, S., Qu, Y., Su, Q., Cheng, R., Dubin, S., Chiu, C.Y., Kaner, R., Huang, Y., Duan, X.: Graphene-supported hemin as a highly active biomimetic oxidation catalyst. Angew. Chem. Int. Ed. **51**, 3822–3825 (2012)

54. Huang, C., Bai, H., Li, C., Shi, G.: A graphene oxide/hemoglobin composite hydrogel for enzymatic catalysis in organic solvents. Chem. Commun. **47**, 4962–4964 (2011)

55. Yue, R., Lu, Q., Zhou, Y.: A novel nitrite biosensor based on single-layer graphene nanoplatelet–protein composite film. Biosens. Bioelectron. **26**, 4436–4441 (2011)

56. Srivastava, R.K., Srivastava, S., Narayanan, T.N., Mahlotra, B.D., Vajtai, R., Ajayan, P.M., Srivastava, A.: Functionalized multilayered graphene platform for urea sensor. ACS Nano **6**, 168–175 (2012)

57. Wang, Y., Wan, Y., Zhang, D.: Reduced graphene sheets modified glassy carbon electrode for electrocatalytic oxidation of hydrazine in alkaline media. Electrochem. Commun. **12**, 187–190 (2010)

58. Xu, C., Wang, J., Wan, L., Lin, J., Wang, X.: Microwave-assisted covalent modification of graphene nanosheets with hydroxypropyl-β-cyclodextrin and its electrochemical detection of phenolic organic pollutants. J. Mater. Chem. **21**, 10463–10471 (2011)

59. Song, W., Li, D.W., Li, Y.T., Li, Y., Long, Y.T.: Disposable biosensor based on graphene oxide conjugated with tyrosinase assembled gold nanoparticles. Biosens. Bioelectron. **26**, 3181–3186 (2011)

60. Zhang, J., Lei, J., Pan, R., Xue, Y., Ju, H.: Highly sensitive electrocatalytic biosensing of hypoxanthine based on functionalization of graphene sheets with water-soluble conducting graft copolymer. Biosens. Bioelectron. **26**, 371–376 (2010)

61. Tu, W., Lei, J., Zhang, S., Ju, H.: Characterization, direct electrochemistry, and amperometric biosensing of graphene by noncovalent functionalization with picket-fence porphyrin. Chem.-Eur. J. **16**, 10771–10777 (2010)

62. Choi, B.G., Park, H., Park, T.J., Yang, M.H., Kim, J.S., Jang, S.Y., Heo, N.S., Lee, S.Y., Kong, J., Hong, W.H.: Solution chemistry of self-assembled graphene nanohybrids for high-performance flexible biosensors. ACS Nano **4**, 2910–2918 (2010)

63. Wang, Y., Zhang, S., Du, D., Shao, Y., Li, Z., Wang, J., Engelhard, M.H., Li, J., Lin, Y.: Self assembly of acetylcholinesterase on a gold nanoparticles–graphene nanosheet hybrid for organophosphate pesticide detection using polyelectrolyte as a linker. J. Mater. Chem. **21**, 5319–5325 (2011)

64. Liu, F., Piao, Y., Choi, K.S., Seo, T.S.: Fabrication of free-standing graphene composite films as electrochemical biosensors. Carbon **50**, 123–133 (2012)

65. Cai, L., Zhan, R., Pu, K.Y., Qi, X., Zhang, H., Huang, W., Liu, B.: Butterfly-shaped conjugated oligoelectrolyte/graphene oxide integrated assay for light-up visual detection of heparin. Anal. Chem. **83**, 7849–7855 (2011)

66. Fu, X., Chen, L., Li, J., Lin, M., You, H., Wang, W.: Label-free colorimetric sensor for ultrasensitive detection of heparin based on color quenching of gold nanorods by graphene oxide. Biosens. Bioelectron. **34**, 227–231 (2012)

67. Guo, C.X., Lu, Z.S., Lei, Y., Li, C.M.: Ionic liquid–graphene composite for ultratrace explosive trinitrotoluene detection. Electrochem. Commun. **12**, 1237–1240 (2010)

68. Fan, L., Hu, Y., Wang, X., Zhang, L., Li, F., Han, D., Li, Z., Zhang, Q., Wang, Z., Niu, L.: Fluorescence resonance energy transfer quenching at the surface of graphene quantum dots for ultrasensitive detection of TNT. Talanta **101**, 192–197 (2012)

69. Li, F., Feng, Y., Zhao, C., Li, P., Tang, B.: A sensitive graphene oxide-DNA based sensing platform for fluorescence "turn-on" detection of bleomycin. Chem. Commun. **48**, 127–129 (2012)

70. Wu, S., Duan, N., Ma, X., Xia, Y., Wang, H., Wang, Z., Zhang, Q.: Multiplexed fluorescence resonance energy transfer aptasensor between upconversion nanoparticles and graphene oxide for the simultaneous determination of mycotoxins. Anal. Chem. **84**, 6263–6270 (2012)

71. Li, Y., Hu, Y., Zhao, Y., Shi, G., Deng, L., Hou, Y., Qu, L.: An electrochemical avenue to green-luminescent graphene quantum dots as potential electron-acceptors for photovoltaics. Adv. Mater. **23**, 776–780 (2011)

72. Pan, D., Zhang, J., Li, Z., Wu, M.: Hydrothermal route for cutting graphene sheets into blue-luminescent graphene quantum dots. Adv. Mater. **22**, 734–738 (2010)

73. Saha, S.K., Baskey, M., Majumdar, D.: Graphene quantum sheets: a new material for spintronic applications. Adv. Mater. **22**, 5531–5536 (2010)

74. Shen, J., Zhu, Y., Chen, C., Yang, X., Li, C.: Facile preparation and upconversion luminescence of graphene quantum dots. Chem. Commun. **47**, 2580–2582 (2011)

75. Zhu, S., Zhang, J., Qiao, C., Tang, S., Li, Y., Yuan, W., Li, B., Tian, L., Liu, F., Hu, R., Gao, H., Wei, H., Zhang, H., Sun, H., Yang, B.: Strongly green-photoluminescent graphene quantum dots for bioimaging applications. Chem. Commun. **47**, 6858–6860 (2011)

76. Gupta, V., Chaudhary, N., Srivastava, R., Sharma, G.D., Bhardwaj, R., Chand, S.: Luminscent graphene quantum dots for organic photovoltaic devices. J. Am. Chem. Soc. **133**, 9960–9963 (2011)

77. Yan, X., Cui, X., Li, L.S.: Synthesis of large, stable colloidal graphene quantum dots with tunable size. J. Am. Chem. Soc. **132**, 5944–5945 (2010)

78. Ponomarenko, L.A., Schedin, F., Katsnelson, M.I., Yang, R., Hill, E.W., Novoselov, K.S., Geim, A.K.: Chaotic Dirac billiard in graphene quantum dots. Science **320**, 356–358 (2008)

79. Burress, J.W., Gadipelli, S., Ford, J., Simmons, J.M., Zhou, W., Yildirim, T.: Graphene oxide framework materials: theoretical predictions and experimental results. Angew. Chem. Int. Ed. **49**, 8902–8904 (2010)

80. Srinivas, G., Burress, J.W., Ford, J., Yildirim, T.: Porous graphene oxide frameworks: synthesis and gas sorption properties. J. Mater. Chem. **21**, 11323–11329 (2011)

81. Li, Y., Wang, H., Xie, L., Liang, Y., Hong, G., Dai, H.: MoS2 nanoparticles grown on graphene: an advanced catalyst for the hydrogen evolution reaction. J. Am. Chem. Soc. **133**, 7296–7299 (2011)

82. Jiang, Z., Wang, J., Meng, L., Huang, Y., Liu, L.: A highly efficient chemical sensor material for ethanol: Al_2O_3/Graphene nanocomposites fabricated from graphene oxide. Chem. Commun. **47**, 6350–6352 (2011)

83. Sint, K., Wang, B., Kral, P.: Selective ion passage through functionalized graphene nanopores. J. Am. Chem. Soc. **130**, 16448–16449 (2008)

84. Qian, Z., Zhou, J., Chen, J., Wang, C., Chen, C., Feng, H.: Nanosized N-doped graphene oxide with visible fluorescence in water for metal ion sensing. J. Mater. Chem. **21**, 17635–17637 (2011)

85. Li, F., Ye, J., Zhou, M., Gan, S., Zhang, Q., Han, D., Niu, L.: All-solid-state potassium-selective electrode using graphene as the solid contact. Analyst **137**, 618–623 (2012)

86. Zhou, M., Gan, S., Cai, B., Li, F., Ma, W., Han, D., Niu, L.: Effective solid contact for ion-selective electrodes: tetrakis(4-chlorophenyl)borate (TB-) anions doped nanocluster films. Anal. Chem. **84**, 3480–3483 (2012)

87. Crespo, G.A., Macho, S., Rius, F.X.: Ion-selective electrodes using carbon nanotubes as ion-to-electron transducers. Anal. Chem. **80**, 1316–1322 (2008)

88. Crespo, G.A., Macho, S., Bobacka, J., Rius, F.X.: Transduction mechanism of carbon nanotubes in solid-contact ion-selective electrodes. Anal. Chem. **81**, 676–681 (2009)

89. Bobacka, J., Ivaska, A., Lewenstam, A.: Potentiometric ion sensors. Chem. Rev. **108**, 329–351 (2008)

90. Mousavi, Z., Bobacka, J., Lewenstam, A., Ivaska, A.: Poly(3,4-ethylenedioxythiophene) (PEDOT) doped with carbon nanotubes as ion-to-electron transducer in polymer membrane-based potassium ion-selective electrodes. J. Electroanal. Chem. **633**, 246–252 (2009)

91. Ping, J., Wang, Y., Wu, J., Ying, Y.: Development of an all-solid-state potassium ion-selective electrode using graphene as the solid-contact transducer. Electrochem. Commun. **13**, 1529–1532 (2011)

92. Hernández, R., Riu, J., Bobacka, J., Vallés, C., Jiménez, P., Benito, A.M., Maser, W.K., Rius, F.X.: Reduced graphene oxide films as solid transducers in potentiometric all-solid-state ion-selective electrodes. J. Phys. Chem. C **116**, 22570–22578 (2012)

93. Ping, J., Wang, Y., Ying, Y., Wu, J.: Application of electrochemically reduced graphene oxide on screen-printed ion-selective electrode. Anal. Chem. **84**, 3473–3479 (2012)

94. Wei, W., Xu, C., Ren, J., Xu, B., Qu, X.: Sensing metal ions with ion selectivity of a crown ether and fluorescence resonance energy transfer between carbon dots and graphene. Chem. Commun. **48**, 1284–1286 (2012)

95. Wen, Y., Xing, F., He, S., Song, S., Wang, L., Long, Y., Li, D., Fan, C.: A graphene-based fluorescent nanoprobe for silver(I) ions detection by using graphene oxide and a silver-specific oligonucleotide. Chem. Commun. **46**, 2596–2598 (2010)

96. Xie, W.Y., Huang, W.T., Li, N.B., Luo, H.Q.: Design of a dual-output fluorescent DNA logic gate and detection of silver ions and cysteine based on graphene oxide. Chem. Commun. **48**, 82–84 (2012)

97. Fu, X., Lou, T., Chen, Z., Lin, M., Feng, W., Chen, L.: "Turn-on" fluorescence detection of lead ions based on accelerated leaching of gold nanoparticles on the surface of graphene. ACS Appl. Mater. Interfaces **4**, 1080–1086 (2012)

98. Hao, L., Song, H., Zhang, L., Wan, X., Tang, Y., Lv, Y.: SiO2/graphene composite for highly selective adsorption of Pb(II) ion. J. Colloid Interface Sci. **369**, 381–387 (2012)

99. Zhao, X.H., Kong, R.M., Zhang, X.B., Meng, H.M., Liu, W.N., Tan, W., Shen, G.L., Yu, R.Q.: Graphene-DNAzyme based biosensor for amplified fluorescence "turn-on" detection of Pb2+ with a high selectivity. Anal. Chem. **83**, 5062–5066 (2011)

100. Wen, Y., Peng, C., Li, D., Zhuo, L., He, S., Wang, L., Huang, Q., Xu, Q.H., Fan, C.: Metal ion-modulated graphene-DNAzyme interactions: design of a nanoprobe for fluorescent detection of lead(II) ions with high sensitivity, selectivity and tunable dynamic range. Chem. Commun. **47**, 6278–6280 (2011)

101. Liu, M., Zhao, H., Chen, S., Yu, H., Zhang, Y., Quan, X.: A "turn-on" fluorescent copper biosensor based on DNA cleavage-dependent graphene-quenched DNAzyme. Biosens. Bioelectron. **26**, 4111–4116 (2011)

102. Liu, M., Zhao, H., Chen, S., Yu, H., Zhang, Y., Quan, X.: Label-free fluorescent detection of Cu(II) ions based on DNA cleavage-dependent graphene-quenched DNAzymes. Chem. Commun. **47**, 7749–7751 (2011)

103. Zhang, T., Cheng, Z., Wang, Y., Li, Z., Wang, C., Li, Y., Fang, Y.: Self-assembled 1-octadecanethiol monolayers on graphene for mercury detection. Nano Lett. **10**, 4738–4741 (2010)

104. Chandra, V., Kim, K.S.: Highly selective adsorption of Hg2+ by a polypyrrole-reduced graphene oxide composite. Chem. Commun. **47**, 3942–3944 (2011)

105. Zhao, Z.Q., Chen, X., Yang, Q., Liu, J.H., Huang, X.J.: Selective adsorption toward toxic metal ions results in selective response: electrochemical studies on a polypyrrole/reduced graphene oxide nanocomposite. Chem. Commun. **48**, 2180–2182 (2012)

106. Zhao, Z.-Q., Chen, X., Yang, Q., Liu, J.-H., Huang, X.-J.: Beyond the selective adsorption of polypyrrole-reduced graphene oxide nanocomposite toward Hg^{2+}: Ultra-sensitive and -selective sensing Pb^{2+} by stripping voltammetry. Electrochem. Commun. **23**, 21–24 (2012)
107. Gong, J., Zhou, T., Song, D., Zhang, L.: Monodispersed Au nanoparticles decorated graphene as an enhanced sensing platform for ultrasensitive stripping voltammetric detection of mercury(II). Sens. Actuators B-Chem. **150**, 491–497 (2010)
108. Huang, W.T., Shi, Y., Xie, W.Y., Luo, H.Q., Li, N.B.: A reversible fluorescence nanoswitch based on bifunctional reduced graphene oxide: use for detection of Hg^{2+} and molecular logic gate operation. Chem. Commun. **47**, 7800–7802 (2011)
109. Zhou, H., Wang, X., Yu, P., Chen, X., Mao, L.: Sensitive and selective voltammetric measurement of Hg^{2+} by rational covalent functionalization of graphene oxide with cysteamine. Analyst **137**, 305–308 (2012)
110. Zhang, J.R., Huang, W.T., Xie, W.Y., Wen, T., Luo, H.Q., Li, N.B.: Highly sensitive, selective, and rapid fluorescence Hg^{2+} sensor based on DNA duplexes of poly(dT) and graphene oxide. Analyst **137**, 3300–3305 (2012)
111. Kong, L., Wang, J., Zheng, G., Liu, J.: A highly sensitive protocol (FRET/SIMNSEF) for the determination of mercury ions: a unity of fluorescence quenching of graphene and enhancement of nanogold. Chem. Commun. **47**, 10389–10391 (2011)
112. Li, M., Zhou, X., Ding, W., Guo, S., Wu, N.: Fluorescent aptamer-functionalized graphene oxide biosensor for label-free detection of mercury(II). Biosens. Bioelectron. **41**, 889–893 (2013)
113. Park, H., Hwang, S.-J., Kim, K.: An electrochemical detection of Hg^{2+} ion using graphene oxide as an electrochemically active indicator. Electrochem. Commun. **24**, 100–103 (2012)
114. Wei, Y., Gao, C., Meng, F.-L., Li, H.-H., Wang, L., Liu, J.-H., Huang, X.-J.: SnO_2/Reduced graphene oxide nanocomposite for the simultaneous electrochemical detection of Cadmium (II), Lead(II), Copper(II), and Mercury(II): an interesting favorable mutual interference. J. Phys. Chem. C **116**, 1034–1041 (2012)

Chapter 6
Graphene in Drug Delivery, Cellular Imaging, Bacteria Inhibition, Versatile Targets Bioassays

Abstract The evaluation of potential risk of graphene to human body has been carried out due to its exceptional promise in various applications, such as glucose detection, drug delivery, and cellular imaging. Small nanosheets entered cells mainly through clathrin-mediated endocytosis, and the increase in graphene size enhanced phagocytotic uptake of the nanosheets. Cellular imaging and drug delivery have also been achieved by using biocompatible material-grafted graphene platforms. Graphene can also be used in pathogen and bacteria inhibition in the form of graphene nanowalls deposited on stainless steel substrates. Recently, versatile bioassay represents one of the main challenges in bioanalytical applications. The large surface area and universal fluorescence quenching ability of graphene sheets enable it to be an efficient platform for multiplex targets assay in a fluorescent manner. Based on this, multiplex analytes, such as DNA, thrombin, Ag^+, Hg^{2+}, cysteine and DNA, thrombin, ATP in logic gate operations, have been successfully detected with high sensitivity and simplicity.

Keywords Graphene · Drug delivery · Cellular imaging · Bacteria inhibition · Targets bioassay

6.1 Graphene Cytotoxicity, Cellular Imaging, and Drug Delivery

Given the exceptional promise of graphene and GO in various applications, it is critically important that a systematic evaluation of their potential risk to human health should be carried out. Research demonstrated that the cytotoxicity of GO nanosheets arose from direct interactions between the cell membrane and GO nanosheets that resulted in physical damage to the cell membrane [1]. This cytotoxicity occurred mostly during the initial contact stage of GO and cells and was independent of exposure duration. This effect was largely attenuated when GO was incubated with fetal bovine serum (FBS), an often employed component in cell culture medium, due

to the extremely high protein adsorption ability of GO. The long-term in vivo bio-distribution of ^{125}I-labeled nanographene sheets functionalized with PEG and the potential toxicity of graphene over time were systematically examined [2]. This PEGylated graphene did not cause appreciable toxicity at tested dose (20 mg/kg) to the treated mice in a period of 3 months as evidenced by blood biochemistry, hematological analysis, and histological examinations. However, a recent study reported that GO with dose less than 20 μg/mL exhibited no toxicity to human fibroblast cells, and the dose of more than 50 μg/mL exhibited obvious cytotoxicity [3]. The experiments to mice also showed a dose-dependent toxicity effect of GO. Hence, GO exhibited dose-dependent toxicity to cells and animals, such as inducing cell apoptosis and lung granuloma formation, and could not be cleaned by kidney. Besides the dose-dependent toxicity, a recent research illustrated that the toxicity of GO and graphene was dependent on the exposure environment (i.e., whether or not in aggregation state) and mode of interaction with cells (i.e., suspension versus adherent cell types) [4]. When GO and graphene are explored for in vivo applications, the dose-dependent cytotoxicity and their present status, such as sheet size, morphology, exfoliation extent, and oxygen content, must be considered. On the other hand, these research results are highly encouraging and pave the way for future graphene-based in vivo biomedical research. Besides, graphene nanoparticles were illustrated to induce photothermal death of U251 human glioma cells in vitro, mediated through induction of oxidative stress and mitochondrial damage [5]. Graphene with different morphologies might induce varying degrees of damage, and the cytotoxicity of GO could be regulated by different reducers. For instance, glucose-reduced GO sheets exhibited excellent NIR photothermal therapy efficiency to LNCaP prostate cancer cells in vitro, which was better than hydrazine-reduced GO and CNT [6]. From the in vivo and in vitro studies, one can see that graphene represents one of the most promising biocompatible nanomaterials in bioapplication.

To fully realize the potential of graphene as biomaterials platforms, pretreatments of graphene are usually needed to enhance its dispersity, stability in electrolytes, and the biocompatibility with drugs and cells. Recently, Hong and coworkers designed two complementary strategies, utilizing either electrostatic or steric stabilization, to enable graphene to stay dispersed in cell culture media and serum [7]. The treated graphene nanosheets exhibited an enhancement of >250 % in the bioconjugation efficiency of streptavidin in comparison with untreated nanosheets, demonstrating the excellent performance as potential drug delivery vehicles. GO nanosheets are able to enter into cells, which renders them to become promising candidates for intracellular delivery of drugs and cellular imaging. However, the mechanisms of how the emerging nanostructures interface with biological systems are still largely unknown. In particular, a fundamental understanding of its ability to penetrate cell membranes and other biological barriers is still lacking. To illustrate these, Mu et al. [8] carried out studies about the cell surface adhesion, subcellular locations, and size-dependent uptake mechanisms of protein-coated GO nanosheets. They found that small nanosheets entered cells mainly through clathrin-mediated endocytosis, and the increase in graphene size enhanced phagocytotic uptake of the

Fig. 6.1 a A working model for cell uptake of protein-coated GO nanosheets. Numbers (*1–4*) and letters (*a–d*) indicate different steps of large and small nanosheets internalizing into cells, respectively. Reprinted with permission from Ref. [8] Copyright 2012 American Chemical Society. **b** Laser confocal fluorescence micrographs of HepG2 cells treated with 0.25 μg/mL DOX (*a, b*) and DOX-loaded GNC-RGO (*c, d*). (*a, c*) Fluorescence micrographs. (*b, d*) Overlay of the morphological and fluorescence images after incubation for 14 h. Images were acquired at 400-fold magnification. Reprinted from Ref. [26] by permission of John Wiley & Sons Ltd.
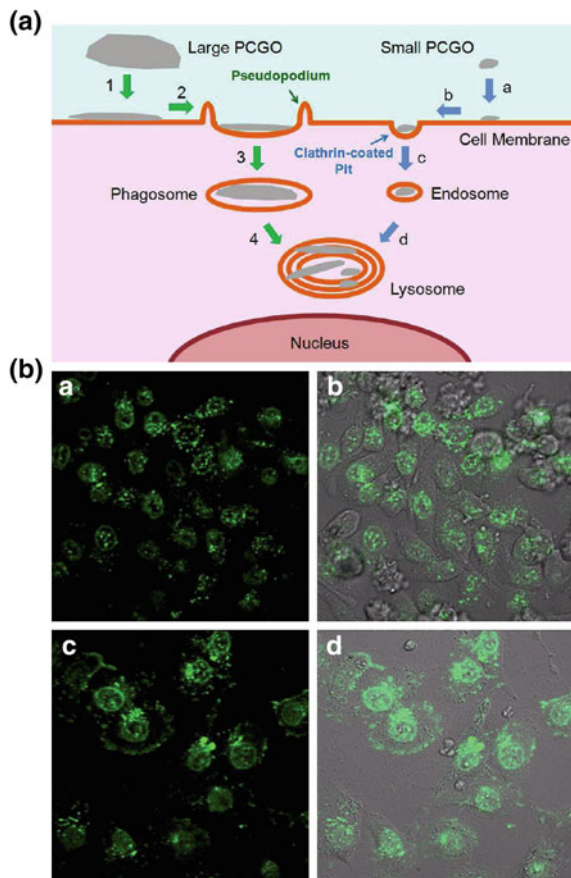
nanosheets (Fig. 6.1a). These results provided fundamental understanding of interactions at the interface of two-dimensional nanostructures and biological systems.

Based on the unique structure and properties of graphene (modified graphene), cancer cells detection had been achieved by using either electrochemical [9, 10] or colorimetric [11] methods with the LOD of 500 cells/mL, 794 cells/mL, and 1,000 Hela cells, respectively. It is revealed that surfaces with good biocompatibility and tissue-specific inductive capabilities are highly desirable in various tissue engineering and cell therapeutic applications. Recently, fluorinated graphene sheets as the scaffold for stem cell growth was reported by Wang et al. [12]. Results showed that fluorinated graphene induced higher proliferation and stronger polarization of mesenchymal stem cells (MSCs). Morphological changes in terms of cytoskeletal and nuclear alignment promoted the differentiation of MSCs toward the neuronal lineage, and the effect could be further enhanced with the addition of neuron-inductive agent, retinoic acid. More importantly, by leveraging on alignment induced neuronal differentiation, the stem cells could be controllably patterned

on fluorinated graphene, pointing to a large-scale and rapid strategy to align MSCs and the ability to induce neuronal lineage in the absence of chemical inducer. Also, cardiomyocyte-like HL-1 cells were recently cultured on graphene-based solution-gated FETs (G-SGFETs) and exhibited a healthy growth [13]. The action potentials of these electrogenic cells could be effectively resolved and tracked across the transistor array. Analysis of the recorded cell signals and the associated electronic noise of the transistors in the arrays confirm that G-SGFETs surpass the performance of state-of-the-art devices for bioelectronic applications.

Cellular imaging and drug delivery have also been achieved by using biocompatible material-grafted graphene platforms. For instance, Dai and coworkers used PEG star polymers to covalently grafting nano-GO sheets for cellular imaging and drug delivery [14, 15]. The PEG–GO conjugate showed photoluminescence from visible to the NIR range, which was used for cellular imaging with little background. This conjugate also served as a carrier for the delivery of water-insoluble aromatic drugs *via* simple adsorption and noncovalent interaction. Later, inspired by Dai's work, fluorescein-functionalized GO was synthesized *via* a PEG bridge and the conjugate could be efficiently taken up by cells and served as a fluorescent nanoprobe for intracellular imaging [16]. It was revealed that cellular uptake of the conjugate possibly relied on direct penetration of cell membranes, rather than energy-dependent pathways. The single sheet structure, high biocompatibility, and loading capability of graphene make it a highly useful and suitable nanocarrier for cellular imaging and drug delivery. To enhance the cellular uptake, various other materials, such as gelatin [17], herceptin [18], o-methacrylate [19], folic acid [20], β-cyclodextrin [21], poly(*N*-isopropylacrylamide) [22], and polyethylenimine [23], have been incorporated into graphene sheets. Recently, nanoscale GO (NGO) was functionalized with sulfonic acid groups, which rendered it stable in physiological solution, followed by covalent binding of folic acid (FA) to the NGO, thus allowing it to specifically target MCF-7 cells, human breast cancer cells with FA receptors [20]. Two anticancer drugs, doxorubicin (DOX) and camptothecin (CPT), were controllably loaded onto the FA-conjugated NGO (FA–NGO) *via* π–π stacking and hydrophobic interactions. It was demonstrated that FA–NGO loaded with the two anticancer drugs showed specific targeting to MCF-7 cells, and remarkably high cytotoxicity compared to NGO loaded with either DOX or CPT only. This work showed the viability of utilizing functionalized GO as the nanocarrier for controlled loading and targeted delivery of multiple drugs, which may have potential clinical advantages pertaining to increased therapeutic efficacy. Besides the biocompatible small aromatic molecules and polymers, nanoparticles, such as Fe_3O_4 [24], AuNPs [25], and gold nanoclusters (GNC) [26], have been anchored onto graphene basal planes by electrostatic, π–π stacking, cation-π, or van der Waals interactions. For instance, GNC–RGO nanocomposites were recently prepared and explored as new cancer therapeutic techniques by Wang et al. [26]. This material caused inhibition of HepG2 cells at high concentration; but more interestingly for oncotherapy, it could carry anticancer agents such as DOX inside the cells while leading to some synergy in inducing karyopyknosis. It was observed that GNCs anchored on RGO retained their NIR fluorescent property and Raman spectroscopy was used to

investigate the performance of DOX-loaded GNC–RGO nanocomposites against hepatocarcinoma and provide important mechanistic clues about their interactions with proteins and DNA. As shown in Fig. 6.1b, DOX alone did not distribute well in the cells, with about half of the DOX molecules resting on the cell membrane surface or in between cells (*a* and *b*). Conversely, when loaded onto GNC–RGO nanocomposites, DOX was well distributed inside the cells (*c* and *d*), establishing that GNC–RGO acted as a drug delivery platform that improved DOX internalization by HepG2 cells. Results suggested that GNC–RGO vectorization might have enhanced membrane permeability through interactions with phospholipids and/or proteins, resulting in high drug transfer into the cells.

Real-time detection of biologically interesting substances in the live cells or on the cell surface has fundamental significance in understanding of cellular functions and pathology, and practical importance in the development of applications in diseases diagnosis and drug discovery. Among these substances, caspase-3 [27, 28], nitric oxide [29], and integrin $\alpha v \beta 3$ [30] have been selectively detected. For instance, Wang et al. designed a novel intracellular protease sensor for caspase-3 *via* the GO–peptide conjugate [27]. Based on the intrinsic properties of GO as a nanocarrier for delivering peptide cargos inside live cells and a fluorescence quencher for fluorophores adjacent to its surface, the GO–peptide conjugate, after being transported into cells followed by cleavage of the peptide by intracellular proteases, provided greatly enhanced fluorescence imaging as a result of the release of fluorophores from the GO surface. Confocal fluorescence microscopy experiments with HeLa cells suggested that the GO–peptide conjugate was efficiently delivered into live cells and acted as a 'signal-on' intracellular sensor for specific, high-contrast imaging of caspase-3 activation. A similar strategy was also reported for real-time imaging and monitoring of caspase-3 activation during the progress of apoptosis in vitro and in vivo [28]. Real-time detection of nitric oxide remains a great difficulty due to its trace level release from cells, and more critically, the rapid reaction of nitric oxide with oxygen and its short half-life. Recently, Guo et al. [29] reported a new approach to build a free-standing biomimetic sensor by covalently binding RGD–peptide on the surface of pyrenebutyric acid functionalized graphene film, in which the RGD–peptide component provided desired biomimetic properties for superior human cell attachment and growth on the film surface to allow real-time electrochemical detection of nitric oxide under drug stimulations. The film sensor exhibited good flexibility and stability by retaining its original response after 45 bending/relaxing cycles and high reproducibility from its almost unchanged current responses after 15 repeated measurements. Based on the ligand–receptor pair of RGD peptide and a cancer cell surface marker, integrin $\alpha v \beta 3$, a nanoscale RGD-pyrene-GO biosensor was prepared for real-time in situ fluorescent detection of the marker [30]. The competitive binding of RGD with integrin $\alpha v \beta 3$ disturbed the adsorption of RGD–pyrene onto the GO surface, resulting in the recovery of pyrene fluorescence.

6.2 Pathogen and Bacteria Inhibition

The edges of graphene nanosheets with extremely high aspect ratio (the ratio of lateral size to the atomic thickness) can be proposed as one of the excellent and ideal nanostructures for an effective direct contact interaction with microorganisms. Bacterial toxicity of graphene nanosheets in the form of graphene nanowalls deposited on stainless steel substrates was investigated for both Gram-positive *Staphylococcus aureus* (*ConA*) and Gram-negative *Escherichia coli* (*E. coli*) bacteria [31]. The efflux of RNA of the bacteria indicated that the cell membrane of the bacteria was effectively damaged by direct contact of the bacteria with the very sharp edges of the nanowalls, resulting in inactivation of the bacteria by the nanowalls. A higher bacterial toxicity of the reduced nanowalls was observed compared to the unreduced nanowalls, which was attributed to more sharpening of the edges of the nanowalls providing stronger contact interaction with the cell membrane and/or better charge transfer between the bacteria and the reduced nanowalls, resulting in more cell membrane damage of the bacteria. Almost at the same time, the antibacterial activity of GO- and rGO-based paper was also studied, which inhibited the growth of *E. coli* bacteria and showed minimal cytotoxicity [32]. Recently, an interesting study was carried out by Akhavan et al. [33] to wrap bacteria by graphene sheets for isolation from environment. In the melatonin-bacterial suspension, aggregation of the graphene sheets resulted in trapping of the *E. coli* bacteria within the aggregated sheets (a kind of bacterial inactivation) (Fig. 6.2a left). The GOs with the oxygen-containing functional groups could better trap the bacteria than the GSs with reduced functional groups (Fig. 6.2a right). On the basis of measuring the glucose consumption of the bacteria, it was found that the bacteria trapped within the aggregated graphene sheets were biologically disconnected from their environment. In addition, the bacteria trapped within the graphene sheets were inactive without any chance for proliferation in a culture medium. After removing the aggregated graphene sheets from the surface of the bacteria by using sonication, they could be reactivated. But, the near-IR irradiation at 808 nm could inactivate the bacteria forever by excessive local heating of the bacteria trapped within the aggregated graphene sheets. Under visible light irradiation, viruses could also be photoinactivated by graphene–tungsten oxide composite [34]. Annealing the composite at 450 °C in air resulted in the formation of W–C and W–O–C bonds of graphene–tungsten oxide (Fig. 6.2b left), which showed visible light photocatalytic performance in photoinactivation of bacteriophage MS2 viruses. The photocatalysis of the viruses on surface of the graphene–tungsten oxide composite resulted in a nearly complete destruction of the viral protein (Fig. 6.2b right) and a sharp increase in the RNA efflux after 3-h light irradiation at room temperature. These results suggested the promising environmentally friendly applications of the low-cost and highly effective carbon nanomaterial in bacteria detection and growth inhibition.

Recently, a graphene-based FET for detection of bacteria was reported, in which large-sized graphene was grown by CVD and functionalized with anti-*E. coli*
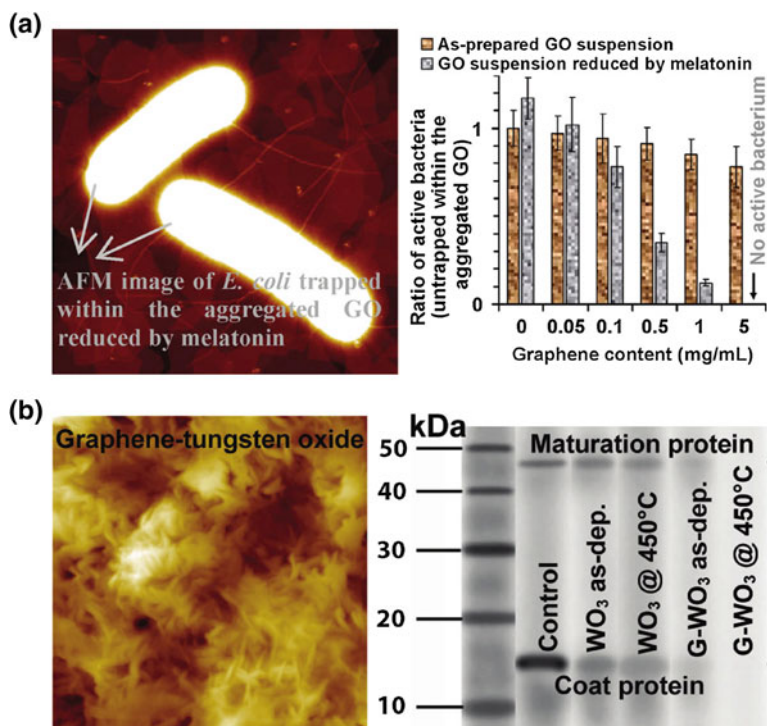
Fig. 6.2 a AFM image of the bacteria trapped between the GO sheets aggregated together after reduction by melatonin (*left*); ratio of the number of the active bacteria obtained from the as-prepared GO-bacterial, the GO-melatonin-bacterial suspensions (*right*). Reprinted with permission from Ref. [33] Copyright 2011 American Chemical Society. **b** AFM image of the graphene–tungsten oxide composite (*left*); SDSP electrophoresis of the viral protein capsid of bacteriophage MS2 after 3-h visible light photocatalysis on surface of the various thin films, as compared to the electrophoresis of a protein marker. Reprinted with permission from Ref. [34] Copyright 2012 American Chemical Society

antibodies and passivation layer [35]. Significant conductance increase in the graphene device was observed after exposure to *E. coli* bacteria at a concentration as low as 10 cfu/mL, while no significant response was triggered by high concentration of the another bacterial strain. Electrochemical detection of bacteria with graphene platforms has also been reported by Wan et al. using silver enhancement [36] and impedimetric immunoassay [37]. In the impedimetric manner, reduced graphene sheets-doped chitosan nanocomposites were electrodeposited on the electrode surface. Based on the specific interaction between the antibodies and sulfate-reducing bacteria (SRB), the bacteria were determined by EIS as the R_{et} signal changes according to the different concentrations of SRB.

Exploiting the fluorescence quenching ability of GO or its own photoluminescence, fluorescent detection of bacteria has been recently developed. A homogenous solution of GO showed a broad fluorescence emission peak around 547 nm

upon excitation at 400 nm, which was due to the disruption of the sp^2 structure of graphene crystals during the oxidation process resulting in the recombination of electron–hole pairs localized within small sp^2 carbon domains that were embedded in an sp^3 matrix [38]. The antibodies for rotavirus were immobilized on GO arrays, where rotavirus was captured by specific antigen–antibody interaction. Ab–DNA–AuNPs complexes were then introduced to the assay system, which quenched the GO photoluminescence by FRET between GO and AuNPs. A LOD of 10^5 pfu/mL was obtained, which was comparable to that of a conventional ELISA technology. Based on the quenching ability of GO, a conjugated oligomer(4,7-bis(9,9-bis(2-(2-(2-(2,3,4,5,6-pentahydroxyhexanal)-ethoxy)ethyl)fluorenyl)benzothiadiazole (FBT) was developed and adopted as a fluorophore for *ConA* and *E. coli* detection [39]. Since GO-based quenching followed long-range nanoscale surface resonance energy transfer that exhibited a $(distance)^{-4}$-dependent quenching efficiency, the binding process switched from the high-quenching (almost non-fluorescent) state to the low-quenching (highly fluorescent) state in the presence of *ConA*. As such, *ConA* was detected with a LOD of 0.5 nM.

6.3 Versatile Targets Bioassays

Versatile bioassay represents one of the main challenges in bioanalytical applications, which need the platforms to be highly efficient, precise, fast, and discriminable in transducing the recognition signal. Efforts have been devoted to this domain. Recently, a fluorescence 'off-to-on' mechanism of GO nanosheets for assays of different biological species by the employment of AgNPs functionalized with ligands, antibodies, and oligonucleotides was proposed by Mei and coworkers [40]. In their design, the fluorescence of GO-*n*-butylamine (NHBu) was strongly quenched by AgNPs through resonance energy transfer or charge-transfer process. When the corresponding analyte was added into the system, specific donor–acceptor interactions occurred between analytes and AgNPs, for example, antigen–antibody reaction and DNA strand hybridization, which led to the disassociation of AgNPs from the GO-NHBu nanosheets and their aggregation. Then, the fluorescence of GO-NHBu nanosheets was immediately recovered, thus providing the rapid identification and quantification of analytes by the fluorescence (Fig. 6.3a). Furthermore, the ink of GO-NHBu was easily printed into the highly uniform word or image for the fabrication of paper-like biosensor (Fig. 6.3b). The GSH, PROTEIN, and DNA words gradually appeared with the increasing amount of analytes under UV light, which was rapid, simple, efficient, and inexpensive. Moreover, if a library of AgNPs with various recognition elements was available, a nearly universal bioassay would be achieved.

The large surface area and universal fluorescence quenching ability of graphene sheets enable it to be an efficient platform for multiplex targets assay in a fluorescent manner. Similar to the fluorescent single-target detection mechanism as mentioned above, multiplex DNA or aptamer sequences labeled with different
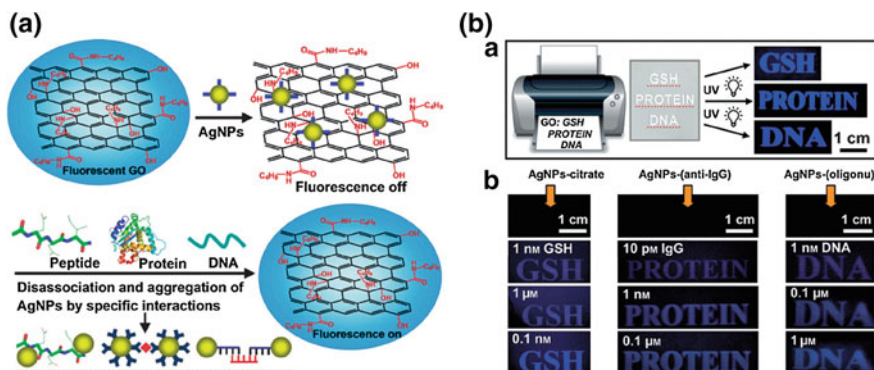
Fig. 6.3 a Fluorescence 'off-to-on' mechanism of GO-NHBu nanosheets for biological assays. **b** Visual biosensors. (*a*) The inkjet printing of GO-NHBu into 'words' on microporous polyvinylidene fluoride membrane. (*b*) Visual detections of GSH, IgG, and DNA under a UV lamp. Reprinted from Ref. [40] by permission of John Wiley & Sons Ltd.

fluorophores are adsorbed on graphene surface, where the fluorescences are all quenched due to the FRET or charge transfer. Probes binding to targets result in desorption of the respective probes and restoration of respective fluorescent signals, indicating the recognition of different targets. Based on this, multiplex analytes, such as DNA, thrombin, Ag^+, Hg^{2+}, cysteine [41] and DNA, thrombin, ATP in logic gate operations [42], have been successfully detected with high sensitivity and simplicity. Combining the merits of graphene platforms, the tailored design of DNA, molecular beacon, or aptamer sequences allows the sensing matrices for numerous targets. Nonetheless, particular prerequisites need to be fulfilled for targets recognition. The association constants of the probe–target complexes must be sufficiently high to release the probes from the graphene platform. While, the binding affinity of the probes to graphene platform should be sufficiently high to eliminate spontaneous desorption leading to perturbing background signals [42]. An equilibrium between the two binding affinity, namely the probe–graphene binding and probe–target binding, should be achieved to get reliable results. Besides, particular emphasis should also be paid to the graphene platform (C/O ratio, defect, structure, number of layer, etc.) and the ambient conditions, such as the ionic strength, pH, solvent, and temperature.

Matrix-assisted laser desorption/ionization time-of-flight MS (MALDI-TOFMS) provides a simple analytical approach for high molecular mass species, such as proteins, DNA/RNA, polysaccharides, and synthetic polymers. For low-mass analytes (<1,000 Da), this method has significant limitation due to the interferences of matrix background ions. To solve this problem, graphene has been, for the first time, used as a novel matrix for MALDI-TOFMS analysis of small molecules [43]. Graphene functioned to trap the analyte molecules and acted as an energy receptacle for laser radiation. Due to its large surface area, it attached to the analytes more tightly. This prevented the detachment of graphene from the analytes under vacuum, which avoided the contamination of the ion source and vacuum system.

On the other hand, the efficiency of desorption/ionization for analytes on a matrix layer of graphene might be enhanced for its simple monolayer structure and unique electronic properties. In positive ion mode, the facile analysis of amino acids, polyamines, anticancer drugs, nucleosides, and steroids had been achieved with simplicity, low interference, and improved reproducibility. Recently, MALDI-TOFMS analysis of small molecules with negative ion LDI on graphene flakes was also developed [44]. Compared to the positive ion desorption/ionization on graphene flakes, in which multiple sodium or potassium adducts were produced, deprotonated monomeric species with significant reduction of matrix interference were detected for the analysis of peptides, amino acids, fatty acids, nucleosides, and nucleotides in negative ion mode. Better sensitivity and reproducibility were achieved in the analysis with negative ion mode than positive ion mode.

References

1. Hu, W., Peng, C., Lv, M., Li, X., Zhang, Y., Chen, N., Fan, C., Huang, Q.: Protein corona-mediated mitigation of cytotoxicity of graphene oxide. ACS Nano **5**, 3693–3700 (2011)
2. Yang, K., Wan, J., Zhang, S., Zhang, Y., Lee, S.T., Liu, Z.: In vivo pharmacokinetics, long-term biodistribution, and toxicology of PEGylated graphene in mice. ACS Nano **5**, 516–522 (2011)
3. Wang, K., Ruan, J., Song, H., Zhang, J., Wo, Y., Guo, S., Cui, D.: Biocompatibility of Graphene Oxide. Nanoscale Res. Lett. **6**, 8 (2010)
4. Liao, K.H., Lin, Y.S., Macosko, C.W., Haynes, C.L.: Cytotoxicity of graphene oxide and graphene in human erythrocytes and skin fibroblasts. ACS Appl. Mater. Interfaces **3**, 2607–2615 (2011)
5. Markovic, Z.M., Harhaji-Trajkovic, L.M., Todorovic-Markovic, B.M., Kepic, D.P., Arsikin, K.M., Jovanovic, S.P., Pantovic, A.C., Dramicanin, M.D., Trajkovic, V.S.: In vitro comparison of the photothermal anticancer activity of graphene nanoparticles and carbon nanotubes. Biomaterials **32**, 1121–1129 (2011)
6. Akhavan, O., Ghaderi, E., Aghayee, S., Fereydooni, Y., Talebi, A.: The use of a glucose-reduced graphene oxide suspension for photothermal cancer therapy. J. Mater. Chem. **22**, 13773–13781 (2012)
7. Hong, B.J., Compton, O.C., An, Z., Eryazici, I., Nguyen, S.T.: Successful stabilization of graphene oxide in electrolyte solutions: enhancement of biofunctionalization and cellular uptake. ACS Nano **6**, 63–73 (2012)
8. Mu, Q., Su, G., Li, L., Gilbertson, B.O., Yu, L.H., Zhang, Q., Sun, Y.P., Yan, B.: Size-dependent cell uptake of protein-coated graphene oxide nanosheets. ACS Appl. Mater. Interfaces **4**, 2259–2266 (2012)
9. Feng, L., Chen, Y., Ren, J., Qu, X.: A graphene functionalized electrochemical aptasensor for selective label-free detection of cancer cells. Biomaterials **32**, 2930–2937 (2011)
10. Yang, G., Cao, J., Li, L., Rana, R.K., Zhu, J.-J.: Carboxymethyl chitosan-functionalized graphene for label-free electrochemical cytosensing. Carbon **51**, 124–133 (2013)
11. Song, Y., Chen, Y., Feng, L., Ren, J., Qu, X.: Selective and quantitative cancer cell detection using target-directed functionalized graphene and its synergetic peroxidase-like activity. Chem. Commun. **47**, 4436–4438 (2011)
12. Wang, Y., Lee, W.C., Manga, K.K., Ang, P.K., Lu, J., Liu, Y.P., Lim, C.T., Loh, K.P.: Fluorinated graphene for promoting neuro-induction of stem cells. Adv. Mater. **24**, 4285–4290 (2012)

13. Hess, L.H., Jansen, M., Maybeck, V., Hauf, M.V., Seifert, M., Stutzmann, M., Sharp, I.D., Offenhausser, A., Garrido, J.A.: Graphene transistor arrays for recording action potentials from electrogenic cells. Adv. Mater. **23**, 5045–5049, 4968 (2011)
14. Sun, X., Liu, Z., Welsher, K., Robinson, J.T., Goodwin, A., Zaric, S., Dai, H.: Nano-graphene oxide for cellular imaging and drug delivery. Nano Res. **1**, 203–212 (2008)
15. Liu, Z., Robinson, J.T., Sun, X., Dai, H.: PEGylated nanographene oxide for delivery of water-insoluble cancer drugs. J. Am. Chem. Soc. **130**, 10876–10877 (2008)
16. Peng, C., Hu, W., Zhou, Y., Fan, C., Huang, Q.: Intracellular imaging with a graphene-based fluorescent probe. Small **6**, 1686–1692 (2010)
17. Liu, K., Zhang, J.-J., Cheng, F.-F., Zheng, T.-T., Wang, C., Zhu, J.-J.: Green and facile synthesis of highly biocompatible graphene nanosheets and its application for cellular imaging and drug delivery. J. Mater. Chem. **21**, 12034–12040 (2011)
18. Guo, C., Book-Newell, B., Irudayaraj, J.: Protein-directed reduction of graphene oxide and intracellular imaging. Chem. Commun. **47**, 12658–12660 (2011)
19. Gollavelli, G., Ling, Y.C.: Multi-functional graphene as an in vitro and in vivo imaging probe. Biomaterials **33**, 2532–2545 (2012)
20. Zhang, L., Xia, J., Zhao, Q., Liu, L., Zhang, Z.: Functional graphene oxide as a nanocarrier for controlled loading and targeted delivery of mixed anticancer drugs. Small **6**, 537–544 (2010)
21. Yang, Y., Zhang, Y.M., Chen, Y., Zhao, D., Chen, J.T., Liu, Y.: Construction of a graphene oxide based noncovalent multiple nanosupramolecular assembly as a scaffold for drug delivery. Chem.-Eur. J. **18**, 4208–4215 (2012)
22. Pan, Y., Bao, H., Sahoo, N.G., Wu, T., Li, L.: Water-soluble poly(*N*-isopropylacrylamide)-graphene sheets synthesized via click chemistry for drug delivery. Adv. Funct. Mater. **21**, 2754–2763 (2011)
23. Kim, H., Namgung, R., Singha, K., Oh, I.K., Kim, W.J.: Graphene oxide-polyethylenimine nanoconstruct as a gene delivery vector and bioimaging tool. Bioconjug. Chem. **22**, 2558–2567 (2011)
24. Zheng, X.T., Li, C.M.: Restoring basal planes of graphene oxides for highly efficient loading and delivery of beta-lapachone. Mol. Pharm. **9**, 615–621 (2012)
25. Liu, Q., Wei, L., Wang, J., Peng, F., Luo, D., Cui, R., Niu, Y., Qin, X., Liu, Y., Sun, H., Yang, J., Li, Y.: Cell imaging by graphene oxide based on surface enhanced Raman scattering. Nanoscale **4**, 7084–7089 (2012)
26. Wang, C., Li, J., Amatore, C., Chen, Y., Jiang, H., Wang, X.M.: Gold nanoclusters and graphene nanocomposites for drug delivery and imaging of cancer cells. Angew. Chem. Int. Ed. **50**, 11644–11648 (2011)
27. Wang, H., Zhang, Q., Chu, X., Chen, T., Ge, J., Yu, R.: Graphene oxide-peptide conjugate as an intracellular protease sensor for caspase-3 activation imaging in live cells. Angew. Chem. Int. Ed. **50**, 7065–7069 (2011)
28. Kong, W.H., Sung, D.K., Kim, K.S., Jung, H.S., Gho, E.J., Yun, S.H., Hahn, S.K.: Self-assembled complex of probe peptide–*E. Coli* RNA I conjugate and nano graphene oxide for apoptosis diagnosis. Biomaterials **33**, 7556–7564 (2012)
29. Guo, C.X., Ng, S.R., Khoo, S.Y., Zheng, X., Chen, P., Li, C.M.: RGD-peptide functionalized graphene biomimetic live-cell sensor for real-time detection of nitric oxide molecules. ACS Nano **6**, 6944–6951 (2012)
30. Wang, Z., Huang, P., Bhirde, A., Jin, A., Ma, Y., Niu, G., Neamati, N., Chen, X.: A nanoscale graphene oxide-peptide biosensor for real-time specific biomarker detection on the cell surface. Chem. Commun. **48**, 9768–9770 (2012)
31. Akhavan, O., Ghaderi, E.: Toxicity of graphene and graphene oxide nanowalls against bacteria. ACS Nano **4**, 5731–5736 (2010)
32. Hu, W., Peng, C., Luo, W., Lv, M., Li, X., Li, D., Huang, Q., Fan, C.: Graphene-based antibacterial paper. ACS Nano **4**, 4317–4323 (2010)
33. Akhavan, O., Ghaderi, E., Esfandiar, A.: Wrapping bacteria by graphene nanosheets for isolation from environment, reactivation by sonication, and inactivation by near-infrared irradiation. J. Phys. Chem. B **115**, 6279–6288 (2011)

34. Akhavan, O., Choobtashani, M., Ghaderi, E.: Protein degradation and RNA efflux of viruses photocatalyzed by graphene-tungsten oxide composite under visible light irradiation. J. Phys. Chem. C **116**, 9653–9659 (2012)
35. Huang, Y., Dong, X., Liu, Y., Li, L.-J., Chen, P.: Graphene-based biosensors for detection of bacteria and their metabolic activities. J. Mater. Chem. **21**, 12358–12362 (2011)
36. Wan, Y., Wang, Y., Wu, J., Zhang, D.: Graphene oxide sheet-mediated silver enhancement for application to electrochemical biosensors. Anal. Chem. **83**, 648–653 (2011)
37. Wan, Y., Lin, Z., Zhang, D., Wang, Y., Hou, B.: Impedimetric immunosensor doped with reduced graphene sheets fabricated by controllable electrodeposition for the non-labelled detection of bacteria. Biosens. Bioelectron. **26**, 1959–1964 (2011)
38. Jung, J.H., Cheon, D.S., Liu, F., Lee, K.B., Seo, T.S.: A graphene oxide based immuno-biosensor for pathogen detection. Angew. Chem. Int. Ed. **49**, 5708–5711 (2010)
39. Wang, L., Pu, K.Y., Li, J., Qi, X., Li, H., Zhang, H., Fan, C., Liu, B.: A graphene-conjugated oligomer hybrid probe for light-up sensing of lectin and *Escherichia coli*. Adv. Mater. **23**, 4386–4391 (2011)
40. Mei, Q., Zhang, Z.: Photoluminescent graphene oxide ink to print sensors onto microporous membranes for versatile visualization bioassays. Angew. Chem. Int. Ed. **51**, 5602–5606 (2012)
41. Zhang, M., Yin, B.C., Tan, W., Ye, B.C.: A versatile graphene-based fluorescence "on/off" switch for multiplex detection of various targets. Biosens. Bioelectron. **26**, 3260–3265 (2011)
42. Liu, X.Q., Aizen, R., Freeman, R., Yehezkeli, O., Willner, I.: Multiplexed aptasensors and amplified DNA sensors using functionalized graphene oxide: application for logic gate operations. ACS Nano **6**, 3553–3563 (2012)
43. Dong, X.L., Cheng, J.S., Li, J.H., Wang, Y.S.: Graphene as a novel matrix for the analysis of small molecules by MALDI-TOF MS. Anal. Chem. **82**, 6208–6214 (2010)
44. Lu, M., Lai, Y., Chen, G., Cai, Z.: Matrix interference-free method for the analysis of small molecules by using negative ion laser desorption/ionization on graphene flakes. Anal. Chem. **83**, 3161–3169 (2011)

Chapter 7
Conclusions and Perspectives

Abstract In this book, we present recent advancements and achievements of graphene and biocompatible materials decorated graphene in bioanalytical applications. We highlight the use of simulations and bioinformatics driven approaches for predictive modeling of the interaction between graphene and biomolecules, the decoration of graphene with various biomaterials, the enhancement of the analytical performances, the effective transduction of recognition event to the detectable signals. Also, future challenges and prospects of graphene in bioanalytical applications are demonstrated.

Keywords Graphene · Biosensing · Biomaterials · Biomolecules · Analytical chemistry

Many efforts have been devoted to elucidating the properties, preparation, and applications of graphene ever since its discovery. Through the collaboration of scientists in physics, chemistry, biology, as well as the interdisciplinary fields, the very tip of the iceberg has been uncovered so far. Great progress and achievement have been observed in large-scale and high-quality preparation, revealing the extraordinary properties, and various applications in electronics, biosensing, and energy, etc. Among these applications, biosensing takes a unique and important position, which is highly associated with human health and environmental protection. In the present book, we present recent advancements and achievements of graphene and biocompatible materials decorated graphene in bioanalytical applications. The unique π-conjugated structure and functional groups, tunable band gap, large surface area, remarkable mechanical, optical, electronic properties make graphene especially suitable for bioanalytical applications. However, these extraordinary properties are only associated with the single-layer graphene sheets, which is still a main challenge for experimentalists to fabricate and isolate graphene sheets in a tailored and fine-tunable manner. One efficient way to solve this may be through the isolation and functionalization of graphene with biological molecules, such as DNA, peptides, and proteins, which endow graphene with biocompatibility. Moreover, the synergetic effects result in the bio-nanocomposites as platforms more

suitable for the anchoring of other substances (NPs, quantum dots, polymers, organic crystals, small molecules, etc.), which are beneficial for probe immobilization and target detection. We highlight the use of simulations and bioinformatics-driven approaches for predictive modeling of the interaction between graphene and biomolecules, various biomaterials decorating graphene based on covalent or non-covalent modes, the enhancement of the analytical performances, the effective transduction of recognition event to the detectable signals through optical, electrochemical, mechanical, electronic, etc., methods. Along this line, various targets, including DNA, amino acid, peptide, protein, enzyme, antigen, glucose, DA, AA, UA, ATP, NADH, cell imaging and drug delivery, gas, other molecules and ions, etc., are detected by adopting well-designed biocompatible graphene platforms. Despite these important achievements, challenges still remain in the exploration of graphene for bioanalytical performances. (a) Graphene sheets with high-quality, tailored functionalization, precise and fine-tunable structures and properties (C/O ratio, defect, edge, etc.) need to be fabricated and adjusted in a more costless, effective, and easy way. (b) Based on the synergetic effects, functional substances are often incorporated into graphene sheets. One should pay attention to the substances distribution, amount, and affinity to graphene sheets, also the nanohybrids' dispersibility and functionality. (c) The mechanisms of probes interacting with graphene or decorated graphene need to be thoroughly investigated. The transduction of detecting signals should be optimized to eliminate background noise. (d) Particular emphasis should be paid to the ambient conditions, such as the ionic strength, pH, organic solvent, and temperature, which have strong impact on the target detection. (e) New techniques and analytical methods need to be developed to exploit and improve the new performance of graphene in bioanalytical applications.